DEVELOPMENT OF A SENSIBLE REDUCED-ORDER MODELING
FRAMEWORK FOR GEOMECHANICS SIMULATION: WITH APPLICATION TO
COUPLED FLOW AND GEOMECHANICS SIMULATION

A Thesis

by

PATRICK ATEF HAKIM MORKOS

Submitted to the Office of Graduate and Professional Studies of
Texas A&M University
in partial fulfillment of the requirements for the degree of

MASTER OF SCIENCE

Chair of Committee,	Eduardo Gildin
Committee Members,	Jihoon Kim
	Yalchin Efendiev
Head of Department,	Jeff Spath

August 2020

Major Subject: Petroleum Engineering

ABSTRACT

With the recent development of unconventional reservoirs, attention has been geared towards the integration of the geomechanical models with traditional flow simulation. A case in point is quantifying rock-fluid interactions in hydraulic fracturing operations. Although much effort has gone into the creation and advancement of commercial simulation software for coupled flow and geomechanics, it is still in its infancy. The models are considerably oversimplified and poorly representative of the problem's complex nature. Throughout history, several contributions have been made into the development of efficient model-order reduction (MOR) techniques for "flow only" simulations. Yet – to date – contributions to the mechanical models in coupled simulations have been minimal.

This study tackles this challenging aspect, by proposing a novel model reduction adaptive workflow, especially for the mechanics simulators, that (1) can be coupled with any simulator that can export mass, stiffness, and load matrices; (2) can achieve 2 orders of magnitude in computational time reduction; and (3) do not add more complexity to the solution.

In the first part of this research, several – widely used – reduction techniques for structural mechanics were implemented based on the construction of the dynamic condensation matrix. Single-step reduction methods were first executed; in particular, Guyan DOFs based reduction techniques. Following that, two-step methods were implemented; where corrections were made to the results obtained from the former. Finally, iterative (three-step) reduction methods were applied; handling the problem of master DOFs selection through consistent updates of the dynamic condensation matrix until convergence is achieved. To that end, two schemes are presented; based on the convergence of the dynamic condensation matrix, as well as, the eigenvalues of the reduced-order model.

In the second part of this research, we provide a rigorous framework for testing the completeness, efficiency, and convergence for all the presented reduction techniques. Regarding the completeness of the reduced models, two main criteria were investigated; namely, modal assurance criterion (MAC) and singular value decomposition (SVD). For efficiency testing, percent error (PE) of natural frequencies and the correlation coefficient for modal vector (CCFMV)

values were considered. Finally, the efficiency of the convergent criterion was demonstrated through the errors associated with the column vectors of the condensation matrix. Several numerical examples are presented to show the efficiency of the presented framework, particularly for coupled simulations.

Based on the adopted framework, we managed to reduce the scale of the finite element models to less than 9% of the full model with error as low as 1%. In terms of computational speed and runtime, we achieved substantial speedups; up to 20X. Given the proposed workflow, large-scale complex simulations – similar to those associated with hydraulic fracturing – could be more feasible and less costly. This, ultimately, would give allowance for incorporating the complex physics pertinent to unconventional reservoirs and motivate the advent of their development at no additional cost.

I dedicate my thesis to my family and my friends. A special feeling of gratitude to my fiancée Christine, my sister Nathalie and my loving parents; Atef and Nagwa Issac whose words of encouragement and tenacity ring in my ear.

ACKNOWLEDGEMENTS

CONTRIBUTORS AND FUNDING SOURCES

Contributors

This work was supervised by a thesis committee consisting of Professor Eduardo Gildin (Chair of Committee), Professor Jihoon Kim (Committee Member) of the Department of Petroleum Engineering and Professor Efendiev (Committee Member) of the Department of Mathematics.

The data analyzed for Chapter II was conceptualized by Professor Thomas Lacy; Department of Mechanical Engineering. The analyses depicted in Chapter III were conceptualized in part by Professor Eduardo Gildin of the Department of Petroleum Engineering. In addition, the analyses conducted in Chapter IV were supported partially by Jihoon Kim of Department of Petroleum Engineering.

All other work conducted for the thesis was completed by the student independently.

TABLE OF CONTENT

LIST OF FIGURES

LIST OF TABLES

CHAPTER I
INTRODUCTION

In oil and gas industry, with the recent development of unconventional reservoirs, attention has been geared towards the integration of the geomechanical models with traditional flow simulation. There are a number of cases in which conventional reservoir simulators fall short in accurately accounting for the effects of rock deformation on flow and vice versa by using the rock compressibility concept and simplistic reservoir property evolution models that are related to pressure/porosity changes via empirical correlations. A case in point is the impact of geomechanical effects on well production [Jun Xiong et al. 2012; T. Kidambi et al. 2017; Alpak F.O. 2019].

Production of oil and gas reservoirs changes the reservoir pore pressure and stress state. These changes in the pore pressure and in-situ stress cause changes in the volume of both reservoir fluids and the reservoir rock. The prediction of the variation of the fluid volume and rock volumetric deformation, and their interaction and influence on the flow conditions, is essential when examining different operating strategies for stress-sensitive reservoirs.

The simultaneous interaction between changes in the pore pressure and variation in the in-situ stress lead to the coupling of two different, yet fully connected, processes: (1) motion of the pore fluid and (2) deformation of the rock solid skeleton. Any attempt to model the interaction of the rock-fluid system should not separate these two processes.

An instance of failure of conventional flow simulations during oil well production operation was presented in Osorio J.G. at al. 1997. In this study, a 3D finite-difference model for the simulation of stress-sensitive reservoirs had been developed. The reservoir was treated as a multiphase poroelastic system consisting of a deforming solid skeleton and a moving compressible pore fluid. The governing equations describing the deformation of the solid and the motion of the pore fluid were fully coupled. Solid displacement and fluid pressure were chosen as the primary variables. Discretization was accomplished by using a 15-point and 7-point operators for the solid-displacement and fluid-flow equations, respectively.

The coupled simulator [used in Osorio et al. 1997] was developed such that a single-input-parameter change permits choosing between explicit, iterative, and implicit coupling approaches. Due its improved stability and rapid convergence characteristics for challenging flow-induced deformation problems, where the geomechanical responses occur on comparable time-scales to flow, the above-described multiphysics system of equations is solved via a fully-implicit formulation in the default mode [Alpak F.O. 2014].

The porosity relative to the initial undeformed bulk volume is defined as follows:

$$\phi - \phi_0 = b(\varepsilon_v - \varepsilon_v^0) + \frac{1}{M}(p - p_0) - \beta_\phi(T - T_0) \tag{1}$$

where b and $1/M$ are the Biot constants, and β_ϕ denotes the volumetric thermal expansion coefficient for porosity. The pore volume is then ϕV_b^0 where V_b^0 is the original undeformed volume of a region containing both the solid and pores. It is important to highlight that the porosity is defined relative to the original volume, not with respect to the current volume.

Numerical results obtained from the application of this model to a centered-well producing at a constant flow rate from a poroelastic medium had been analyzed. The discretization grid consisted of 15 blocks in each x- and y-direction, and 5 blocks in the z-direction, each block having a length of 10 ft. At the boundaries, the pore pressure was constant and equal to the initial pore pressure, and the displacements were zero.
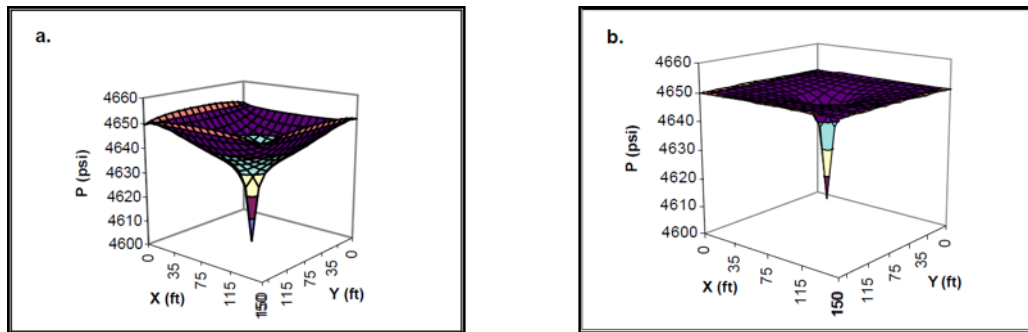
Figure 1: Pore pressure distribution at: (a) 5 days (b) 200 days [Reprinted from Osorio, 1997]

Figure 1 shows the pore pressure distribution at 5 and 200 days. After 5 days of production, the radius of investigation had already arrived to the outer boundaries and, consequently, the

pressure maintenance at the boundaries became active. As production time increased, a conventional fluid-flow model will predict, for this particular example, a constant pore pressure distribution with time. In Osorio's study, with using fluid-flow/geomechanical model, a stress-transfer effect was observed. As the solid part of the rock expanded, the pore fluid received the load change caused by the rock expansion. Accordingly, after the radius of investigation reached the outer boundaries the pore pressure distribution didn't remain constant with time, but rose until equilibrium conditions were attained, as observed in *Figure 1b* after 200 days of production.

Figure 1a also shows that after 5 days of production, the pore pressure in the region close to the outer boundaries reaches values slightly greater than the initial pore pressure. This behavior is possible because the load caused by the initial expansion of the solid skeleton is higher than the decrease in the pore pressure which results in pressure rises above the initial pressure. After equilibrium condition is reached, this excess in pore pressure is dissipated as observed after 200 days of production (*Figure 1b*).

Besides the pore pressure, the stress state also alters the physical properties (e.g., permeability and porosity) which are important to the performance of stress-sensitive reservoirs. A convenient way of expressing the stress state of the rock is through the effective stress, which is a measure of the "actual" stress acting on the solid part of the porous system. *Figure 2* shows the distribution of the change in the effective stress in the x-direction (compressive stress is taken negative). Note that after 5 days of production (*Figure 2a*), the change in effective stress (with respect to the initial effective stress) switches from compression to extension. The region under compressive stress is due to production and, therefore, is located around the wellbore where the pore pressure is always minimum. The region in extension is close to the outer boundaries where zero-displacement is specified. After 200 days of production, the increment in pore pressure (caused by the pressure maintenance and the load received from the rock expansion) reduces the magnitude of the change in the effective stress in the tensile region (*Figure 2b*).
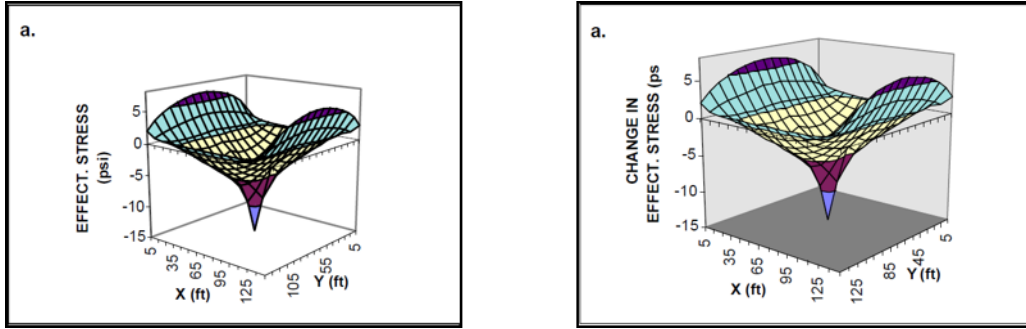
***Figure 2**: Change of effective stress in x-direction at: (**a**) 5 days (**b**) 200 days [Reprinted from Osorio, 1997]*

Although much effort has gone into the creation and advancement of commercial simulation software for coupled simulations, this area of research is still in its infancy. The models are considerably oversimplified and poorly representative of the problem's complex nature. Detailed and complex coupled flow and geomechanics simulations can model such systems, but they are computationally expensive. This is due to the nonlinear nature of governing equations, and the complex domain over which geomechanical problem must be solved. Moreover, computational demands can be excessive in applications such as optimization and uncertainty quantification, where hundreds or thousands of simulation runs might be required.

In general, finite element methods (FEM) is used for the mechanics part of the solution, whereas finite difference (FD) methods are used for the flow part. On field-scale problems, 70 to 80% of the run time is spent in the geomechanics model solving the system of linear equations. The compute-intensive nature of this model is a function of several items. First, the finite element formulation of the geomechanics model has a 27-point stencil compared to the standard seven-point stencil in the reservoir-simulation model [***Figure 3***]. Another factor is the number of unknowns in the geomechanics model, which is three at each node compared to one at each cell in an IMPES finite-difference simulation model [Aziz, K., & Settari, A., 2002]. In addition, the total number of gridblocks used in the geomechanics model, is larger because of the overburden, underburden, and side-burden regions that are simulated in this model in addition to the reservoir gridblocks [Thomas L.K. et al. 2002]. Moreover, computational demands can be excessive in applications such as optimization and uncertainty quantification, where hundreds or thousands of simulation runs might be required [Alpak F.O. 2019].
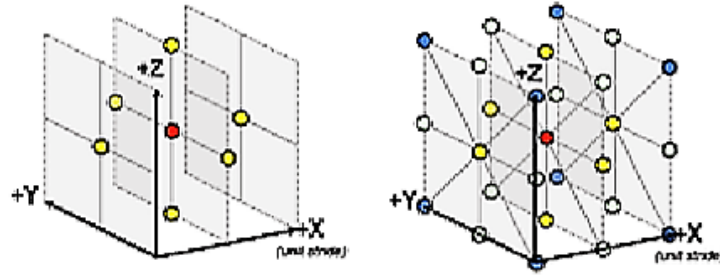
Figure 3: (a) Seven-point stencil shown as three adjacent planes (b) twenty seven-point stencil shown as three adjacent planes [Reprinted from Bui et al., 2020].

Traditionally, the reservoir simulation community has emphasized flow modeling and oversimplified the mechanical response of the formation through the use of the rock compressibility, taken as a constant coefficient or a simple function of porosity [Hyun C. Yoon et al., 2019; Ertekin et al. 2001]. However, with the recent development in computational techniques, a number of efficient schemes for the simulation of coupled flow and geomechanics problems have been presented [Jihoon Kim et al., 2015; Alpak F.O., 2019; Yoon HC et al., 2019].

The coupled process between mechanics and flow in porous media is described through "***poroelasticity***". Its theoretical basis goes back to the mid-1920s when Terzaghi described analytically the one-dimensional consolidation of a soil column under a constant load [Terzaghi, 1923, 1943]. Biot [Biot, 1941] developed the first three-dimensional coupled poroelastic system to describe the dynamics of porous media with the coupling between the fluid flow and the stress. This pioneering work is a basic isothermal theory with saturated single phase flow inside solid matrix, which is based on a linear stress-strain constitutive relationship and a linear form of Darcy's flow law. An important reformulation of Biot's theory was done by Rice and Cleary [Rice and Cleary, 1976]. They formulated the equations by using material coefficients which are more concise and easier to use in practical applications [Liu, 2004]. Other more sophisticated approaches have been recently proposed, e.g. [Coussy, 2004], however, Biot's theory still remains the most popular approach used in geomechanics.

Lewis and Schrefler [Lewis and Schrefler, 1998] presented and applied finite element methods (FEM) to one- and two-dimensional problems in consolidation and to the problem of subsidence in Venice. Other numerical works have been conducted at the Center for Subsurface Modeling, at

5

the University of Texas at Austin. There, Liu [Liu, 2004] implemented a scheme involving Taylor–Hood elements and, subsequently, a Discontinuous Garlekin (DG) variant based on the work of Phillips and Wheeler [Phillips and Wheeler, 2007]. Gai [Gai, 2004] used continuous elements for displacements and a cell-centered finite difference method for pressure and implemented an iteratively coupled scheme to find the numerical solution. She also studied the multiphase flow version of the poroelasticity equations. Phillips and Wheeler [Phillips and Wheeler, 2007] presented the theoretical convergence of two-dimensional models that couple both continuous and discontinuous Galerkin elements for the displacements with mixed spaces for the fluid flow. In addition, [Girault et al., 2009] presented a domain decomposition method for solving linear elasticity. Their algorithm uses mortar spaces as displacement boundary conditions and was designed to eliminate rigid body motions. Information is transferred by jumps, and mortars are introduced at the interfaces to dissociate the computation between neighboring subdomains [Girault et al., 2009].

One of the first applications of the Continuous Galerkin Finite Element Method (CG-FEM) was published in 1969 by Sanhu and Wilson [Sandhu and Wilson, 1969]. They applied a Finite Element Method (FEM) formulation to three-dimensional soil consolidation problems which was later revisited by Yokoo [Muller et al., 2009; Santarelli et al., 1992]. Fluid's compressibility was considered by Ghaboussi and Wilson [Belayneh, 2004]. They briefly commented on the stability of Continuous Galerkin (CG) schemes as well [Kim et al., 2009]. Zienkiewicz et al. [Zienkiewicz et al., 1977] introduced the compressibility of the solid grains. The stability analysis in time was performed by Booker and Small [Booker and Small, 1987].

Zienkiewicz and Shiomi [Zienkiewicz and Shiomi, 1984] discussed various CG formulations for soil consolidation problems. Mixed finite elements [Phillips, 2005; Phillips and Wheeler, 2007], reduced integrations [Souza-Neto et al., 2008] and penalty methods [Wheeler, 1978], which were studied and used for dealing with incompressible elasticity problems, were proposed for consolidation problems with incompressible fluid models. Multiple CG applications have been applied to various practical poromechanics problems. In particular, applications in the area of petroleum engineering can be found in [Chin et al., 2000; Dean et al., 2006; Settari and Walters, 2001; Shao, 1997].

Domain decomposition methods (DDM) are very efficient algorithms to compute the solution of large scale problems on parallel computers. These methods mainly consist of splitting the global domain into several subdomains and to compute the solution on the global domain through the resolution of the problem associated with each subdomain [Maday and Magoules, 2006]. The theory for DDM can be found elsewhere [Quarteroni and Valli, 1999; Toselli and Widlund, 2004]. However, for porous media problems, a DDM with optimal scalability has yet to be found [Ferronato et al., 2008; Girault et al., 2009; Turska and Schrefler, 1993; Turska et al., 1994].

The interactions between flow and geomechanics have been modeled using various coupling schemes [Prevost, 1997; Settari and Mourits, 1998; Settari and Walters, 2001; Mainguy and Longuemare, 2002; Minkoff et al., 2003; Thomas et al., 2003; Tran et al., 2004, 2005; Dean et al., 2006; Jha and Juanes, 2007]. Coupling methods are typically classified into *four* types: fully coupled, iteratively coupled, explicitly coupled, and loosely coupled [Settari and Walters, 2001; Dean et al., 2006].

For the fully coupled solution schemes, the coupled governing equations of flow and geomechanics are solved simultaneously at every time step. On the contrary, for iteratively coupled (or sequential) solution schemes, either the flow, or mechanical, problem is solved first, and then the other problem is solved using the intermediate solution information. Similar to sequential solution schemes, staggered solution schemes offer to solve the governing equations of flow and geomechanics in a sequential manner. However, the staggered methods implement only one iteration at each time step. That is why staggered methods are also known as single-pass sequential methods. Finally, regarding loosely coupled solution schemes, the coupling between the two problems is resolved only after a certain number of flow time steps.

Given the enormous investment in software development and the high computational cost of fully coupled flow–mechanics simulation, sequential solution methods seem to be a more preferable solution option as compared to the fully coupled approach. Sequential, or staggered, solution schemes offer wide flexibility and are highly desirable from a software engineering perspective. Moreover, sequential schemes allow for using specialized numerical methods for each of the mechanics and flow problems [Felippa and Park, 1980].

However, the pertinent computational time and cost of the coupling flow/geomechanics simulations are much higher in comparison to conventional reservoir flow simulation. This is

7

owing to the dramatic increase in the scale of coupled simulation models, as well as, number of iterations taken with increasing geometric complexity and involvement of non-linearity in problem of interest. This motivates the implementation of model-order reduction (MOR) techniques together with coupling solution schemes. MOR techniques have proven to handle those effects (i.e. geometric complexity and non-linearity) efficiently through providing a much smaller, yet representative, reduced model (ROM) for the full-order model (FOM) in hand.

Model-order-reduction (MOR) techniques represent a broad family of computational techniques that have received significant attention in the last decade [Athanasios C.A., 2005; Benner P. et al., 2015]. MOR has been successfully applied for reservoir simulation (flow only) to alleviate the high computational cost [Cardoso M.A. et al., 2010; He J. et al. 2014; Ghommem M. et al., 2015; Jansen J.D. et al., 2017; Tan X. et al. 2019] but, its application to coupled multiphysics, as in the problem herein, has been minimal [Florez H. 2017; Florez H. et al., 2018; Jin Z.L. et al., 2019]. MOR, in this setting, has been developed based on the so-called *snapshot-based* MOR, whereby the reduction is attained by projecting these snapshots in smaller subspaces, known as the proper orthogonal decomposition (POD) method [Cardoso M.A., 2010]. Generally, this involves two major steps: (a) an offline step (preprocessing) where training runs are performed - at least one run of the full order system is required - and relevant solution information is processed and saved; (b) an online step (run-time) where new test runs are performed based on a set of reduced states. This technique has been enhanced for nonlinear systems so that only a small set of nonlinear terms need to be computed. The reader can refer to published work of the Discrete Empirical Interpolation (DEIM) or the POD-DEIM [Ghommom M. et al., 2015; Tan X. et al., 2019] and the Trajectory-Piecewise-Linear (POD-TPWL) [Cardoso M.A. et al. 2010; He J. et al., 2014] frameworks. However, it is well known that POD heavily depends on the set of collected snapshots obtained in the offline step of the algorithm, and judicious selection of such snapshots is an important step in our framework. Several combinations of training and tuning are required to create a robust reduced model thereof.

As mentioned before, POD is a posteriori method and requires previous computation of the solution of the problem (snapshots) using the simulation of the full order model (original model) to build the reduced basis. Although it implementation is somewhat easy and it has been successfully implemented in the reservoir simulation community, its applicability to parametric

systems is dauting, given the optimal basis are as good as the input used to obtain the snapshots. If the boundary conditions or model parameters vary during the online phase to the model reduction implementation, the solution may not converge or be not be accurate. A different approach proposed in the partial differential community is the use of Proper Generalized Decomposition (PGD), which is a priori method, that is, it does not need any previous computation of the solution. The reduced order model (ROM) is directly built by means of the solution as a separation of variables in an iterative fashion. The reader may refer to [Cueto E. et al. 2014; Keunings R. et al., 2013]. There has been serval applications of PDG to thermodynamics and mechanics problems, especially in the field of linear elastic solid mechanics [Garikapati H.Z. et al., 2013], and recently for fracture mechanics problems [Oliver J. et al. 2017].

In this study, we propose a less laborious alternative to POD or PDG for computing the projection. To do so, we recall methods streaming from the structural mechanics community [Guyan R.J. 1965; Qu Z.Q., 2004; Gildin E. et al., 2009]. There exists a vast literature of model reduction for structural mechanical problems [Qu Z.Q., 2004] and in particular, for the structure persevering MOR for second-order systems whereby, the mass, stiffness and damping matrices are preserved as in the original form. This has not been the path taken in the area of geomechanics so far [Florez H., 2017; Florez H. et al., 2018; Florez H. et al., 2019; Jin Z.L. et al., 2019], and thus, to the author's best knowledge, the methodology proposed here is novel. The reader can find a helpful summary of recent MOR developments in geomechanics in the very same publications [Florez H., 2017; Florez H. et al., 2018; Florez H. et al., 2019; Jin Z.L. et al., 2019].

1.1. Thesis Objective

Owing to the high computational cost associate with simulating coupled flow and geomechanics, we propose here to reduce the computational cost by means of the application of practical model reduction frameworks to handle the mechanics part. To this end, this study aims at:

- Creation and advancement of an in-house simulation software that utilizes numerous computational techniques to capture and integrate mechanical responses of reservoir rocks with conventional flow simulations.
- Development of a rigorous reduced-order modeling (ROM) framework for scale reduction of complex simulation models using various condensation techniques, as well as, modal analysis.

- Modification of the developed workflow so it can be easily coupled with commercial simulation software without adjustment to their source code.

- Optimization of the developed workflow through testing the completeness, efficiency, and convergence for all the implemented reduction techniques.

- Adjustment of developed workflow to adapt to coupled flow/geomechancis systems.

1.2.   Thesis Outline

In chapter 2, we provide a review of some mathematical preliminaries that prove to be useful in the formulation of mathematical models for structured problems in general and geomechanical models in particular. Various numerical methods are presented including conventional variational methods, such as the Ritz, Galerkin, Collocation and least-squares methods, as well as finite element methods. In addition, key distinctions between various numerical techniques are presented to justify the use of the specific numerical techniques in the sequel.

In chapter 3, several – widely used – reduction techniques for structural mechanics were implemented based on the construction of the dynamic condensation matrix. Single-step reduction methods were first executed; in particular, Guyan DOFs-based reduction techniques [Guyan R.J., 1965; Qu Z.Q., 2004]. Following that, two-step methods were implemented; where corrections were made to the results obtained from the former [Qu Z.Q., 2004]. Finally, iterative (three-step) reduction methods were applied; handling the problem of master DOFs selection through consistent updates of the dynamic condensation matrix until convergence is achieved. To that end, two schemes are presented; based on the convergence of the dynamic condensation matrix, as well as, the eigenvalues of the reduced-order model [Friswell M.I. et al., 1994; Qu Z.Q. et al., 1998].

In the second part of chapter 2, we provide a rigorous framework for testing the completeness, efficiency, and convergence for all the presented reduction techniques [Allemang R.J. et al., 1982; Penny J.E.T. et al., 1994]. Regarding the completeness of the reduced models, two main criteria were investigated; namely, modal assurance criterion (MAC) and singular value decomposition (SVD). For efficiency testing, percent error (PE) of natural frequencies and the correlation coefficient for modal vector (CCFMV) values were considered. Finally, the efficiency of the convergent criterion was demonstrated through the errors associated with the column vectors of

the condensation matrix. Several numerical examples are presented to show the efficiency of the presented framework.

In chapter 4, we present a general framework for linear formulations of coupled flow and geomechanics, and we describe the constitutive relations consistent with Biot's theory [Biot, 1941]. The formulation integrates the approaches proposed by several researchers [Coussy, 1995; Lewis and Schrefler, 1998; Borja, 2006]. Numerical demonstration is presented to show the efficiency of the presented framework. Then, we extend the formulation to nonlinear formulation of coupled systems.

INTRODUCTION FOR MATHEMATICAL MODELING FOR GEOMECHANICS

Virtually every phenomenon in nature can be described in terms of algebraic, differential, and/or integral equations relating various quantities of interest. A case in point is hydraulic fracturing processes in oil and gas industry; where multistage fractures are created in unconventional reservoir. The set of equations that expresses the essential features of a physical system in terms of variables that describe the system are called mathematical models. Mathematical models of a process are developed using assumptions concerning how the process works and using appropriate axioms or laws governing the process, and they are often characterized by very complex differential and/or integral equations posed on geometrically complicated domains. While the derivation of the governing equations for most problems is not unduly difficult, their solution by exact methods of analysis is often difficult due to geometric and material complexities.
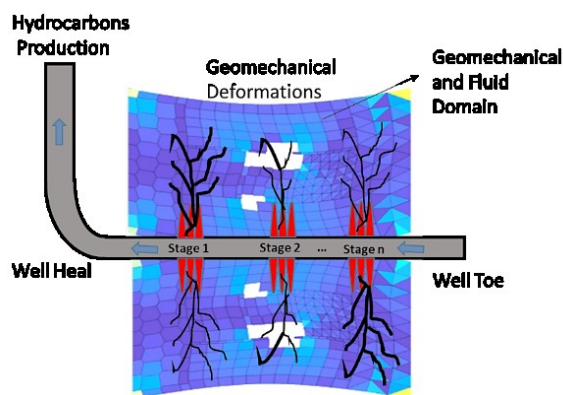
Figure 4: Geomechanical Effect in Hydraulic Fracture Process. Here the hydraulic fractures are represented by red color, wellbore trajectory represented by grey color and geomechanical deformations represented by blue color. Hydraulic fractures are created by the injection of a fluid at high pressure at particular positions of the wellbore. The black swarms represent possible fracture propagation in the geological media with different intensity as shown by the thickness of the ramifications. Multiple hydraulic fracture stages (3 in this case) are used to enhance reservoir production in unconventional reservoirs.

Historically, the processes were drastically simplified so that the governing equations can be solved analytically. Over the last few decades, however, computers have made it possible, with

the help of suitable mathematical models and numerical methods, to solve many practical problems of engineering. Numerical methods typically transform differential equations governing a continuum to a set of algebraic equations of a discrete model of the continuum that are to be solved using computers. There exist a number of numerical methods, many of which are developed to solve differential equations.

This chapter is devoted to review some of the mathematical preliminaries that prove to be useful in the sequel and to study integral formulations and more commonly used variational methods such as the Ritz, Galerkin, collocation, and least-squares methods. Since the finite element method can be viewed as an elementwise application of a variational method, it is useful to learn how variational methods work.

2.1. Mathematical Model for Geomechanics

The starting point for the discussion of the numerical methods is the differential equations governing the physical phenomena under study. We start our derivation with the model shown below. Here – on the left panel – we have a reservoir; represented by one layer (the middle green layer), surrounded by various stresses; in our case an overburden (the top red layer) and an underburden (the bottom blue layer). A further simplification of the case on the left can be done by studying the stresses on a little specimen (or mesh element) of that reservoir [as shown on the right panel].
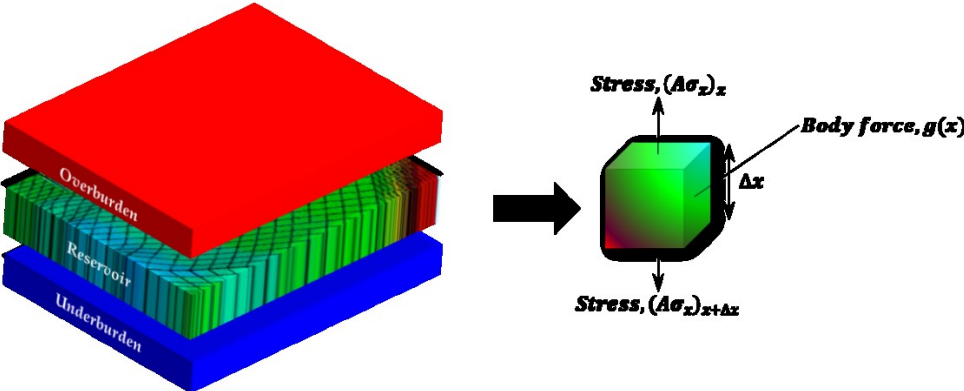
Figure 5: Geomechanical Model for Reservoir Simulation: (Left) A one-layer reservoir [represented in green color] surrounded by overburden stresses [top red layer] and underburden layer [bottom blue layer] (Right) A simplified representation of the reservoir model showing all acting forces at equilibrium.

Below we consider a simple example drawn from solid mechanics to illustrate how mathematical model of geomechanical problem is formulated. This example is concerned with the mathematical formulation of the axial deformation of a bar of variable cross section as shown below. The term bar is used in solid and structural mechanics to mean a structural element that carries *only* axial loads (tensile as well as compressive).
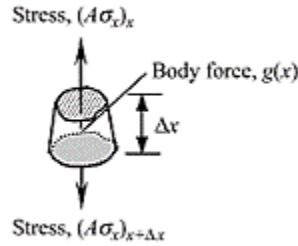
Figure 6: *An element of length Δx with axial forces acting at both ends of the element.*

For an *elastostatic* structural problem, it is assumed that masses are displaced so slowly that *no significant inertia forces* are generated. Application of Newton's second law in the x direction; where all applied forces on the elastic body sum to zero and the displacements are not a function of time, yields

$$-[A\sigma_x]_x + [A\sigma_x]_{x+\Delta x} + gA\Delta x = 0 \tag{2}$$

where g is the body force, σ_x denotes stress in the x direction, $[A\sigma_x]_x$ and $[A\sigma_x]_{x+\Delta x}$ are the net tensile force on the volume element at x and $x + \Delta x$, respectively.

Dividing throughout by Δx and taking the limit $\Delta x \to 0$, we obtain

$$\frac{d}{dx}A\sigma_x + Ag = 0 \tag{3}$$

which represents the equilibrium of forces in the x-direction.

Using *Hooke's law*, the stress σ_x can be related to the axial displacement

$$\sigma_x = E \cdot \varepsilon_x = E \cdot \frac{du}{dx} \tag{4}$$

where E is Young's modulus, u denotes the axial displacement, and ε_x is the axial strain.

Now using Eq. (4) in Eq. (3), we arrive at the equilibrium equation in terms of the displacement

$$\frac{d}{dx}\left(EA\frac{du}{dx}\right) + gA = 0 \tag{5}$$

Application of the finite element method [Reddy J., 2006] to the second-order differential equation [Eq. (5)], the equation of equilibrium can be written in variational form as

$$\mathbf{KX} = \mathbf{F} \tag{6}$$

where $\mathbf{K}$ is the stiffness matrix; which gives the relationship between the stresses and the strains (resulting deformations). $\mathbf{F}$ is the vector of applied forces (e.g. external stresses). $\mathbf{X}$ is the displacement (response) vector.

For an *elastodynamic* structural problem, the static equilibrium of applied forces is disturbed, and the material undergoes accelerations. Such accelerations generate *inertia forces* acting on all masses in the structure.

According to Newton's second law, when a body is acted on by a *nonzero* net force, the net force is equal to the *time rate of change of the body's linear momentum*.

$$\mathbf{F}_{inertia} = \frac{d}{dt}\left[\mathbf{M}\dot{\mathbf{X}}(t)\right] \tag{7}$$

where $\mathbf{M}$ is the mass matrix. $\dot{\mathbf{X}}(t)$ is the velocity vector. $\mathbf{F}_{inertia}$ is the *total external* applied force vector.

Using the chain rule, Eq. (7)can be defined as

$$\mathbf{F}_{inertia} = \dot{\mathbf{M}}\dot{\mathbf{X}}(t) + \mathbf{M}\ddot{\mathbf{X}}(t) \tag{8}$$

where $\dot{\mathbf{M}}$ is the time derivative of mass matrix. $\ddot{\mathbf{X}}(t)$ is the acceleration vector.
In many applications, the masses are *constant*, then Eq. (*8*) reduces to

$$\mathbf{F}_{inertia} = \mathbf{M}\ddot{\mathbf{X}}(t) \tag{9}$$

where $\mathbf{M}\ddot{\mathbf{X}}(t)$ is defined as the inertial force.

According to *D'Alembert's Principle* [Reddy J., 2006] which states that a system may be set in a state of dynamic equilibrium by adding to the external forces a fictitious force that is the inertial force, Eq. (*9*). Accordingly, the equation of dynamic equilibrium will take the form

$$\mathbf{K}\mathbf{X}(t) = \mathbf{F}(t) + \mathbf{F}_{inertia} \tag{10}$$

$$\mathbf{M}\ddot{\mathbf{X}}(t) + \mathbf{K}\mathbf{X}(t) = \mathbf{F}(t) \tag{11}$$

2.2. Weighted-Integral Statements

In almost all approximate methods used to determine the solution of differential and/or integral equations [Eq. (5)], we seek a solution in the form

$$U(X) = U_N(X) = \sum_{j=1}^{N} c_j \emptyset_j(X) \tag{12}$$

where U represents the solution of a particular differential equation and associated boundary conditions, and U_N is its approximation that is represented as a linear combination of unknown parameters c_j and known functions $\emptyset_j$ of position X in the domain Ω on which the problem is posed.

Consider the problem of solving the differential equation

$$-\frac{d}{dX}\left[a(X)\frac{du}{dx}\right] + c(X)u = f(X) \tag{13}$$

subjected to the boundary conditions

$$u(0) = u_0, \qquad \left[a(X)\frac{du}{dX}\right]_{X=L} = Q_0 \tag{14}$$

where $a(X)$, $c(X)$, and $f(X)$ are known functions, u_0 and Q_0 are known parameters, and $u(X)$ is the function to be determined.

We seek an approximate solution over the entire domain $\Omega = (0, L)$ in the form

$$U_N(X) = \sum_{j=1}^{N} c_j \emptyset_j(X) + \emptyset_0(X) \tag{15}$$

where the c_j are coefficients to be determined and $\emptyset_j(X)$ and $\emptyset_0(X)$ are functions chosen such that the specified boundary conditions of the problem are satisfied by the N-parameter approximate solution U_N.

2.3. Computational Methods

Ideally speaking, an effective computational method should have the following features:

a) It should have a *sound mathematical as well as physical basis* (i.e., yield convergent solutions and be applicable to practical problems).

b) It *should not have limitations* with regard to the geometry, the physical composition of the domain, or the nature of the "loading."

c) The formulative procedure should be *independent* of the shape of the domain and the specific form of the boundary conditions.

d) It should be *flexible* enough to allow different degrees of approximation without reformulating the entire problem.

e) It should involve a *systematic procedure* that can be automated for use on digital computers.

2.3.1. Classical Variational Methods

Our objective in this section is to study the variational methods of approximation as *they provide a background for the development of finite element models* [Reddy J., 2006]. The methods to be discussed include:

1. *The Rayleigh Ritz Method.*
2. *The weighted-residual Methods*
   a) *The Petrov-Galerkin Method.*
   b) *The Galerkin Method.*
   c) *The Least-squares Method.*
   d) *The Collocation Method.*

Various variational methods, e.g., the Ritz, Galerkin, collocation, and least-squares methods, differ from each other in *the choice of the integral form*, *weight functions*, and/or *approximation functions*.

The classical variational methods, which are truly meshless methods, are powerful methods that provide globally continuous solutions but suffer from the disadvantage that the approximation functions for problems with arbitrary domains are difficult to construct.

Table 1: *Solution scheme of differential equation using classical variational methods*

Step 1. The equation is put into an equivalent weighted-integral form.

Step 2. The approximate solution over the domain is assumed to be a linear combination $(\sum_j c_j \emptyset_j)$ of appropriately chosen approximation functions $\emptyset_j$ and undetermined coefficients c_j .

$$U(X) = U_N(X) = \sum_{j=1}^{N} c_j \emptyset_j(X) + \emptyset_0(X)$$

Step 3. The coefficients c_j are determined such that the residual error associated with the approximate solution to differential equations is minimized.

2.3.1.1. The Rayleigh Ritz Method

In the Ritz method, we seek an approximate solution

$$U_N(X) = \sum_{j=1}^{N} c_j \emptyset_j(X) + \emptyset_0(X) \tag{16}$$

to be the solution to the variational form (or the weak form) to the boundary-value problem (BVP)

$$B(w, u) = l(w) \tag{17}$$

where the constants c_j, called the *Ritz coefficients,* are determined such that Eq. (17) holds for each

$$w = \phi_i \ (i = 1,2, \dots, N) \tag{18}$$

Substituting Eq. (16) and Eq. (18) in Eq. (17) yields

$$B\left(\phi_i, \sum_{j=1}^{N} c_j \emptyset_j + \emptyset_0\right) = l(\phi_i) \tag{19}$$

Since $B(\cdot, \cdot)$ is linear in u, we have

$$\sum_{j=1}^{N} B(\phi_i, \emptyset_j) \cdot c_j = l(\phi_i) - B(\phi_i, \emptyset_0) \tag{20}$$

Or

$$\sum_{j=1}^{N} K_{ij} \cdot c_j = F_i \tag{21}$$

Where

$$K_{ij} = B(\phi_i, \emptyset_j) \tag{22}$$

$$F_i = l(\phi_i) - B(\phi_i, \emptyset_0) \tag{23}$$

2.3.1.2. The Method of the Weighted Residuals

The weighted-residual method is a *generalization* of the Ritz method in that the weight functions can be chosen from an independent set of functions, and it requires only the weighted-integral form to determine the parameters.

The method of weighted residuals can be described in its generality by considering the operator equation

$$\mathcal{A}(u) = f \tag{24}$$

where $\mathcal{A}$ is an operator (linear or nonlinear), often a differential operator, acting on the dependent variable u, and f is a known function of the independent variables.

Similar to the Ritz method, , the solution u is approximated by the expression

$$U_N(X) = \sum_{j=1}^{N} c_j \emptyset_j(X) + \emptyset_0(X) \tag{25}$$

Substitution of the approximate solution U_N into the left-hand side of Eq. (24) gives a function $\mathcal{A}(U_N)$ that, in general, is not equal to the specified function f. The difference $\mathcal{A}(U_N) - f$, called the *residual of the approximation*, is nonzero:

$$R = \mathcal{A}(U_N) - f = \mathcal{A}\left(\sum_{j=1}^{N} c_j \emptyset_j + \emptyset_0\right) - f \neq 0 \tag{26}$$

Note that the residual R is a function of position as well as of the parameters c_j.

In the weighted-residual method, as the name suggests, the parameters c_j are determined by requiring the residual R to vanish in the weighted-integral sense:

19

$$\int_{\Omega} \Psi_i(\boldsymbol{X}) \cdot R(\boldsymbol{X}, c_j) \, d\boldsymbol{X} = 0 \tag{27}$$

where Ω is a multi-dimensional domain and Ψ_i are *weight functions,* which, in general, are not the same as the approximation functions $\emptyset_j$. The set $\{\Psi_i\}$ must be a linearly independent set; otherwise, the equations will not be linearly independent and hence will not be solvable.

2.3.1.2.1. The Petrov-Galerkin Method

The weighted-residual method is referred to as the *Petrov–Galerkin method* when $\Psi_i \neq \emptyset_i$. Using linear operator $\mathcal{A}$, Eq. (27) can be simplified to the form

$$\sum_{j=1}^{N} [\Psi_i \cdot \mathcal{A}(\emptyset_j) d\boldsymbol{X}] \cdot c_j = \int_{\Omega} \Psi_i \cdot [f - \mathcal{A}(\emptyset_0)] \, d\boldsymbol{X} \tag{28}$$

$$\sum_{j=1}^{N} A_{ij} \cdot c_j = F_i \tag{29}$$

Where

$$\boldsymbol{A_{ij}} = \int_{\Omega} \Psi_i \cdot \mathcal{A}(\emptyset_j) \, d\boldsymbol{X} \neq \boldsymbol{A_{ji}} \tag{30}$$

$$\boldsymbol{F_i} = \int_{\Omega} \Psi_i \cdot [f - \mathcal{A}(\emptyset_0)] \, d\boldsymbol{X} \tag{31}$$

2.3.1.2.2. The Galerkin Method

If the weight function Ψ_i is chosen to be equal to the approximation function $\emptyset_j$, the weighted-residual method is better known as the Galerkin method. The algebraic equations of the Galerkin approximation are

$$\boldsymbol{Ac} = \boldsymbol{F} \tag{32}$$

where

$$\boldsymbol{A_{ij}} = \int_{\Omega} \emptyset_i \cdot \mathcal{A}(\emptyset_j) \, d\boldsymbol{X} \neq \boldsymbol{A_{ji}} \tag{33}$$

$$F_i = \int_\Omega \emptyset_i \cdot [f - \mathcal{A}(\emptyset_0)] \, dX \tag{34}$$

Once again, the coefficient matrix $[A]$ is not symmetric.

In general, the Galerkin method is *not the same as* the Ritz method. This should be clear from the fact that the former uses the weighted-integral form whereas the latter uses the weak (or variational) form to determine the coefficients c_j. Consequently, the approximation functions used in the Galerkin method are required to be of higher order than those in the Ritz method.

If the equation permits, differentiation from the dependent variable(s) can be transferred to the weight function $w = \emptyset_j$, thereby obtaining the weak form. Then there is *no difference* between the Galerkin method and the Ritz method. Thus, Ritz and Galerkin methods yield the same solutions in two cases: **(a)** when the specified boundary conditions of the problem are all of the essential type, and therefore the requirements on $\emptyset_j$ in the two methods become the same and the weighted-integral form reduces to the weak form; and **(b)** when the approximation functions of the Galerkin method are used in the Ritz method.

2.3.1.2.3. The Least-Squares Method

In least-squares method, we determine the parameters c_j by minimizing the integral of the square of the residual Eq.(26):

$$\frac{\partial}{\partial c_i} \int_\Omega R^2(X, c_j) \, dX = 0 \tag{35}$$

or

$$\int_\Omega \frac{\partial R}{\partial c_i} \cdot R \, dX = 0 \tag{36}$$

Comparison of Eq. (35) with Eq. (27) shows that $\Psi_i = \partial R / \partial c_i$. If $\mathcal{A}$ is a linear operator, $\Psi_i = \mathcal{A}(\emptyset_j)$, and Eq. (35) becomes

$$\sum_{j=1}^{N} \left[\mathcal{A}(\Psi_i) \cdot \mathcal{A}(\emptyset_j) dX \right] \cdot c_j = \int_{\Omega} \mathcal{A}(\Psi_i) \cdot [f - \mathcal{A}(\emptyset_0)] \, dX \tag{37}$$

$$Ac = F \tag{38}$$

Where

$$A_{ij} = \int_{\Omega} \Psi_i \cdot \mathcal{A}(\emptyset_j) \, dX \neq A_{ji} \tag{39}$$

$$F_i = \int_{\Omega} \Psi_i \cdot [f - \mathcal{A}(\emptyset_0)] \, dX \tag{40}$$

Note that the coefficient matrix A_{ij} is *symmetric*, but it involves the same order of differentiation as in the governing differential equation $A(u) - f = 0$.

2.3.1.2.4. The Collocation Method

In the collocation method, we seek an approximate solution U_N to Eq. (24) in the form of Eq. (25) by requiring the residual to vanish identically at N selected points within the domain Ω.

$$R(X, c_j) = 0 \tag{41}$$

The selection of the points is *crucial* in obtaining a well-conditioned system of equations and ultimately in obtaining an accurate solution. The collocation method can be shown to be a special case of Eq. (26) with $\psi_i = \delta(X)$, where $\delta(X)$ is the Dirac delta function, which is defined by

$$\int_{\Omega} f(X) \cdot \delta(X - \xi) \, dX = f(\xi) \tag{42}$$

With this choice of weight functions, the weighted-residual statement Eq. (5) becomes

$$\int_{\Omega} \delta(X) \cdot R(X, c_j) \, dX = 0 \tag{43}$$

The key distinctions between Rayleigh Ritz Method and Methods of Weighted Residuals are summarized below in **Table 2**.

Table 2: *Comparison between Ritz method and weighted-residual methods*

Rayleigh Ritz Method	Weighted-Residual Methods
▪ The Ritz method uses *the weak form* to determine the parameters c_i.	▪ The weighted-residual methods use the *weighted-integral form* to determine the parameters c_j.
▪ The approximation solution, U_N, must *satisfy the reduced differentiability* requirements associated with the weak form of the boundary-value problem (BVP).	▪ The approximation solution, U_N, must be *differentiable in accordance with the operator equation*: $\mathcal{A}(u) = f$.
▪ The approximation functions, $\emptyset_j$, must satisfy the homogenous form of the *essential boundary conditions* (EBCs).	▪ The approximation functions, $\emptyset_j$, must satisfy the homogenous form of *all boundary conditions*; *essential* (EBCs) and *natural* (NBCs).
▪ The approximation functions, $\emptyset_0$, must satisfy the *essential boundary conditions* (EBCs).	▪ The approximation functions, $\emptyset_j$, must satisfy *all boundary conditions*; *essential* (EBCs) and *natural* (NBCs).
▪ The order of the polynomial expressions used for the Ritz method is *lower*.	▪ The order of the polynomial expressions used for the weighted-residual method is *higher*.

2.3.2. The Finite Element Method

The finite element method is a numerical method like the finite difference method but is more general and powerful in its application to real-world problems that involve complicated physics, geometry, and/or boundary conditions.

In the finite element method, a *given domain is viewed as a collection of subdomains, and over each subdomain the governing equation is approximated by any of the traditional variational methods*. The main reason behind seeking approximate solution on a collection of subdomains is the fact that it is easier to represent a complicated function as a collection of simple polynomials, as can be seen from *Figure 7*. Each individual segment of the solution should fit with its neighbors

in the sense that the function and possibly derivatives up to a chosen order are continuous at the connecting points.

$$u_h(x) = \sum_{e=1}^{N=6} u_h^e(x)$$
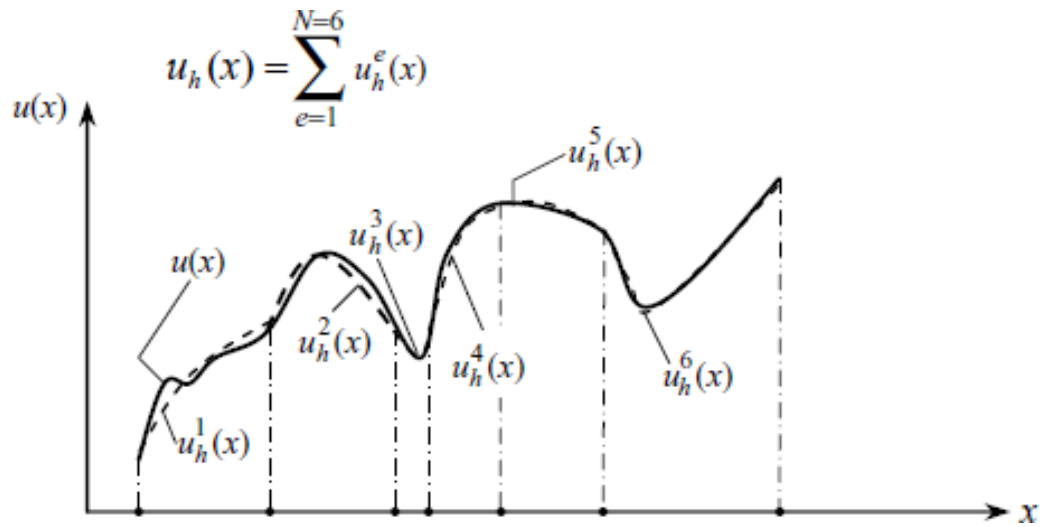
Figure 7: *Piecewise approximation of an arbitrary function [Reprinted from Reddy J., 2006]*

2.3.2.1. The fundamental steps of the finite element method

Table 3: *Steps involved in finite element analysis (FEA) of a typical problem*

Step 1. **Discretization of the given domain into a collection of preselected finite elements**.

- Construct the finite element mesh of preselected elements.
- Number the nodes and the elements.
- Generate the geometric properties (e.g., coordinates and cross-sectional areas) needed for the problem.

Step 2. **Derivation of element equations for all typical elements in the mesh**.

- Construct the variational formulation of the given differential equation over the typical element.
- Assume that a typical dependent variable u is of the form

$$u = \sum_{i=1}^{n} u_i \Psi_i$$

and substitute it into Step 2a to obtain element equations in the form

$$[K^e]\{u^e\} = \{F^e\}$$

- Select, if already available in the literature, or derive element interpolation functions Ψ_i and compute the element matrices.

Step 3. **Assembly of element equations to obtain the equations of the whole problem**.

- Identify the interelement continuity conditions among the primary variables (relationship between the local degrees of freedom and the global degrees of freedom—connectivity of elements) by relating element nodes to global nodes.
- Identify the "equilibrium" conditions among the secondary variables (relationship between the local source or force components and the globally specified source components).
- Assemble element equations using Steps 3a and 3b.

Step 4. **Imposition of the boundary conditions of the problem**.

- Identify the specified global primary degrees of freedom.

- Identify the specified global secondary degrees of freedom (if not already done in Step 3b).

Step 5. **Solution of the assembled equations**.

Step 6. **Postprocessing of the results**.

- Compute the gradient of the solution or other desired quantities from the primary degrees of freedom computed in Step 5.
- Represent the results in tabular and/or graphical form.

.

In the preceding sections, a brief *breakdown* of the major steps involved in the finite element analysis is presented.

2.3.2.2.1. Discretization of the Domain

Here, the domain is represented as a collection of a finite number of subdomains. Each subdomain is called an element. The collection of elements is called the finite element mesh. The elements are connected to each other at points called nodes.

The *reason* for dividing a domain into a set of subdomains is two-fold:

a) Domains of most *systems are a composite of geometrically and/or materially different parts*, and the solution on these subdomains is represented by different functions that are continuous at the interfaces of these subdomains. Therefore, it is appropriate to seek approximation of the solution over each subdomain.

b) *Approximation of the solution over each element of the mesh is simpler than its approximation over the entire domain*. Approximation of the geometry of the domain in the present case is not a concern, since it is a straight line. We must, however, seek a suitable approximation of the solution over each subdomain (i.e., finite element).

The number of elements into which the total domain is divided in a problem depends mainly on:

a) The geometry of the domain
b) The desired accuracy of the solution.

In a given problem, the exact solution is not known a priori. Hence, we begin with a number of elements that are considered to be reasonable. Most often, the analyst has knowledge of the qualitative behavior of the solution, and this helps to choose a starting mesh.

Whenever a problem is solved by the finite element method for the first time, it is required to investigate the convergence of the finite element solution by gradually refining the mesh (i.e., increasing the number of elements) and comparing the solution with those obtained by higher-order elements. The order of an element refers to the degree of polynomial used to represent the solution over the element. This is made clearer in the sequel.

2.3.2.2.2. *Derivation of Element Equations*

We develop the algebraic equations among the unknown parameters, much the same way as we did in the classical variational methods. The main difference is that we work with a finite element as opposed to the total domain. This step results in a matrix equation of the form

$$[K^e]\{c^e\} = \{F^e\}$$

which is called *the finite element model* of the original equation. Since the element is physically connected to its neighbors, the resulting algebraic equations will contain more unknowns than the number of algebraic equations. Then it becomes necessary to put the elements together to eliminate the extra unknowns.

The derivation of finite element equations, i.e., algebraic equations among the unknown parameters of the finite element approximation, involves the following *three* steps:

Step 1.   Construct the weighted-residual or weak form of the differential equation.

Step 2.   Assume the form of the approximate solution over a typical finite element.

Step 3.   Derive the finite element equations by substituting the approximate solution into the weighted-residual or weak form.

A typical element is isolated from the mesh. Then, we seek an approximate solution to the governing differential equation over the element. In principle, any method that allows the derivation of necessary algebraic relations among the nodal values of the dependent variable can be used.

2.3.2.2.3. Connectivity of Elements

In deriving the element equations, we isolated a typical element from the mesh and formulated the variational problem (or weak form) and developed its finite element model. The finite element model of a typical element contains n equations among $2n$ unknowns. Hence, they cannot be solved without using the equations from other elements to get rid of extra unknowns.

To obtain the finite element equations of the total problem, we must put the elements back into their original positions. In putting the elements with their nodal degrees of freedom back into their original positions, we must require that the solution is uniquely defined, and their source terms are "balanced" at the points where elements are connected to each other. Of course, if the primary variable is not continuous, we do not impose its continuity, the primary variables are assumed to be continuous. The continuity of the primary variables refers to the single-valued nature of the solution; balance of secondary variables refers to the equilibrium of point sources. Thus, the assembly of elements is carried out by imposing those two conditions.

2.3.2.2.4. Imposition of Boundary Conditions

Each problem differs from the other in the specification of the data and boundary conditions on the primary and secondary variables. Generally, the boundary conditions of a problem (i.e. The known primary degrees of freedom and the known secondary degrees of freedom) are imposed on the assembled set of finite element (algebraic) equations.

2.3.2.2.5. Solution of Equations

As a standard procedure in finite element analysis, the unknown primary degrees of freedom are determined first by *considering the algebraic equations corresponding to the unknown primary variables*. Then, the unknown secondary variables are determined by considering the remaining equations; those that contain the unknown secondary variables.

2.3.2.2.6. Postcomputation of the Solution

The solution of the finite element equations gives the nodal values of the primary unknowns. Once the nodal values of the primary variables are known, we can use the finite element approximation to compute the desired quantities. The process of computing desired quantities in

numerical form or graphical form from the known finite element solution is termed *postcomputation* or *postprocessing;* these phrases are meant to indicate that further computations are made after obtaining the solution of the finite element equations for the nodal values of the primary variables.

2.3.3. Comparison between Computational Methods

In the preceding sections, various computational methods used for solving differential and/or integral equations of mechanical systems were introduced and a brief analysis of their key components was presented. In this section, a comprehensive comparison between the different computational methods and their major differences are presented in **Table 4**. Based on the provided analysis, it has been decided to implement finite element methods (FEM) in the sequel study for two reason: (1) their ability to handle the complexity of any system (e.g. nonlinearity and large scale) and (2) their consistency in deriving the solution of any system unlike the conventional variational methods.

Table 4: Key distinctions between classical variational methods and finite element method

Classical Variational Methods	Finite Element Method
▪ The construction of the approximation functions is arbitrary, moreover, is difficult when the given domain is geometrically complex.	▪ The construction of the approximation functions is accomplished through a systematic scheme, that qualifies the FEM to be computationally competitive.
▪ The solution u is represented as a linear combination $(u_h = \sum c_j \emptyset_j)$ in terms of arbitrary parameters c_j.	▪ The solution u is represented as a linear combination $(u_h = \sum c_j \emptyset_j)$ in terms of the values u_j of u_h (and possibly its derivatives as well) at the nodal points.
▪ They are meshless methods.	▪ It includes the use of meshes.
▪ They cease to be effective when the geometry of the problem is far more complex.	▪ It Allows accurate representation of complex geometry and inclusion of dissimilar material properties.
▪ Due to the fact that classical variational methods are meshless, they are powerful	▪ Due to the subdivision of the whole domain, it has the ability of capturing

Classical Variational Methods	Finite Element Method
for capturing the global effects. Yet, they are hard to capture high gradient local effects.	local effects (e.g., large gradients of solution), thus, enabling easy representation of the solution.

2.4. The Sources of Error

Although finite element methods (FEM) are more robust than conventional variational methods in different aspects, yet there are a variety of errors introduced during the process of implementing the FEM to any system that increase the complexity of their application. Accordingly, a huge attention must be paid in order to successfully implement these methods. The following is a listing of the major error sources introduced:

2.4.1. Errors due to the Approximation of the Domain

The division of the whole domain into finite elements *may not be exact* (i.e., the assemblage of elements, Ω_h, does not match the original domain Ω), introducing error in the domain being modeled.

2.4.2. Errors due to the Approximation of the Solution

During the derivation of element equations, typically, the dependent unknowns (u) of the problem are approximated using the basic idea that any continuous function can be represented by a linear combination of known functions $\emptyset_i$ and undetermined coefficients c_i ($u \approx u_h = \sum c_i \emptyset_i$). Algebraic relations among the undetermined coefficients c_i are obtained by satisfying the governing equations, in a weighted-integral sense, over each element. *The approximation functions $\emptyset_i$ are often taken to be polynomials, and they are derived using concepts from interpolation theory*. Therefore, they are termed *interpolation functions*. Thus, approximation errors in the second stage are introduced both in representing the solution u as well as in evaluating the integrals.

2.4.3. Errors due to Mesh Size

Accuracy refers to the difference between the exact solution and the finite element solution, while convergence refers to the accuracy as the number of elements in the mesh is increased.

The *accuracy* and *convergence* of the finite element solution depends on:

- The differential equation that represents the problem
- The integral form of the differential equation.
- The finite elements being used.

Meshes that are of *irregularly shaped elements* or *don't have sufficient number of elements* in a region containing high gradients in the solution, both of which result in loss of accuracy or, in the case of nonlinear problems, nonconvergence of solutions.

2.4.4. Errors in Solving the Assembled System of Equations

Errors are introduced due to *numerical computation* (e.g., numerical integration and round-off errors in a computer). The estimation of these errors, in general, is not simple. However, under certain conditions, they can be estimated for an element and problem.

2.4.5. Errors due to Approximation in Time

For time-dependent problems, a two-stage formulation is usually followed. In the first stage, the differential equations are *approximated* by the finite element method to obtain a set of ordinary differential equations in time. In the second, the differential equations in time are solved exactly or *further approximated* by either variational methods or finite difference methods to obtain algebraic equations, which are then solved for the nodal values.

Obviously, some of the errors discussed above can be zero. When all the errors are zero, we obtain the exact solution of the problem (which is not the case in most problems).

Although great progress has been made on the theory and applications of the finite element method during the past several decades, yet more attention must be geared towards the accuracy, reliability and computational effort involved in finite element modeling (FEM). It is well known that the computational effort of finite element analysis is approximately proportional to the cubic of the size of a problem. The computational work , then, could be reduced drastically if the size of

the problem is reduced. Therefore, the development of efficient model reduction methods for creating accurate low-order dynamic models has recently become a major goal of simulation and modeling research.

Many techniques have been proposed to reduce the size of a large-sized model before a detailed analysis is performed. Some popular examples are component mode synthesis, dynamic condensation, dynamic substructure, and the Ritz vector approach. With the application of model reduction technique, the size of a full model may be reduced significantly. However, due to the truncated errors, the reduced model cannot retain all features of the full model. Even for the features within an interested frequency range, they may not be exactly kept in the reduced model resulting from most of the model reduction techniques. Therefore, there is a tradeoff between the size of the model and its accuracy. The crux of model reduction is to pursue a smallest model that contains the highest degree of information of the full model.

Dynamic condensation (proposed in 1965) is considered one of the most efficient methods for model reduction. In this technique, the total degrees of freedom are first divided into the master and slave degrees-of-freedom (DOFs). Then, the relationship, called dynamic condensation matrix, of the responses or mode shapes between these two sets of degrees of freedom is defined by dynamic condensation schemes. Using the dynamic condensation matrix, the system matrices of a full model can be condensed to the size spanned only by the master degrees of freedom. Also, the measured data from a modal test can be expanded to the size of the full finite element model.

Next chapter sets out to explain the principles and applications of dynamic condensation techniques. It covers all the potentially useful condensation methods including static condensation, exact condensation, and iterative dynamic condensation. The effects of the selection of master degrees of freedom on the accuracy and application of dynamic condensation technique are described in detail. The applications of these methods to the finite element analyses (FEA) are demonstrated through several examples.

CHAPTER III

MODEL-ORDER REDUCTION TECHNIQUES FOR STRUCTURAL PROBLEMS

The numerical simulation of the response of complex engineering systems usually requires the solution of large systems of simultaneous algebraic (and/or differential) equations, which may be computationally expensive, particularly for nonlinear and time-dependent (dynamic) problems.

Many techniques have been proposed to reduce the size of a large-sized model. Some popular examples are component mode synthesis, dynamic condensation, dynamic substructure, and the Ritz vector approach. The techniques for reducing the degrees of freedom have been referred to as reduced-basis techniques, reduction methods, and condensation methods.

Reduction methods can be applied to various linear and nonlinear boundary-value, initial-value, and eigenvalue problems, sensitivity analysis, reanalysis and design optimization problems; as well as to different nonstructural problems (e.g., heat transfer, fluid-structure interaction, etc.).

With the application of model reduction technique, the size of a full model may be reduced significantly. However, the reduced model cannot retain all features of the full model. Even for the features within an interested frequency range, they may not be exactly kept in the reduced model resulting from most of the model reduction techniques. Therefore, there is a tradeoff between the size of the model and its accuracy. The crux of model reduction is to pursue a smallest model that contains the highest degree of information of the full model.

This chapter is intended to summarize and assess some recent developments of reduction methods and their application to various mechanics problems. To fix ideas, the details of application of reduction methods to linear problems are described in the succeeding sections. Numerical results are presented which demonstrate the effectiveness of reduction methods. Also, a number of research areas which have high potential for application of reduction methods are identified.

3.1.   The Basic Idea of Reduction Techniques

The basic idea of model reduction methods is the condensation of a large system to a similar but much smaller substitute. In structural dynamic analyses [21], the dynamic equation of equilibrium

of the full-order model (FOM) can be expressed as a set of linear second-order differential equations:

$$\mathbf{M}\ddot{\mathbf{X}}(t) + \mathbf{C}\dot{\mathbf{X}}(t) + \mathbf{K}\mathbf{X}(t) = \mathbf{F}(t) \tag{44}$$

in which $\mathbf{M}$, $\mathbf{C}$, and $\mathbf{K} \in R^{n \times n}$ are the mass, damping, and stiffness matrices of the full order model; $\ddot{\mathbf{X}}(t)$, $\dot{\mathbf{X}}(t)$, and $\mathbf{X}(t) \in R^n$ are the acceleration, velocity, and displacement response vectors, respectively, of the full model under the external loads. The vector $\mathbf{X}$ is also referred to as the full order coordinates; $\mathbf{F}(t) \in R^n$ is the equivalent force vector acting on the model; n denotes the number of degrees of freedom of the full model.

Since the number n is generally very large for a practical structural problem, dynamic analyses, simulations, and design require very expensive computational efforts. Thus, model reduction technique is usually introduced to reduce the size of the full model and leads to a reduced order model.

The response of the large system, which was originally described in terms of a large number of degrees of freedom - components of a vector $\mathbf{X}$, is approximated by a linear combination of few preselected global approximation vectors (modes or basis vectors). The problem is then reformulated in terms of a few discrete variables - components of a vector $\mathbf{Z}$, which represent the amplitudes of the global approximation vectors. This is accomplished by using the following transformation (or mapping):

$$\mathbf{X}(t) = \mathbf{T}\,\mathbf{Z}(t) \tag{45}$$

where $\mathbf{T} \in R^{n \times m}$ is the coordinate transformation matrix, $\mathbf{Z} \in R^m$ is the reduced-order coordinates. Knowing that the dimension of the reduced system, m, is much less than the problem dimension (or, full dimension), n, assuming appropriate selection of transformation matrix, T.

Similarly, the derivatives of the response vector; velocity and acceleration.

$$\dot{\mathbf{X}}(t) = \mathbf{T}\,\dot{\mathbf{Z}}(t) \tag{46}$$

$$\ddot{\mathbf{X}}(t) = \mathbf{T}\,\ddot{\mathbf{Z}}(t) \tag{47}$$

Introducing Eqs. (45) to (47) into Eq. (44) and premultiplying both sides by the transpose of transformation matrix T leads to the equilibrium equation of the reduced-order model (ROM) as follows

$$\mathbf{M_R}\ddot{\mathbf{Z}}(t) + \mathbf{C_R}\dot{\mathbf{Z}}(t) + \mathbf{K_R}\mathbf{Z}(t) = \mathbf{F_R}(t) \tag{48}$$

in which M_R, C_R, and $K_R \in R^{m \times m}$ are the mass, damping, and stiffness matrices of the reduced order model; $\ddot{Z}(t)$, $\dot{Z}(t)$, and $Z(t) \in R^n$ are the acceleration, velocity, and displacement response vectors, respectively, of the reduced model under the external loads. $F_R(t) \in R^m$ is the equivalent force vector acting on the model.

The process of transforming the equilibrium equation of the full-order model (FOM) [Eq. (48)] into the equilibrium equation of the reduced-order model (ROM) [Eq. (44)] is sometimes called "*Condensation*" for reasons that will be explained in greater detail in the sequel. The resulting reduced-order model (ROM) should offer a good representation of the corresponding full-order model (FOM) and its solution (i.e. MOR solution) should be comparable to that of full-order model (FOM). The aforementioned conditions are achieved contingent good selection of transformation matrix, T.

3.2. Classification of Model Order Reduction Techniques

Dynamic condensation is considered one of the most efficient methods for model reduction. In this technique, the total degrees of freedom are first divided into the master and slave degrees of freedom. Then, the relationship, called dynamic condensation matrix, of the responses or mode shapes between these two sets of degrees of freedom is defined by dynamic condensation schemes. Using the dynamic condensation matrix, the system matrices of a full model can be condensed to the size spanned only by the master degrees of freedom.

Based on various criteria, the dynamic model order reduction techniques can be classified into four major categories. Each category may include several subcategories as follows:

3.2.1. Based on the Type of Coordinates Retained as the Reduced Order Coordinates

  a. Physical Coordinate Reduction.
  b. Generalized Coordinate Reduction.
  c. Hybrid Coordinate Reduction.

3.2.2. Based on the Construction of the Dynamic Condensation Matrix

    a. Single-Mode-Dependent Dynamic Condensation Matrix.

    b. Multimode-Dependent Dynamic Condensation Matrix.

    c. Response-Dependent Dynamic Condensation Matrix.

3.2.3. Based on the Information Required to Compute the Dynamic Condensation Matrix

    a. Physical-Type Dynamic Condensation.

    b. Modal-Type Dynamic Condensation.

    c. Hybrid Dynamic Condensation.

3.2.4. Based on the Schemes used for Dynamic Condensation

    a. Single-Step Dynamic Condensation.

    b. Two-Step Dynamic Condensation.

    c. Iterative Dynamic Condensation.

Basic definitions and key distinctions between the four major categories; as well as their subcategories are summarized in *Table 5* through *Table 8*.

Table 5: *Classification Based on the Type of Reduced Order Coordinates*

Physical	Generalized	Hybrid
Definition		
The coordinates of the reduced model belong to a subset of the physical coordinates of the full model.	The coordinates of the reduced model belong to a subset of the Modal coordinates of the full model.	The coordinates of the reduced model consist of some physical coordinates of the full model and part of the modal coordinates of the model.
Coordinate Transformation Matrix		
$$T = \begin{bmatrix} I \\ R \end{bmatrix}$$ where • I is an identity matrix of order m. • R is the dynamic condensation matrix.	$$X = \phi_m q_m$$ where • $\phi_m \in R^{n \times m}$ is the eigenvector matrix of the full model. • X is the physical space. • q_m is the modal space.	$$T_{CMS} = \begin{bmatrix} \phi_N & R_{Guyan} \\ 0 & I \end{bmatrix}$$ where • $\phi_m \in R^{n \times m}$ is the eigenvector matrix of the full model. • I is an identity matrix of order m. • R is the dynamic condensation matrix.

Table 6: _Classification Based on the Construction of the Dynamic Condensation Matrix_

Single-Mode-Dependent	Multi-Mode-Dependent	Response-Dependent
Definition		
It represents the relation of an eigenvector between the master and slave degrees of freedom.	It represents the relations of the multi-eigenvectors, $p,$ for example, between the master and slave degrees of freedom.	It represents the relations of responses between the master and slave degrees of freedom
Dynamic Condensation Matrix		
$$\boldsymbol{\phi_s} = \boldsymbol{R}\,\boldsymbol{\phi_m}$$ where $\boldsymbol{\phi_s}$ is the subvector of the eigenvector at the slave degrees of freedom. $\boldsymbol{\phi_m}$ is the subvector of the eigenvector at the master degrees of freedom.	$$\boldsymbol{\phi_{sp}} = \boldsymbol{R}\,\boldsymbol{\phi_{mp}}$$ where $\boldsymbol{\phi_{sp}}$ is the submatrix of the eigenvector matrix at the slave degrees of freedom. $\boldsymbol{\phi_m}$ is the submatrix of the eigenvector matrix at the master degrees of freedom.	$$\boldsymbol{X_s}(t) = \boldsymbol{R}\,\boldsymbol{X_m}(t)$$ where $\boldsymbol{X_s}(t)$ is the displacement vector at the slave degrees of freedom. $\boldsymbol{X_m}(s)$ is the displacement vector of the at the master degrees of freedom.

Table 7: *Classification Based on the types of information required to compute the dynamic condensation matrix*

Physical-Type	Modal-Type	Hybrid
Definition		
Only the system matrices, stiffness and mass matrices, for example, of the full model are included in the dynamic condensation matrix.	Only the mode shapes of the full model are included in the dynamic condensation matrix.	Both the physical parameters and the mode shapes of the full model are included in the dynamic condensation matrix.
Remarks		
• More computationally efficient than the other two. • The accuracy or convergent rate depends on what and how many degrees of freedom are selected as the master degrees of freedom.	• The reduced model preserves all the modes selected. • Because this reduction is exact, the selection of master degrees of freedom does not affect the accuracy of reduced model.	

Table 8: *Classification Based on the Schemes Used for Dynamic Condensation.*

Single-Step	Two-Step	Iterative
Definition		
The dynamic condensation matrix is explicitly defined by either the system matrices or the modal matrix or both of a full model.	The results computed from the single-step condensation methods are usually considered as an initial prediction. Then, correction will be made in the second step.	It is an extension of the two-step method. After the reduced model is obtained from the second step, it is used to estimate the dynamic condensation matrix in the next step. This process is repeated until the required accuracy is obtained
Key Distinctions		
• All the interested modes can be computed from the reduced model one by one. • The convergence of this technique strongly depends on the selection of the initial approximation and the approximation for the next mode. • The speed of convergence of the latter is generally faster.		▪ All the interested modes are computed from the reduced model simultaneously. ▪ The convergence of this technique is guaranteed. ▪ The speed of convergence of the latter is generally slower.

3.3.   Formulation of Dynamic Equations of Motion

This section lays the foundation for the exact condensation techniques and iterative condensation techniques [sections 3.4.2 and 3.4.3, respectively] by offering an alternative solution to the dynamic equations of motion [Eq. (44)] through transformation into frequency-based space (using Fourier Transform) instead of the original physical space.

We start with the general form of the dynamic equations of motion [Eq. (44)], that is defined as

$$\mathbf{M}\ddot{\mathbf{X}}(t) + \mathbf{C}\dot{\mathbf{X}}(t) + \mathbf{K}\mathbf{X}(t) = \mathbf{F}(t) \tag{49}$$

where $\ddot{\mathbf{X}}(t)$, $\dot{\mathbf{X}}(t)$ and $\mathbf{X}(t)$ are the acceleration response vector, velocity response vector, and displacement response vector, respectively. $\mathbf{M}$, $\mathbf{C}$ and $\mathbf{K}$ are the mass, damping, and stiffness matrices, respectively. $\mathbf{F}(t)$ is the vector of applied forces.

In the absence of damping and external forces, Eq. (49) reduces to

$$\mathbf{M}\ddot{\mathbf{X}}(t) + \mathbf{K}\mathbf{X}(t) = 0 \tag{50}$$

The motion of a dynamic structure may be represented by a set of simultaneous differential equations using some discretization scheme, such as the finite element method, if necessary. The *dynamic characteristics* (dynamic responses, strains, stresses, etc.) of the system can be obtained from these equations using the direct integration methods (finite difference method, Newmark method, for example) in the time domain. Alternatively, these coupled equations of motion may be solved by transforming them into a set of independent equations by a modal matrix.

 Generally, the solution of Eq. (50) has the form

$$\mathbf{X}(t) = \boldsymbol{\varphi} \sin(\omega t + \emptyset) \tag{51}$$

where $\boldsymbol{\varphi}$ is the vector of amplitudes, ω is the frequency of harmonic response, and $\emptyset$ is the phase angle. Differentiation of Eq. (51) twice with respect to time produces

$$\ddot{\mathbf{X}}(t) = -\omega^2 \boldsymbol{\varphi} \sin(\omega t + \emptyset) \tag{52}$$

Substituting Eqs. (51) and (52) into Eq. (50) and rearranging it results in

$$(\mathbf{K} - \omega^2 \mathbf{M})\boldsymbol{\varphi} = 0 \tag{53}$$

Now, the n simultaneous homogeneous differential equations are reduced to a set of n homogeneous algebraic equations. Eq. (53) has the form of an algebraic eigenvalue problem. It is usually simply termed as an eigenproblem.

Nontrivial solutions exist if the determinant of the coefficient matrix is equal to zero (as shown in **Figure 8**)

$$|\mathbf{K} - \omega^2 \mathbf{M}| = 0 \tag{54}$$
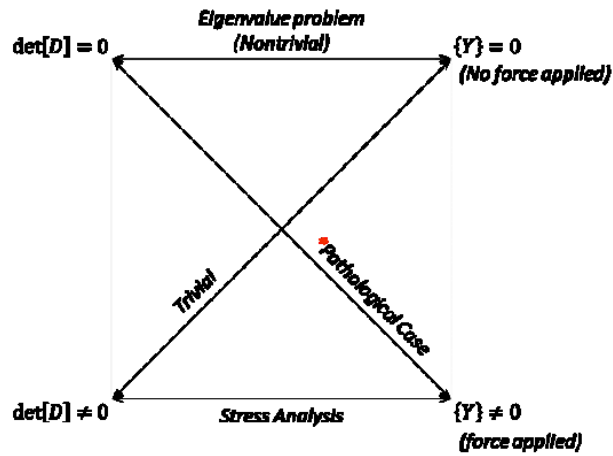
Figure 8: Comparison between different solutions to eigenproblem

The above equation leads to a polynomial of order n in ω^2 that has n distinct roots. These roots, denoted by $\lambda_1, \lambda_2, \lambda_3, \dots, \lambda_n$, and are called *eigenvalues*. Their square roots are called *natural frequencies*. Associated with each eigenvalue, ω_i^2, there is an n-dimensional vector, $\boldsymbol{\varphi}_i$ whose elements are real numbers.

The vector $\boldsymbol{\varphi}_i$ is known as eigenvector (also, modal vector, mode shape or natural mode) and can be obtained by using Eq. (53) as follows

$$(\mathbf{K} - \omega_i^2 \mathbf{M})\boldsymbol{\varphi}_i = 0 \tag{55}$$

For operational efficiency, an $n \times n$ *eigenvector matrix* or *normal modal matrix* is defined by placing all of the eigenvectors columnwise in this matrix with the form

$$\Phi = [\boldsymbol{\varphi_1} \quad \boldsymbol{\varphi_2} \quad \cdots \quad \boldsymbol{\varphi_n}] \tag{56}$$

Using this matrix, the compact form of the eigenproblem shown in Eq. (53) is given by

$$\mathbf{K}\Phi = \mathbf{M}\Phi\boldsymbol{\Lambda} \tag{57}$$

Where the eigenvalue matrix $\boldsymbol{\Lambda}$ is defined as

$$\boldsymbol{\Lambda} = \text{diag}(\lambda_1 \quad \lambda_2 \quad \cdots \quad \lambda_n) \tag{58}$$

It is an $n \times n$ diagonal matrix whose diagonal elements are the *eigenvalues* of the model.

The eigenvectors are *orthogonal* with respect to the mass matrix $\boldsymbol{M}$ and stiffness matrix $\boldsymbol{K}$. This orthogonality indicates that all the eigenvectors are *linearly independent*. The orthogonal conditions are given by

$$\Phi^{\mathbf{T}}\mathbf{M}\Phi = \mathbf{I} \tag{59}$$

$$\Phi^{\mathbf{T}}\mathbf{K}\Phi = \boldsymbol{\Lambda} \tag{60}$$

3.4. Dynamic Condensation Techniques

Based on the construction of the dynamic condensation matrix, the dynamic condensation techniques can be categorized as follows [see ***Figure 9***]:

3.4.1. Single-Step Dynamic Condensation

In the single-step method, the dynamic condensation matrix is *explicitly* defined by either the system matrices or the modal matrices or both of a full model, as well as, the corresponding reduced model. Guyan condensation and its variants are examples of single-step methods.

3.4.2. Two-Step Dynamic Condensation

In the two-step method, the results computed from the single-step methods are usually considered as an initial approximation. These values usually have relatively high errors. Correction will be made in the second step. Accordingly, the two-step method is also referred to as the *prediction-correction* method.

3.4.3. Iterative Dynamic Condensation

The iterative dynamic condensation is considered an extension of the two-step method. After the reduced model is obtained from the second step, it is used to estimate the dynamic condensation matrix in the following step. This process is repeated until the reduced model with required accuracy is obtained.
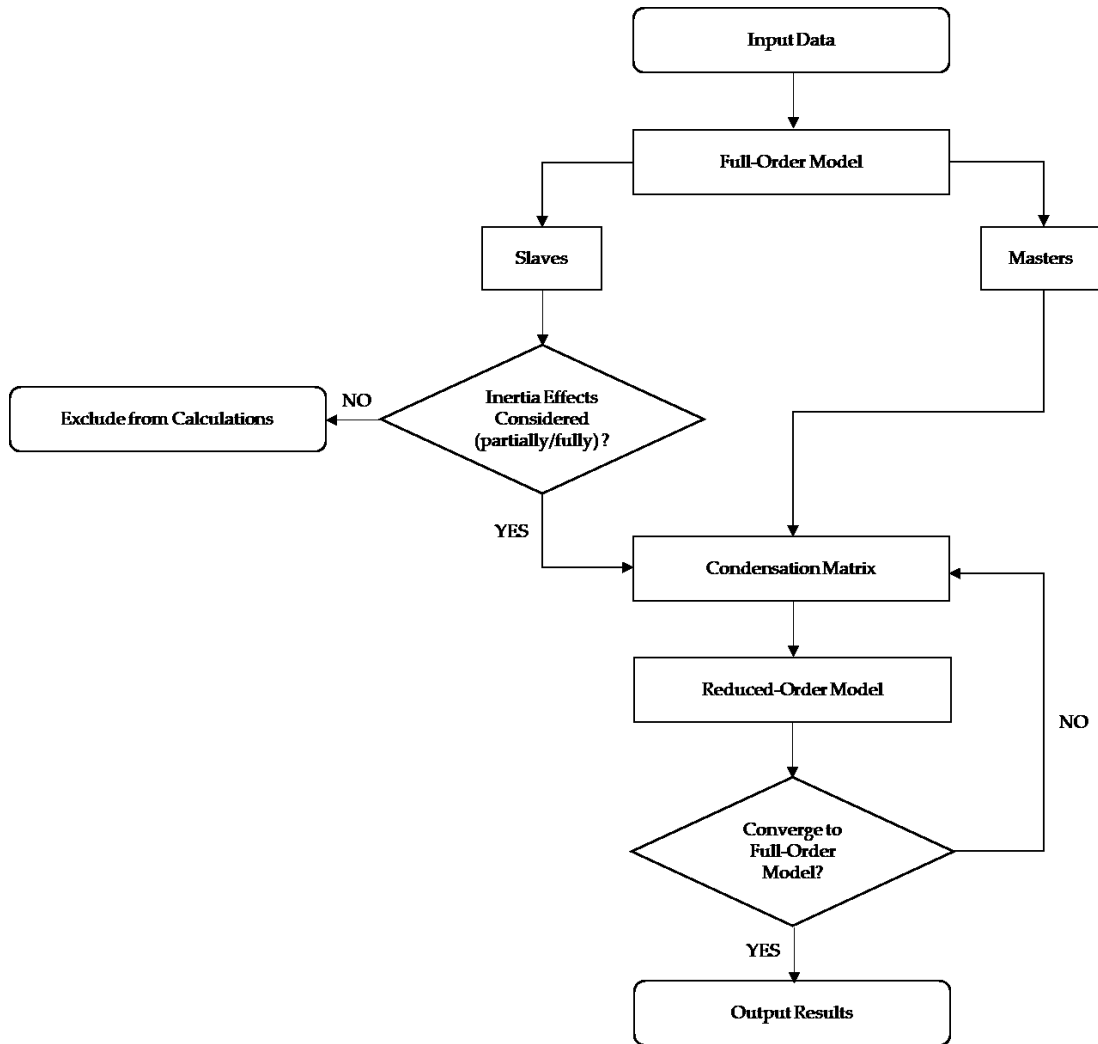
Figure 9: General Scheme for Dynamic Condensation Techniques

3.5.   Guyan Condensation

This technique was first proposed by Guyan and Irons (1965) and is considered as one of the most popular condensation techniques. This method is usually referred to as "*static*" condensation since the dynamic effect is ignored in the condensation.

3.5.1   Basic Idea of Guyan Condensation

Guyan condensation is considered as the initial approximation of exact dynamic condensation. Its valid frequency range is $[0, \omega_c)$. ω_c is called the cut frequency and is equal to the lowest frequency of the full model with all its master degrees of freedom grounded. This model is referred to as the slave model.

Because the frequencies of the full model will increase if some of its degrees of freedom are fixed, the frequencies in the lowest frequency range of the full model are usually smaller than the lowest frequency of the slave model, that is, the cut frequency. This is the reason why Guyan condensation is generally valid in the lowest frequency range of the full model and the corresponding results have reasonable accuracy within this range. The error in Guyan condensation depends upon the ratio of cut frequency to the interested frequency. The higher the ratio, the more accurate the reduced model.

Based on the fundamental features of Guyan condensation, its accuracy may be improved from the ways listed below besides the partial and full inclusion of inertia effects:

1. Optimal selection of master degrees of freedom. From the definition of a slave model, we know that different master degrees of freedom result in a different slave model with a different lowest frequency. Therefore, optimal selection of these degrees of freedom may increase the lowest frequency, that is, the cut frequency. As a result, the ratio will be increased.
2. Increase of the number of master degrees of freedom. The lowest frequency of the slave model may be increasing significantly by increasing the number of master degrees of freedom.

3.5.2 Formulation of Guyan Condensation for Static Problems

Considering the static equations of equilibrium, that is,

$$KX = F \qquad (61)$$

the total degrees of freedom of the full model are categorized as *master* degrees of freedom; retained in the reduced model and *slave* degrees of freedom; deleted from the model or condensed. Accordingly, the static Eq. (61) can be rewritten as

$$\begin{bmatrix} K_{mm} & K_{ms} \\ K_{sm} & K_{ss} \end{bmatrix} \begin{Bmatrix} X_m \\ X_s \end{Bmatrix} = \begin{Bmatrix} F_m \\ F_s \end{Bmatrix} \qquad (62)$$

where m and s indicate the master degrees of freedom and slave degrees of freedom, respectively.

The expansion of Eq. (62) leads to the following two equations:

$$K_{mm}X_m + K_{ms}X_s = F_m \qquad (63)$$

$$K_{sm}X_m + K_{ss}X_s = F_s \qquad (64)$$

X_s the displacement vector at the slaves can be expressed in terms of X_m the displacement vector at the masters as follows

$$X_s = -K_{ss}^{-1}K_{sm}X_m + K_{ss}^{-1}F_s \qquad (65)$$

Assuming $F_s = 0$ in Eq. (65) leads to

$$X_s = R_G X_m \qquad (66)$$

where R_G is called the static condensation matrix due to the ignorance of dynamic effects. This matrix relates the displacements between the masters and the slaves and is defined as

$$R_G = -K_{ss}^{-1}K_{sm} \qquad (67)$$

Substitution of Eq. (65) into Eq. (63) leads to

$$K_G X_m = F_G \qquad (68)$$

Where K_G and F_G are the reduced stiffness matrix and reduced force vector, respectively. They are defined as follows

$$K_G = K_{mm} - K_{ms}K_{ss}^{-1}K_{sm} \qquad (69)$$

$$F_G = F_m - K_{ms}K_{ss}^{-1}F_s \qquad (70)$$

3.5.3. Numerical Demonstration

In this section, we present the performance of the proposed scheme through one structural problem. For the finite element modeling, we use the well-known 4-node quadrilateral flat shell finite elements. A detailed description of the problem is presented in Abousleiman et el. (1996).

A two-dimensional reservoir [**Figure 10**] is considered with boundary conditioned as specified in **Table 9**. The specifications of our model are listed in **Table 10**. In the model, a uniform mesh of the size 20×10 is used, in which 231 nodes, 200 elements and 419 degrees-of-freedom are contained.
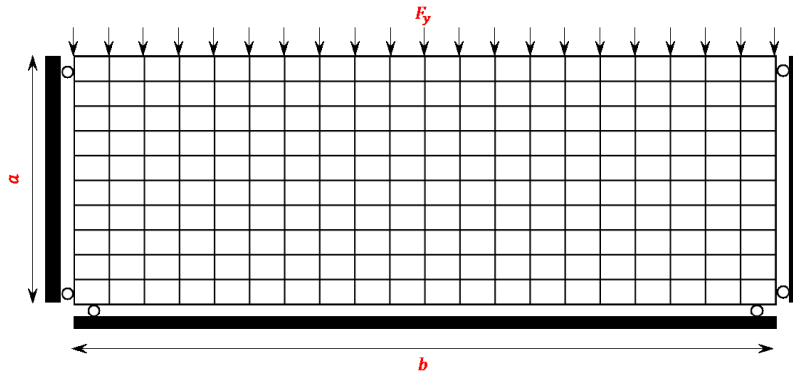
Figure 10: *Two-dimensional reservoir*

Table 9: *Boundary Conditions for Two-dimensional Reservoir*

1. Constant vertical stress on the top ($\sigma_y = F / a$; where $F = 1.00E08 \ N$ and $a = 100 \ m$).

2. No vertical displacement in the bottom (i.e. $u_y = 0$).

3. No horizontal displacement on the right side (i.e. $u_x = 0$).

4. No horizontal displacement on the left side (i.e. $u_x = 0$).

Table 10: *Data Input for Two-dimensional Reservoir*

Young's Modulus, E *	=	0.10	GPa
Poisson Ratio, v *	=	0.20	fraction
Stress, σ	=	1.00	MPa

* Only two elastic moduli are needed to describe fully material behavior of homogeneous, isotropic material

Two numerical cases are considered with different master degrees-of-freedom for the two-dimensional reservoir. Summary of the two models is listed in ***Table 11***. The master degrees-of-freedom are selected as shown in ***Figure 11***.
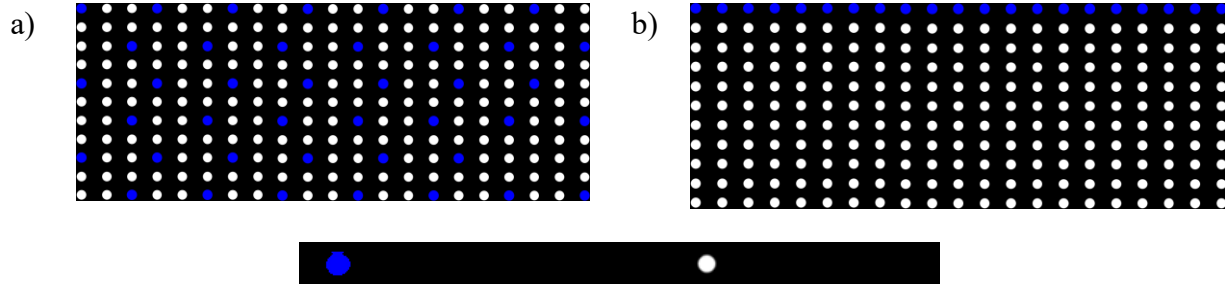
Figure 11: (a) *70 degrees-of-freedom selected for the reduced-model of the two-dimensional reservoir* ***(b)*** *40 degrees-of-freedom selected for the reduced-model of the two-dimensional reservoir.*

Table 11: *Summary of Four Cases for Two-Dimensional Reservoir*

Model	Number of Master DOFs	Number of Slave DOFs	Relative Size of Reduced-Order Model
A	70	347	17.1 %
B	40	379	9.55 %
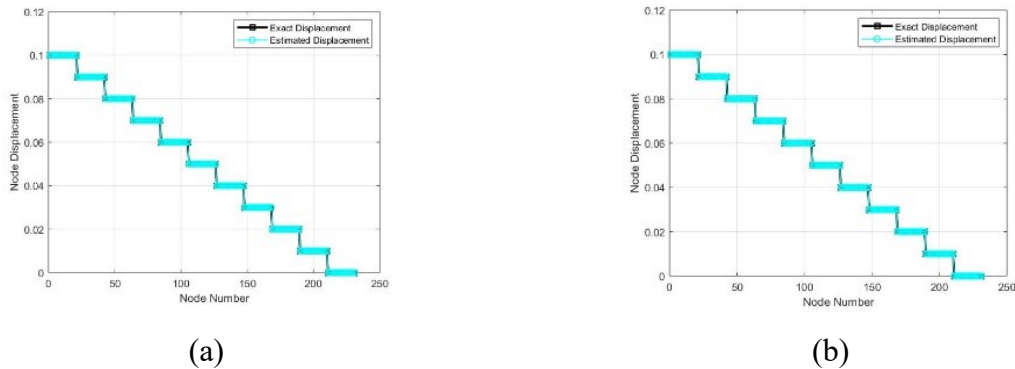
Figure 12: (a) *Exact* ***(Black)*** *and estimated* ***(Cyan)*** *node displacement for Static two-dimensional reservoir using Guyan Condensation with 70 master degrees-of-freedom* ***(b)*** *Exact and estimated node displacement for Static two-dimensional reservoir using Guyan Condensation with 40 master degrees-of-freedom.*

The exact and estimated node displacements are shown in *Figure 12*. As expected, Guyan condensation is *exact* for the static problem regardless of the choice of master degrees of freedom.

3.5.4. Formulation of Guyan Condensation for Dynamic Problems

Considering the dynamic equations of equilibrium without damping, that is,

$$\mathbf{M}\ddot{\mathbf{X}}(t) + \mathbf{K}\mathbf{X}(t) = \mathbf{F}(t) \tag{71}$$

where $\ddot{\boldsymbol{X}}(t)$ is the acceleration vector of the full model, and $\boldsymbol{M}$ is the mass matrix of the full-order model.. Similar to the static equations of equilibrium, Eq. (71) can be rewritten as

$$\begin{bmatrix} \mathbf{M}_{mm} & \mathbf{M}_{ms} \\ \mathbf{M}_{sm} & \mathbf{M}_{ss} \end{bmatrix} \begin{Bmatrix} \ddot{\mathbf{X}}_m \\ \ddot{\mathbf{X}}_s \end{Bmatrix} + \begin{bmatrix} \mathbf{K}_{mm} & \mathbf{K}_{ms} \\ \mathbf{K}_{sm} & \mathbf{K}_{ss} \end{bmatrix} \begin{Bmatrix} \mathbf{X}_m \\ \mathbf{X}_s \end{Bmatrix} = \begin{Bmatrix} \mathbf{F}_m \\ \mathbf{F}_s \end{Bmatrix} \tag{72}$$

where $\boldsymbol{m}$ and $\boldsymbol{s}$ indicate the master degrees of freedom and slave degrees of freedom, respectively.

The expansion of Eq. (72) leads to the following two equations:

$$\mathbf{M}_{mm}\ddot{\mathbf{X}}_m + \mathbf{M}_{ms}\ddot{\mathbf{X}}_s + \mathbf{K}_{mm}\mathbf{X}_m + \mathbf{K}_{ms}\mathbf{X}_s = \mathbf{F}_m \tag{73}$$

$$\mathbf{M}_{sm}\ddot{\mathbf{X}}_m + \mathbf{M}_{ss}\ddot{\mathbf{X}}_s + \mathbf{K}_{sm}\mathbf{X}_m + \mathbf{K}_{ss}\mathbf{X}_s = \mathbf{F}_s \tag{74}$$

Assuming $\boldsymbol{F}_s = \boldsymbol{0}$ in Eq. (74) and letting $\ddot{\boldsymbol{X}}_m = \ddot{\boldsymbol{X}}_s = \boldsymbol{0}$ leads to

$$\mathbf{X}_s = \mathbf{R}_G\mathbf{X}_m \tag{75}$$

Differentiating Eq. (75) twice with respect to time leads to

$$\ddot{\mathbf{X}}_s = \mathbf{R}_G\ddot{\mathbf{X}}_m \tag{76}$$

Substitution of Eqs. (75) and (76)into Eq. (73) leads to

$$\mathbf{M}_G\ddot{\mathbf{X}}_m + \mathbf{K}_G\mathbf{X}_m = \mathbf{F}_G \tag{77}$$

Where $\boldsymbol{M_G}$, $\boldsymbol{K_G}$ and $\boldsymbol{F_G}$ are the reduced mass matrix, stiffness matrix and reduced force vector, respectively. They are defined as follows

$$\mathbf{M}_R = \mathbf{M}_{mm} - \mathbf{K}_{ms}\mathbf{K}_{ss}^{-1}\mathbf{M}_{sm} - \mathbf{M}_{ms}\mathbf{K}_{ss}^{-1}\mathbf{K}_{sm} + \mathbf{K}_{ms}\mathbf{K}_{ss}^{-1}\mathbf{M}_{ss}\mathbf{K}_{ss}^{-1}\mathbf{K}_{sm} \tag{78}$$

$$\mathbf{K}_G = \mathbf{K}_{mm} - \mathbf{K}_{ms}\mathbf{K}_{ss}^{-1}\mathbf{K}_{sm} \tag{79}$$

$$\mathbf{F}_G = \mathbf{F}_m - \mathbf{K}_{ms}\mathbf{K}_{ss}^{-1}\mathbf{F}_s \tag{80}$$

Notice that the reduced system of equations for dynamic system [Eq. (78) through (80)] is similar – to some extent – and somehow a generalization to the reduced system of equations for the static system [Eqs. (69) and (70)]. The only difference is that the former [i.e. reduced system for dynamic problem] accounts for the inertia effects, unlike the latter [i.e. reduced system for static system].

3.5.5. Numerical Demonstration

In this section, we present the performance of the proposed scheme through one structural problem. For comparison reasons, we have adopted the same structural problem as in the static case [*Figure 10*] with same specifications as in *Table 9* and *Table 10*. The only difference that inertia effects were integrated in the calculations.

Two numerical cases are considered with different master degrees-of-freedom for the two-dimensional reservoir. Summary of the two models is listed in *Table 11*. The master degrees-of-freedom are selected as shown in *Figure 11*.

The exact and estimated node displacements are shown in *Figure 13*. It is clear that although Guyan Condensation is exact for static problems, its accuracy is *very low* for dynamic problems.

(a)   (b)
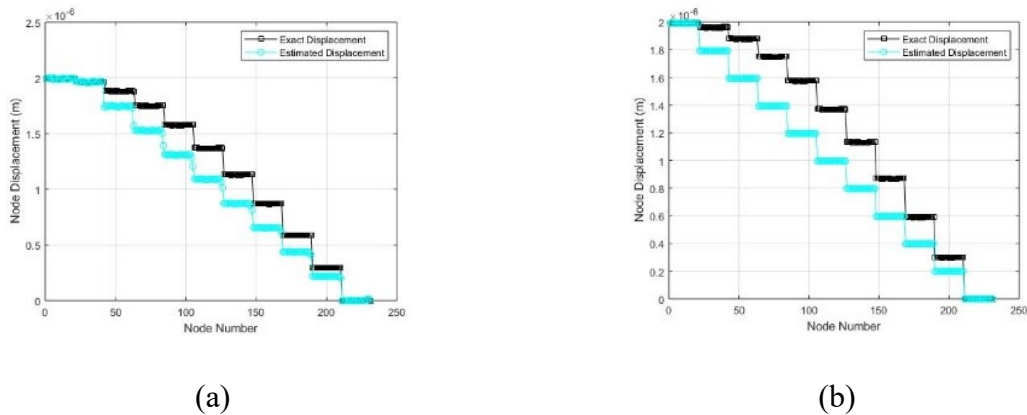
Figure 13: (a) Exact (Black) and estimated (Cyan) node displacement for dynamic two-dimensional reservoir using Guyan Condensation with 70 master degrees-of-freedom (b) Exact and estimated node displacement for dynamic two-dimensional reservoir using Guyan Condensation with 40 master degrees-of-freedom.

The natural frequencies are selected to check the accuracy of the reduced model. If the frequencies of the reduced model are close to those of the full model, the reduced model is

considered a good approximation of the full model at that frequency range. The percent error of natural frequency is used for the comparison and is defined as follows

$$\text{PE}\left(\omega_j^{(i)}\right) = \frac{\omega_j^{(i)} - \omega_j}{\omega_j} \times 100 \ (\%) \tag{81}$$

where ω_j and $\omega_j^{(i)}$ are the exact and the ith approximation of the $j^{th}(j = 1,2,\dots,m)$ frequency. The lowest 15 natural frequencies from the full-order model, and the reduced-order model are listed in **Table 12** for the two cases; 70 master degrees-of-freedom and 40 master degrees-of-freedom, respectively.

Table 12: *Comparison of natural frequencies of a two-dimensional reservoir*

Mode	Full Model Frequency (f)	Reduced Model Case 1 (70 Masters) Frequency (f_R)	Percent Error (PE)	Case 2 (40 Masters) Frequency (f_R)	Percent Error (PE)
1	7.177045	7.342037	2.29889	7.403909	3.16096
2	14.39838	15.57420	8.16631	16.02467	11.2949
3	21.70855	24.95394	14.9498	26.23697	20.8601
4	29.15246	34.27970	17.5876	36.10206	23.8388
5	34.95285	37.71653	7.90687	39.21829	12.2033
6	35.18489	37.83921	7.54391	39.41228	12.0148
7	35.31034	37.95869	7.50019	39.43424	11.6789
8	35.64859	38.12092	6.93526	39.52847	10.8836
9	35.88522	38.46486	7.18857	39.86258	11.0835
10	36.46714	39.62306	8.65414	42.05507	15.3231
11	36.77536	41.09397	11.7432	42.68695	16.0748
12	38.51842	44.53755	15.6266	46.4399	20.5654
13	41.48070	47.70197	14.9980	51.29357	23.6564
14	44.62237	48.96842	9.73962	52.42924	17.4954
15	45.32531	54.35583	19.9237	57.26358	26.3390

As shown in **Table 12**, Guyan condensation shows some error for dynamic problems. The accuracy of the reduced model is highly *dependent* on the selection procedure of the master degrees-of-freedom. Generally, *case 1* (70 master degrees-of-freedom) is better than *case 2* (40 master degrees-of-freedom) in terms of accuracy. This is due to the higher number of the master degrees-of-freedom. Also, the frequencies resulting from the reduced-order model are *higher* than those from the full-order model. This indicates that the reduced-order model will always be *stiffer* than the full-order model. Finally, the accuracy of the higher modes is normally *lower* than that of the lower modes.

3.5.6. Selection of the Masters for Guyan Reduced Model

In modal analysis [see **Figure 14**] of a structure by the Guyan reduction, <u>two</u> approximations are made:

1. Selection of masters.
2. Reduction of the size of the eigenproblem, i.e. Guyan condensation, etc.
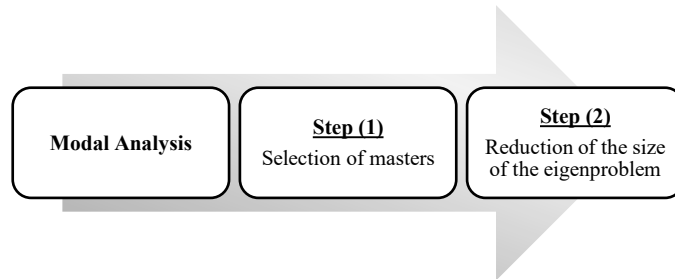
Figure 14: *Modal Analysis of Complex Structure*

As shown in previous section, optimal selection of the masters is a necessary first step to increase the accuracy of the reduced-order model. Shah and Raymund (1982) introduced selection procedure that assures that a large number of lower frequencies are preserved in the reduced eigenvalue problem.

There are two ways to implement the proposed guideline. The key distinctions between both techniques are summarized in **Table 13** below

Table 13: *Comparison of implementation techniques for analytical selection scheme*

Scenario I	Scenario II
▪ All the master degrees-of-freedom are selected simultaneously.	▪ Master degrees-of-freedom are selected one-by-one, or equivalently, one slave degree-of-freedom is eliminated at a time.
▪ Iterative process is required to find a set of masters that satisfies the proposed guidelines.	▪ Iterative process is not required in this case.
▪ Has a higher computational cost, especially with large complex structures.	▪ Has a lower computational cost due to the exclusion of recursive iteration.

Based on the previous comparison, the *second* scenario has been chosen to proceed with, provided that the static coupling among slaves is stronger than dynamic coupling.

3.5.7. The Basic Idea of the Proposed Scheme [Algorithm 1]

The full eigenvalue problem of size $[n \times n]$, is given by

$$\mathbf{KX} = \omega^2 \mathbf{MX} \tag{82}$$

where $\lambda_i^{(0)} = \omega_i \ for \ i = 1, \dots, n$ are the eigenvalues and are ordered in an *ascending* order.

Elimination of one slave at a time requires finding a degree-of-freedom for which the ratio $\gamma_i^2 = K_{ii}/M_{ii}$ is the highest, provided that the ratio, γ_i, is greater than the cut-off frequency, ω_c.

This would result in a reduced eigenvalue problem of size $[(n-1) \times (n-1)]$, and is given by

$$\mathbf{K}^{(1)}\mathbf{X} = \omega^2 \mathbf{M}^{(1)}\mathbf{X} \tag{83}$$

where $\lambda_i^{(1)} = \omega_i \ for \ i = 1, \dots, n$ are the eigenvalues and are ordered in an ascending order. Note that $\lambda_i^{(1)}$ can be considered as an upper bound of $\lambda_i^{(0)}$. Also, the accuracy of the approximation will decrease as the superscript increases, or equivalently, as more slave degrees-of-freedom are eliminated.

This process is repeated successively until the ratio, γ_i, becomes smaller than the cut-off frequency, ω_c. The remaining degrees-of-freedom in the reduced system would represent the master degrees-of-freedom.

Algorithm 1: *Procedure to Select Master Degrees-of-freedom.*

Step 1. Find a degree-of-freedom for which the ratio K_{ii} / M_{ii} is the largest.

Step 2. If this ratio is greater than the cutoff frequency, ω_c^2, eliminate this degree-of-freedom from mass and stiffness matrices by the Guyan reduction method.

Step 3. Apply steps 1 and 2 to the reduced matrices obtained in step 2.

Step 4. Repeat steps 1-3, until the largest ratio found in step 1 is less than or equal to ω_c^2.

Step 5. At this point, the degrees-of-freedom associated with the resultant reduced matrices represent the selected masters.

One limitation of this procedure, however, is the *critical choice* of cut-off frequency since increasing the frequency ratio between cut-off frequency and calculated frequencies, increases the accuracy of the reduced model.

3.6.   Two-Step Dynamic Condensation

To achieve reasonably accurate results, the inertia effects could be partially or fully included in the condensation. The corresponding condensation approaches are generally called dynamic condensation.

3.6.1. Formulation of Equations for The Exact Condensation (Direct Back-Substitution)

The general eigenproblem of full model is given by

$$(\mathbf{K} - \lambda\mathbf{M})\boldsymbol{\varphi} = 0 \tag{84}$$

Similar to static problem, this equation may be rewritten as

$$\left(\begin{bmatrix} K_{mm} & K_{ms} \\ K_{sm} & K_{ss} \end{bmatrix} - \lambda \begin{bmatrix} M_{mm} & M_{ms} \\ M_{sm} & M_{ss} \end{bmatrix} \right) \begin{Bmatrix} \varphi_m \\ \varphi_s \end{Bmatrix} = \begin{Bmatrix} 0 \\ 0 \end{Bmatrix} \tag{85}$$

A simple multiplication expands this equation into two equations, namely,

$$(\mathbf{K}_{mm} - \lambda \mathbf{M}_{mm})\boldsymbol{\varphi}_m + (\mathbf{K}_{ms} - \lambda \mathbf{M}_{ms})\boldsymbol{\varphi}_s = \mathbf{0} \tag{86}$$

$$(\mathbf{K}_{sm} - \lambda \mathbf{M}_{sm})\boldsymbol{\varphi}_m + (\mathbf{K}_{ss} - \lambda \mathbf{M}_{ss})\boldsymbol{\varphi}_s = \mathbf{0} \tag{87}$$

The relation of the eigenvector between the masters and slaves may be obtained from Eq. (86) as

$$\boldsymbol{\varphi}_s = \mathbf{R}(\lambda)\boldsymbol{\varphi}_m \tag{88}$$

The condensation matrix is defined as

$$\mathbf{R}(\lambda) = (\mathbf{K}_{ss} - \lambda \mathbf{M}_{ss})^{-1}(\mathbf{K}_{sm} - \lambda \mathbf{M}_{sm}) \tag{89}$$

Unlike static condensation, inertia effects are considered in this condensation matrix. Hence, the condensation matrix is considered dynamic. One limitation is that the dynamic condensation matrix in Eq. (86) is single-mode dependent. Consequently, having different modes may lead to different dynamic condensation matrices.

Back-substituting Eq. (88) into Eq. (86), we obtain is

$$\mathbf{D}_R(\lambda)\boldsymbol{\varphi}_m = \mathbf{0} \tag{90}$$

The reduced dynamic stiffness matrix

$$\mathbf{D}_R(\lambda) = (\mathbf{K}_{mm} - \lambda \mathbf{M}_{mm}) + (\mathbf{K}_{ms} - \lambda \mathbf{M}_{ms})(\mathbf{K}_{ss} - \lambda \mathbf{M}_{ss})^{-1}(\mathbf{K}_{sm} - \lambda \mathbf{M}_{sm}) \tag{91}$$

Because no error is introduced during the derivation of the condensation matrix in Eq. (89) and the reduced eigenproblem in Eq. (91), the condensation matrix is usually referred to as the exact condensation matrix and the corresponding method is called exact dynamic condensation or exact condensation. Therefore, the accuracy of the reduced model does not depend on the selection of masters except in the rare case when the energy of the system does not contribute to the whole set of masters and convergence to all the modes of interest is guaranteed.

If the stiffness and mass matrices of a system are denoted by K^* and M^*, the dynamic stiffness matrix is given by

$$\mathbf{D}^*(\lambda) = \mathbf{K}^* - \lambda \mathbf{M}^* \tag{92}$$

The following equation may be used to *exactly* compute the stiffness and mass matrices from the dynamic stiffness matrix

$$M_R = -\frac{\partial D_R(\lambda)}{\partial \lambda} \tag{93}$$

$$K_R = D_R(\lambda) + \lambda M_R = D_R(\lambda) - \lambda \frac{\partial D_R(\lambda)}{\partial \lambda} \tag{94}$$

Introducing Eq. (91) into Eq. (93), we have

$$M_R = -\frac{\partial D_R(\lambda)}{\partial \lambda} = -\frac{\partial D_{mm}}{\partial \lambda} + \frac{\partial D_{ms}}{\partial \lambda} D_{ss}^{-1} D_{sm} + D_{ms} \frac{\partial D_{ss}^{-1}}{\partial \lambda} D_{sm} + D_{ms}^{-1} D_{ss} \frac{\partial D_{sm}}{\partial \lambda} \tag{95}$$

The reduced mass matrix is given by

$$M_R(\lambda) = M_{mm} - M_{ms} D_{ss}^{-1} D_{sm} - D_{ms} D_{ss}^{-1} M_{sm} + D_{ms} D_{ss}^{-1} M_{ss} D_{ss}^{-1} D_{sm} \tag{96}$$

The reduced stiffness matrix is given by

$$K_R(\lambda) = K_{mm} - K_{ms} D_{ss}^{-1} D_{sm} - D_{ms} D_{ss}^{-1} K_{sm} + D_{ms} D_{ss}^{-1} K_{ss} D_{ss}^{-1} D_{sm} \tag{97}$$

Similar to the full eigenproblem, the reduced stiffness and mass matrices given in Eqs. (96) and (97) are eigenvalue- or frequency-dependent.

3.7. Iterative Dynamic Condensation

As described in the preceding section. Dynamic condensation approaches – Generally – can significantly improve the accuracy of static condensation. Unfortunately, these methods have one or more disadvantages:

1. The reduced model is frequency-dependent, and a special eigensolver is required to solve the reduced eigenproblem. Furthermore, it is difficult to use this reduced model in further dynamic analyses.

2. The eigenpairs of the reduced model have to be computed one by one which is considered computationally expensive.

3.7.1. Formulation of the Equations for Dynamic Condensation Matrix

Assume that the ith approximation of the first m eigenvectors is denoted by matrix $\Phi_m^{(i)}$ (the size of $n \times m$). Considering Eq. (88), $\Phi_m^{(i)}$ can be expressed in partitioned form as

$$\Phi_m^{(i)} = \begin{bmatrix} \Phi_{mm}^{(i)} \\ \Phi_{sm}^{(i)} \end{bmatrix} = \begin{bmatrix} I \\ R^{(i)} \end{bmatrix} \Phi_{mm}^{(i)} \tag{98}$$

where the ith approximate dynamic condensation matrix, $\mathbf{R}^{(i)}$, is defined as

$$\mathbf{R}^{(i)} = \Phi_{sm}^{(i)}\left(\Phi_{mm}^{(i)}\right)^{-1} \tag{99}$$

According to subspace iteration method in eigenproblems, the $(i+1)^{th}$ approximation of eigenvector matrix $\Phi_m^{(i+1)}$ is obtained by two steps:

Step 1. A subspace, $\mathbf{X}_m^{(i+1)}$, is calculated with an inverse power method

$$\mathbf{X}_m^{(i+1)} = \mathbf{C}\Phi_m^{(i+1)} \tag{100}$$

where $\mathbf{C} = \mathbf{K}^{-1}\mathbf{M}$

Step 2. An orthonormalization process is adopted to construct new m eigenvectors.

$$\Phi_m^{(i+1)} = \mathbf{X}_m^{(i+1)}\mathbf{\Psi}^{(i+1)} = \begin{bmatrix} \mathbf{X}_{mm}^{(i+1)} \\ \mathbf{X}_{sm}^{(i+1)} \end{bmatrix}\mathbf{\Psi}^{(i+1)} \tag{101}$$

Where the eigenvector matrix, $\mathbf{\Psi}^{(i+1)}$, is defined as

$$\overline{\mathbf{K}}_R^{(i+1)}\mathbf{\Psi}^{(i+1)} = \overline{\mathbf{M}}_R^{(i+1)}\mathbf{\Psi}^{(i+1)}\Omega^{(i+1)} \tag{102}$$

Where

$$\overline{\mathbf{K}}_R^{(i+1)} = \left(\mathbf{X}_m^{(i+1)}\right)^{-1}\mathbf{K}\mathbf{X}_m^{(i+1)} \tag{103}$$

$$\overline{\mathbf{M}}_R^{(i+1)} = \left(\mathbf{X}_m^{(i+1)}\right)^{-1}\mathbf{M}\mathbf{X}_m^{(i+1)} \tag{104}$$

Substitution of Eq. (101) in Eq. (99), we get

$$\mathbf{R}^{(i+1)} = \mathbf{X}_{sm}^{(i+1)}\left(\mathbf{X}_{mm}^{(i+1)}\right)^{-1} \tag{105}$$

Rewriting Eq. (100) in partitioned form leads to

$$\mathbf{X}_m^{(i+1)} = \begin{bmatrix} \mathbf{X}_{mm}^{(i+1)} \\ \mathbf{X}_{sm}^{(i+1)} \end{bmatrix} = \begin{bmatrix} \mathbf{C}_{mm} & \mathbf{C}_{ms} \\ \mathbf{C}_{sm} & \mathbf{C}_{ss} \end{bmatrix}\begin{bmatrix} \mathbf{I} \\ \mathbf{R}^{(i)} \end{bmatrix}\Phi_{mm}^{(i)} \tag{106}$$

Eq. (106) can be expanded into

$$\mathbf{X}_{mm}^{(i+1)} = \left(\mathbf{C}_{mm} + \mathbf{C}_{ms}\mathbf{R}^{(i)}\right)\Phi_{mm}^{(i)} \tag{107}$$

$$\mathbf{X}_{sm}^{(i+1)} = \left(\mathbf{C}_{sm} + \mathbf{C}_{ss}\mathbf{R}^{(i)}\right)\Phi_{mm}^{(i)} \tag{108}$$

Substitution of Eqs. (107) and (108) into Eq. (105)

$$R^{(i+1)} = \left(C_{sm} + C_{ss}R^{(i)}\right)\left(C_{mm} + C_{ms}R^{(i)}\right)^{-1} \tag{109}$$

The reduced stiffness matrix would be

$$K_R = K_{mm} + R^T K_{sm} + K_{ms}R + R^T K_{ss}R \tag{110}$$

The reduced mass matrix would be

$$M_R = M_{mm} + R^T M_{sm} + M_{ms}R + R^T M_{ss}R \tag{111}$$

The equivalent force vector would be

$$F_R = F_m + R^T F_s \tag{112}$$

As noticed, the reduced system of equations (using iterative techniques) [Eq. (110) through (112)] shows a huge progress over the reduced system of equations (using Guyan Condensation) [Eq. (69) and (70)] for *two* major reasons: **(1)** the former reduced system (using iterative techniques) accounts for the inertia effects represented by inclusion of mass matrix and **(2)** guarantees convergence to true solution (of full system) regardless of masters selection due to the implementation of inverse power theory for construction of condensation matrix.

3.7.2. Solution Schemes for Dynamic Condensation Matrix

Two iterative schemes are provided in this section, which are based on the convergence of the eigenvalues of the reduced model and the column vectors of the dynamic condensation matrix, respectively. The key steps for the two schemes are provided in *Table 14* and *Table 15*, respectively. The pseudo-codes for both schemes are provided in *Algorithm 2* and *Algorithm 3*.

Table 14: *Key Steps for iterative scheme (I)*

Step 1.	Formulate the matrix, C.
Step 2.	Calculate the initial approximation of dynamic condensation matrix, R^0.
Step 3.	For $i = 0, 1, 2, ...$
	i. Calculate the $(i + k)^{th}$ approximate dynamic condensation matrix, $R^{(i+k)}$.
	ii. Calculate the condensed stiffness, $K_R^{(i+k)}$, and mass, $M_R^{(i+k)}$, matrices.
	iii. Solve the eigenproblem of the condensed model.
	iv. Check the convergence.
Step 4.	Output the results and stop.

Table 15: *Key Steps for Iterative Scheme (II)*

Step 1.	Formulate the matrix, C.
Step 2.	Calculate the initial approximation of dynamic condensation matrix, R^0.
Step 3.	For $i = 0, 1, 2, ...$
	i. Calculate the $(i + k)^{th}$ approximate dynamic condensation matrix, $R^{(i+k)}$.
	ii. Check the convergence.
Step 4.	Calculate the condensed stiffness, $K_R^{(i+k)}$, and mass, $M_R^{(i+k)}$, matrices.
Step 5.	Solve the eigenproblem of the condensed model.
Step 6.	Output the results and stop.

Calculate the initial approximation of dynamic condensation matrix R

$R^{(0)} = C_{sm} C_{mm}^{-1}$

for error $< \varepsilon$

Calculate the condensed matrices for the (i)th approximate dynamic condensation matrix $R^{(i)}$

$K_R^{(i)} = K_{mm} + \left(R^{(i+k)}\right)^T k_{sm} + K_{ms} R^{(i+k)} + \left(R^{(i+k)}\right)^T k_{ss} R^{(i+k)}$

$M_R^{(i)} = M_{mm} + \left(R^{(i+k)}\right)^T M_{sm} + M_{ms} R^{(i+k)} + \left(R^{(i+k)}\right)^T M_{ss} R^{(i+k)}$

Solve the eigenproblem of the condensed model

$\left[U^{(i)}, E^{(i)}\right] = eig(K_R^{(i)}, M_R^{(i)})$

Calculate the $(i+k)$th approximate dynamic condensation matrix $R^{(i+k)}$ by iteration.

for $i = 1:k$

$R^{(i+1)} = \left(C_{sm} + C_{ss} R^{(i)}\right)\left(C_{mm} + C_{ms} R^{(i)}\right)^{-1}$

Update

$R^{(i)} = R^{(i+1)}$

end

Calculate the condensed matrices for the $(i+1)$th approximate dynamic condensation matrix $R^{(i+1)}$

$K_R^{(i+k)} = K_{mm} + \left(R^{(i+k)}\right)^T k_{sm} + K_{ms} R^{(i+k)} + \left(R^{(i+k)}\right)^T k_{ss} R^{(i+k)}$

$M_R^{(i+k)} = M_{mm} + \left(R^{(i+k)}\right)^T M_{sm} + M_{ms} R^{(i+k)} + \left(R^{(i+k)}\right)^T M_{ss} R^{(i+k)}$

Solve the eigenproblem of the condensed model

$\left[U^{(i+k)}, E^{(i+k)}\right] = eig(K_R^{(i+k)}, M_R^{(i+k)})$

Check the convergence by using the following convergent criterion

for $j = 1:m$

$error(j, 1) = \left|\dfrac{\lambda_j^{(i+k)} - \lambda_j^{(i)}}{\lambda_j^{(i+k)}}\right|$

end

$R^{(i)} = R^{(i+1)}$

end

60

Algorithm 3: *The pseudo-code for iterative scheme (II)*

Calculate the initial approximation of dynamic condensation matrix R

$R^{(0)} = C_{sm}C_{mm}^{-1}$

for error $< \varepsilon$

Calculate the $(i + k)$th approximate dynamic condensation matrix $R^{(i+k)}$ by iterating the following equation for k times

for i $= 1:k$

$R^{(i+1)} = (C_{sm} + C_{ss}R^{(i)})(C_{mm} + C_{ms}R^{(i)})^{-1}$

Update

$R^{(i)} = R^{(i+1)}$

end

Check the convergence by using the following convergent criterion

for j $= 1:m$

$$error(j, 1) = 1 - \frac{\left(r_j^{(i+k)}\right)^T r_j^{(i)}}{\left\|r_j^{(i+k)}\right\|_2 \left\|r_j^{(i)}\right\|_2}$$

end

Update

$R^{(i)} = R^{(i+k)}$

end

Calculate the condensed stiffness and mass matrices for the $(i + 1)$th approximate dynamic condensation matrix $R^{(i+1)}$

$K_R^{(i+k)} = K_{mm} + \left(R^{(i+k)}\right)^T k_{sm} + K_{ms}R^{(i+k)} + \left(R^{(i+k)}\right)^T k_{ss}R^{(i+k)}$

$M_R^{(i+k)} = M_{mm} + \left(R^{(i+k)}\right)^T M_{sm} + M_{ms}R^{(i+k)} + \left(R^{(i+k)}\right)^T M_{ss}R^{(i+k)}$

Solve the eigenproblem of the condensed model

$\left[U^{(i+k)}, E^{(i+k)}\right] = eig(K_R^{(i+k)}, M_R^{(i+k)})$

3.7.3. Numerical Demonstration

In this section, we present the performance of the proposed iterative technique (*Iterative scheme I*) through one structural problem. For comparison reasons, we have adopted the same structural problem as in the previous sections.

Two numerical cases are considered with different master degrees-of-freedom for the two-dimensional reservoir. Summary of the two models is listed in **Table 11**. The master degrees-of-freedom are selected as shown in **Figure 11**.

Comparison of natural frequencies of a full-order model, f, and reduced-order model, f_R, for the two cases: 70 masters and 40 masters, are listed in **Table 16**, for both Guyan condensation and iterative techniques. Graphical representation of the exact and estimated node displacements, and the exact and estimated natural frequencies are shown in **Figure 15** and **Figure 16**, respectively.

(a)   (b)
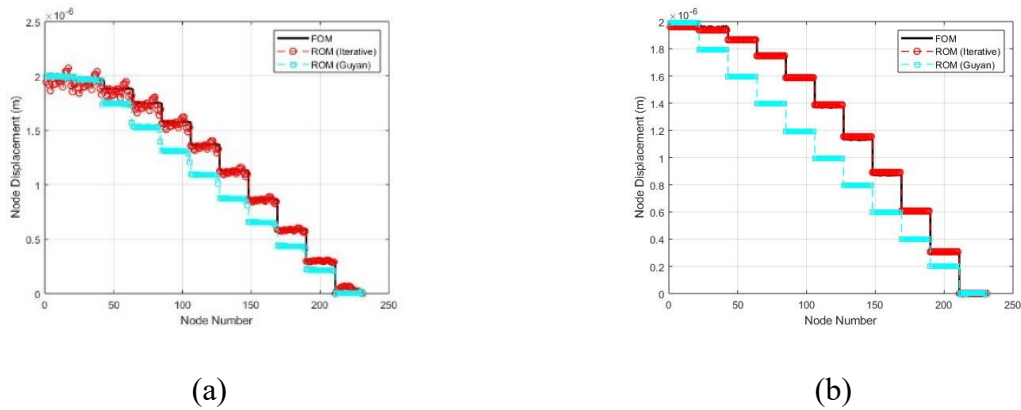
Figure 15: (a) Exact and estimated node displacement for dynamic two-dimensional reservoir problem using guyan condensation (cyan) and iterative technique (red) for the selected 70 master degrees-of-freedom (b) Exact and estimated node displacement for dynamic two-dimensional reservoir problem using guyan condensation (cyan) and iterative technique (red) for the selected 40 master degrees-of-freedom

Table 16: Comparison of natural frequencies of a full-order model and reduced-order model (using guyan condensation and iterative techniques)

Mode	Full Model	Reduced Model			
		Guyan		Iterative	
		Case 1 (70 dofs)	Case 2 (40 dofs)	Case 1 (70 dofs)	Case 2 (40 dofs)
	Frequency f	Frequency f_R	Frequency f_R	Frequency f_R	Frequency f_R
1	7.177045	7.218943	7.403909	7.177045	7.177045
2	14.398382	14.690802	16.024665	14.398382	14.398382
3	21.708545	22.771715	26.236969	21.708545	21.708545
4	29.152458	31.357743	36.102064	29.152458	29.152458
5	34.952854	38.620170	39.218288	34.952854	34.952854
6	35.184888	39.057133	39.412284	35.184888	35.184888
7	35.310344	39.358188	39.434237	35.310344	35.310344
8	35.648592	39.532995	39.528471	35.648592	35.648592
9	35.885224	40.256565	39.862583	35.885224	35.885224
10	36.467141	40.879297	42.055067	36.467141	36.467141
11	36.775363	41.575773	42.686952	36.775363	36.775363
12	38.518421	43.921807	46.439901	38.518421	38.518421
13	41.480695	44.904219	51.293569	41.480695	41.480695
14	44.622372	49.922279	52.429244	44.622372	44.622373
15	45.325314	52.626637	57.263584	45.325314	45.325314
16	50.005533	58.145880	64.336545	50.005533	50.005533
17	51.731441	62.721284	65.018487	51.731441	52.737420
18	52.737394	63.906454	72.494879	52.737394	55.471782
19	53.981439	65.718173	77.824069	53.981439	61.161490
20	55.471782	68.713754	81.715391	55.471782	61.673560
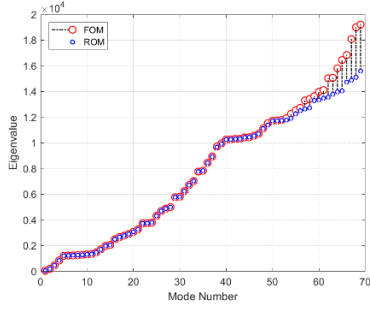
(a)
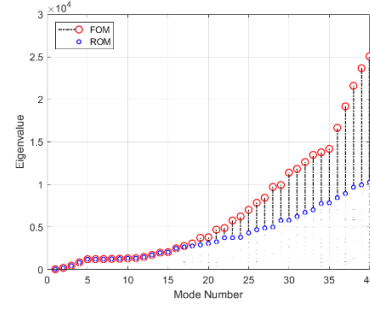
(b)

Figure 16: *(a) Comparison of natural frequencies of a full-order model (**blue**) and reduced-order model (**red**) for dynamic two-dimensional reservoir problem for the selected 70 master degrees-of-freedom (b) Comparison of natural frequencies of a full-order model (**blue**) and reduced-order model (**red**) for dynamic two-dimensional reservoir problem for the selected 40 master degrees-of-freedom*

It is clear that the proposed iterative schemes assure the convergence of the estimated displacements towards the exact displacement *regardless of the choice of the master* and slave degrees-of-freedom unlike Guyan condensation that suffers from huge error when dynamic problem is considered.

3.8. Assessment of the model efficiency

To demonstrate the efficiency of the proposed iterative technique, *three* aspects were assessed:

1. Assessment of the Convergent Criterion.
2. Assessment of the Reduced Model Accuracy.
3. Assessment of the Suitability of the Measurement Locations.

3.8.1. Assessment of the Convergent Criterion

One major criterion is used to assess the efficiency of the convergent criterion. *The errors of the column vectors of the dynamic condensation matrix should decrease consistently as the number of iterations increases*. This assures the convergence of the proposed method.

The errors of the first 20 column vectors of the dynamic condensation matrix in every iteration for the two case; 70 masters and 40 masters, are listed in ***Table 17*** and ***Table 18***,

respectively. A graphical representation of the errors in column vectors of dynamic condensation matrix over iterations for the two cases is presented in ***Figure 17***, as well.

(a)   (b)
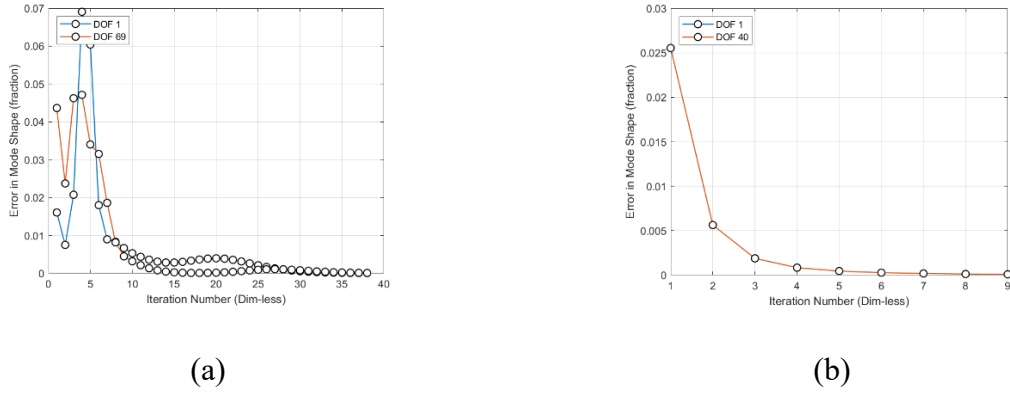
Figure 17: *(a) The Errors for Reduced-Order Model (ROM) Using Iterative Technique for Dynamic Two-dimensional Reservoir Problem for the selected 70 master degrees-of-freedom (b) The Errors for Reduced-Order Model (ROM) Using Iterative Technique for Dynamic Two-dimensional Reservoir Problem for the selected 40 master degrees-of-freedom*

Table 17: *The Errors of the Column Vectors of Dynamic Condensation Matrix (Case 1 ~ 70 DOFs)*

Column no.	Iteration Number				
	1	**2**	**3**	**4**	**5**
1	0.196728	0.064519	0.015191	0.005431	0.002682
2	0.208473	0.038028	0.02385	0.014232	0.008235
3	0.207968	0.057544	0.010014	0.003160	0.002136
4	0.173874	0.02399	0.01041	0.006140	0.005849
5	0.194601	0.066862	0.022303	0.007194	0.002713
6	0.154075	0.018048	0.012873	0.010358	0.00638
7	0.212048	0.068038	0.013325	0.004838	0.003287
8	0.144615	0.019572	0.014867	0.008871	0.006167
9	0.219732	0.061151	0.013996	0.005989	0.002643
10	0.141171	0.020707	0.014275	0.009102	0.006075
11	0.219646	0.059836	0.014533	0.005308	0.002701
12	0.140419	0.020692	0.014312	0.009041	0.006096
13	0.218706	0.060221	0.01423	0.005422	0.002681
14	0.140393	0.020598	0.014325	0.009048	0.006091
15	0.218315	0.060309	0.01425	0.005411	0.002736
16	0.140448	0.020582	0.014322	0.009048	0.006146
17	0.218223	0.06029	0.014257	0.00542	0.002837
18	0.140478	0.020583	0.014322	0.009055	0.006595
19	0.21821	0.060285	0.014256	0.005442	0.003540
20	0.140495	0.020584	0.014323	0.009134	0.010120

Table 18: *The Errors of the Column Vectors of Dynamic Condensation Matrix (Case 2 ~ 40 DOFs)*

Column no.	Iteration Number			
	1	**2**	**3**	**4**
1	0.025542	0.005634	0.001883	0.000838
2	0.051784	0.016211	0.006866	0.003488
3	0.038214	0.008153	0.002141	0.000727
4	0.045193	0.011116	0.004164	0.002179
5	0.031824	0.00929	0.003692	0.001663
6	0.036664	0.010643	0.005425	0.003174
7	0.036834	0.009206	0.002832	0.001157
8	0.036788	0.012843	0.005532	0.002706
9	0.037759	0.008303	0.002738	0.001309
10	0.040011	0.012819	0.005209	0.002765
11	0.03714	0.008333	0.002859	0.001262
12	0.042409	0.012483	0.005257	0.00279
13	0.036718	0.008431	0.002816	0.001247
14	0.043548	0.012404	0.005281	0.00278
15	0.036599	0.008431	0.002806	0.001253
16	0.043984	0.012415	0.005278	0.002787
17	0.036593	0.008419	0.00281	0.001254
18	0.044141	0.012424	0.005277	0.002817
19	0.036605	0.008417	0.002811	0.001256
20	0.044216	0.012426	0.005278	0.003088

As shown in ***Table 17*** and ***Table 18***, the errors of the column vectors of the dynamic condensation matrix *decrease consistently* as the number of iterations increases. This assures the convergence of the proposed method.

3.8.2. Assessment of the Model Accuracy

The natural frequencies and the corresponding mode shapes are selected to check the accuracy of the reduced model. If the eigenpairs of the reduced model are close to those of the full model, the reduced model is considered a good approximation of the full model at that frequency range.

Two major criteria are used to assess the accuracy of the reduced models:

3.8.2.1.   *The percent errors (PE) of natural frequencies*

$$\text{PE}\left(\omega_j^{(i)}\right) = \frac{\omega_j^{(i)} - \omega_j}{\omega_j} \times 100 \ (\%) \tag{113}$$

where ω_j and $\omega_j^{(i)}$ are the exact and the ith approximation of the $j^{th}(j = 1,2,\ldots,m)$ frequency. *A value of PE close to zero suggests that the two corresponding frequencies of the reduced model and full model are equivalent*, hence the reduced model is a good representation of the full model.

The percent errors (PE) of the lowest 20 frequencies obtained from the proposed iterative technique for the two cases; 70 masters and 40 masters, using Eq. (113) and are listed in ***Table 19*** and ***Table 20***, respectively. A graphical representation of the percent errors (PE) for the two cases is presented in ***Figure 18***, as well.

Table 19: *The Percent Errors calculated with the Proposed Iterative Technique (Case 1 ~ 70 DOFs)*

	Iteration Number				
	1	**2**	**3**	**4**	**5**
Mode	**Percent Error (PE)**	**Percent Error (PE)**	**Percent Error (PE)**	**Percent Error (PE)**	**Percent Error (PE)**
1	0.0000	0.0000	0.0000	0.0000	0.0000
2	0.0014	0.0000	0.0000	0.0000	0.0000
3	0.0259	0.0000	0.0000	0.0000	0.0000
4	0.1620	0.0004	0.0000	0.0000	0.0000
5	0.3268	0.0028	0.0000	0.0000	0.0000
6	0.5762	0.0042	0.0000	0.0000	0.0000
7	0.1077	0.0011	0.0000	0.0000	0.0000
8	0.0870	0.0009	0.0000	0.0000	0.0000
9	0.0456	0.0005	0.0000	0.0000	0.0000
10	0.1277	0.0012	0.0000	0.0000	0.0000
11	0.0121	0.0000	0.0000	0.0000	0.0000
12	0.1363	0.0018	0.0000	0.0000	0.0000
13	0.1824	0.0033	0.0000	0.0000	0.0000
14	1.4145	0.0238	0.0003	0.0000	0.0000
15	0.2663	0.0070	0.0001	0.0000	0.0000
16	0.4508	0.0211	0.0005	0.0000	0.0000
17	2.6177	0.0939	0.0022	0.0001	0.0000
18	2.9143	0.4871	0.0284	0.0017	0.0001
19	10.0111	0.1999	0.0106	0.0006	0.0000
20	8.7607	0.5904	0.0369	0.0024	0.0002

Table 20: The Percent Errors calculated with the Proposed Iterative Technique (Case 2 ~ 40 DOFs)

Mode	Iteration Number			
	1	2	3	4
	Percent Error (PE)	Percent Error (PE)	Percent Error (PE)	Percent Error (PE)
1	0.0000	0.0000	0.0000	0.0000
2	0.0068	0.0000	0.0000	0.0000
3	0.1108	0.0011	0.0000	0.0000
4	0.5711	0.0183	0.0006	0.0000
5	0.6551	0.0376	0.0014	0.0000
6	1.6143	0.1152	0.0085	0.0006
7	0.3267	0.0373	0.0050	0.0007
8	0.2794	0.0384	0.0063	0.0010
9	0.1534	0.0211	0.0044	0.0009
10	0.3494	0.0275	0.0028	0.0003
11	0.0909	0.0007	0.0000	0.0000
12	0.2862	0.0258	0.0022	0.0002
13	0.3767	0.0336	0.0030	0.0003
14	3.4410	0.4143	0.0529	0.0064
15	0.5259	0.0623	0.0080	0.0011
16	0.8368	0.1763	0.0470	0.0135
17	5.3804	1.013	0.1987	0.0375
18	3.5683	2.5363	2.1398	1.8762
19	12.9687	10.1452	8.6612	7.7263
20	12.6351	8.1613	6.8100	5.2548

<center>(a)   (b)</center>
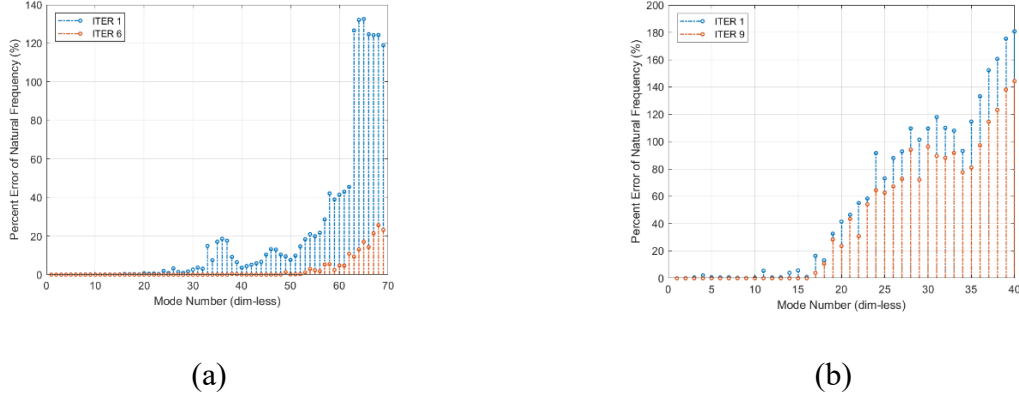
Figure 18: (a) The percent errors for the reduced-order model (ROM) using iterative technique for dynamic two-dimensional reservoir problem for the selected 70 masters degrees-of-freedom (b) The percent errors for the reduced-order model (ROM) using iterative technique for dynamic two-dimensional reservoir problem for the selected 40 masters degrees-of-freedom

3.8.2.2.   *The correlated coefficient for modal vector (CCFMV)*

$$
\text{CCFMV}\left(\varphi_{mj}^{(i)}\right) = \frac{\varphi_{mj}^{T} \cdot \varphi_{mj}^{(i)}}{\left\{\left[\varphi_{mj}^{T} \cdot \varphi_{mj}\right] \cdot \left[\left(\varphi_{mj}^{(i)}\right)^{T} \cdot \varphi_{mj}^{(i)}\right]\right\}^{1/2}}
\tag{114}
$$

where φ_{mj} and $\varphi_{mj}^{(i)}$ are the exact and the ith approximation of the $j^{th}(j = 1,2, \dots, m)$ eigenvector, respectively. *A value of CCFMV close to one suggests that the two corresponding eigenvectors (or, mode shapes) of the reduced model and full model are well correlated*, hence the reduced model is a good representation of the full model. Equivalently, a value of one suggests that the two eigenvectors are uncorrelated.

The correlated coefficient for modal vector (CCFMV) of the lowest 20 frequencies obtained from the proposed iterative technique for the two cases; 70 masters and 40 masters, using Eq. (114) and are listed in **Table 21** and **Table 22**, respectively. A graphical representation of the correlated coefficient for modal vector (CCFMV) for the two cases is presented in **Figure 19**, as well.

<center>71</center>

Table 21: The Correlated Coefficient for Modal Vector (CCFMV) calculated with the Proposed Iterative Technique (Case 1 ~ 70 DOFs)

Mode	Iteration Number					
	1	2	3	4	5	6
	CCFMV	CCFMV	CCFMV	CCFMV	CCFMV	CCFMV
1	1.000000	1.000000	1.000000	1.000000	1.000000	1.000000
2	1.000000	1.000000	1.000000	1.000000	1.000000	1.000000
3	0.999987	1.000000	1.000000	1.000000	1.000000	1.000000
4	0.999995	1.000000	1.000000	1.000000	1.000000	1.000000
5	0.999914	0.999995	1.000000	1.000000	1.000000	1.000000
6	0.998894	0.999929	0.999998	1.000000	1.000000	1.000000
7	0.998250	0.999989	1.000000	1.000000	1.000000	1.000000
8	0.999781	0.999971	0.999999	1.000000	1.000000	1.000000
9	0.998802	0.999853	0.999999	1.000000	1.000000	1.000000
10	0.999868	0.999984	1.000000	1.000000	1.000000	1.000000
11	0.999202	0.999934	0.999999	1.000000	1.000000	1.000000
12	0.999588	0.999987	1.000000	1.000000	1.000000	1.000000
13	0.999688	0.999963	0.999999	1.000000	1.000000	1.000000
14	0.999491	0.999916	0.999998	1.000000	1.000000	1.000000
15	0.998309	0.999884	0.999997	1.000000	1.000000	1.000000
16	0.997544	0.999634	0.999955	0.999998	1.000000	1.000000
17	0.992602	0.995377	0.999710	0.999996	1.000000	1.000000
18	0.991209	0.996787	0.999794	0.999997	1.000000	1.000000
19	0.998336	0.999409	0.999939	0.999999	1.000000	1.000000
20	0.989630	0.995096	0.999093	0.999972	1.000000	1.000000

Table 22: The Correlated Coefficient for Modal Vector (CCFMV) calculated with the Proposed Iterative Technique (Case 2 ~ 40 DOFs)

Mode	Iteration Number				
	1	**3**	**5**	**7**	**9**
	CCFMV	**CCFMV**	**CCFMV**	**CCFMV**	**CCFMV**
1	1.000000	1.000000	1.000000	1.000000	1.000000
2	0.999998	1.000000	1.000000	1.000000	1.000000
3	0.999955	0.999998	1.000000	1.000000	1.000000
4	0.999948	0.999959	0.999997	1.000000	1.000000
5	0.992178	0.999042	0.999869	0.999982	0.999998
6	0.993297	0.998848	0.999794	0.999963	0.999994
7	0.988820	0.999247	0.999926	0.999992	0.999999
8	0.996927	0.999338	0.999853	0.999968	0.999993
9	1.000000	1.000000	1.000000	1.000000	1.000000
10	0.956178	0.997292	0.999997	0.999998	1.000000
11	0.928158	0.990784	0.999716	0.999989	0.999999
12	0.999994	0.999878	0.999975	0.999997	1.000000
13	0.999941	0.999881	0.999977	0.999997	1.000000
14	0.000000	0.996941	0.999530	0.999926	0.999988
15	0.000112	0.999904	0.999978	0.999997	1.000000
16	0.999954	0.999931	0.999979	0.999996	0.999999
17	0.000000	0.000001	0.000000	0.000000	0.000000
18	0.975819	0.000000	0.000000	0.000000	0.000000
19	0.000000	0.000000	0.000003	0.000001	0.000000
20	0.000177	0.000076	0.000000	0.000000	0.000000
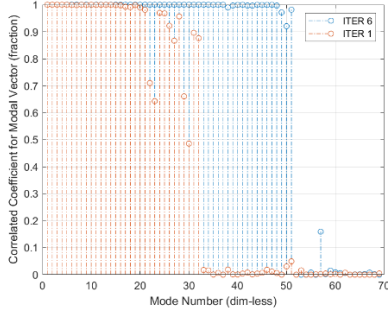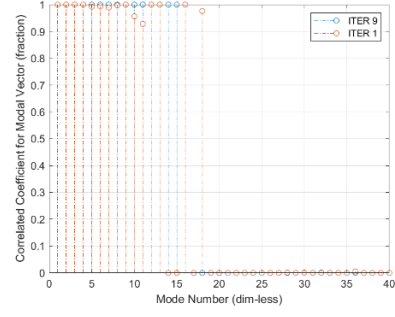
Figure 19: *(a) The correlated coefficient for modal vector (CCFMV) calculated using iterative technique for dynamic two-dimensional reservoir problem for the selected 70 master degrees-of-freedom (b) The correlated coefficient for modal vector (CCFMV) calculated using iterative technique for dynamic two-dimensional reservoir problem for the selected 40 master degrees-of-freedom*

3.8.3.   Assessment of the Suitability of Measurement Locations

Here *two possible criteria* are investigated:

3.8.3.1.   *Modal Assurance Criterion (MAC)*

In any modal test, the mode shapes are useful when they can be distinguished from each other. That is, *the mode shape vectors should be linearly independent*.

The easiest way to check the linear dependence of mode shapes is to use modal assurance criterion

$$\text{MAC}_{ij} = \frac{\left[u^{(i)^T}u^{(j)}\right]^2}{\left[u^{(i)^T}u^{(i)}\right]\left[u^{(j)^T}u^{(j)}\right]} \tag{115}$$

where $u^{(i)}$ and $u^{(j)}$ are the ith and j^{th} mode shapes at the selected measurement locations.

The off-diagonal terms are close to zero, which supports the fact that they are less dependent. Yet, the eigenvectors are not exactly zero due to the fact that they are orthogonal with respect to the mass and stiffness matrices and the MAC does not account for that.

74

A graphical representation of the MAC matrices is presented in ***Figure 20*** for the two cases; 72 masters and 40 masters, respectively. Due to the symmetry of the MAC matrix, the lower triangle for both cases was omitted.

<div align="center">(a)   (b)</div>

Figure 20: *(a) Modal Assurance Criterion (MAC) for Reduced-Order Models Using Iterative Technique for Dynamic Two-dimensional Reservoir Problem for the selected 70 master degrees-of-freedom (b) Modal Assurance Criterion (MAC) for Reduced-Order Models Using Iterative Technique for Dynamic Two-dimensional Reservoir Problem for the selected 40 master degrees-of-freedom*

3.8.3.2.   *Singular Value Decomposition (SVD)*

A singular value decomposition of the eigenvector matrix based on the selected degrees-of-freedom can be used to determine the suitability of the chosen masters. The method basically evaluates the ratio of the largest to the smallest singular value of the eigenvector matrix. *The larger the ratio, the worst the choice of the masters*.

A graphical representation of the SVD results is presented in ***Figure 21*** for the two cases; 72 masters and 40 masters, respectively. The ratio of the largest to the lowest singular value for both cases is presented on both figures.

Figure 21: (a) Singular Value Decomposition (SVD) for Reduced-Order Models Using Iterative Technique for Dynamic Two-dimensional Reservoir Problem for the selected 70 master degrees-of-freedom (b) S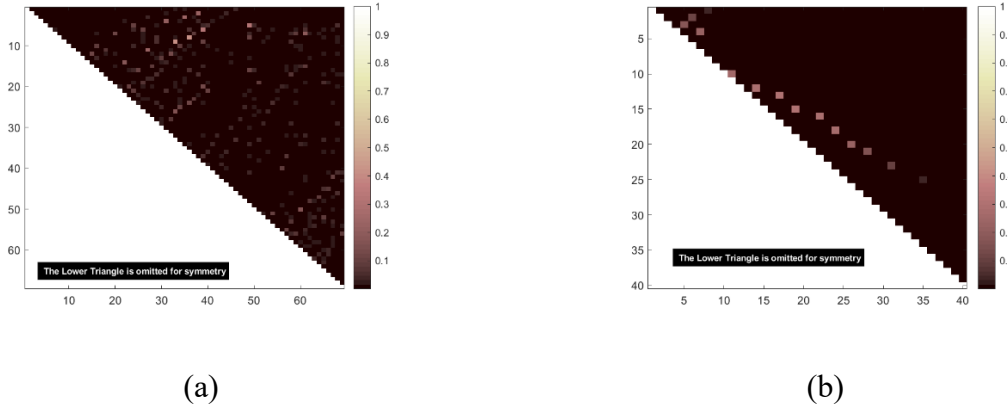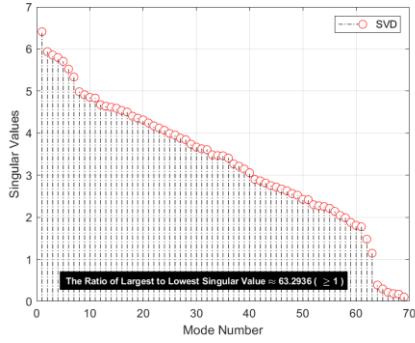ingular Value Decomposition (SVD) for Reduced-Order Models Using Iterative Technique for Dynamic Two-dimensional Reservoir Problem for the selected 40 master degrees-of-freedom
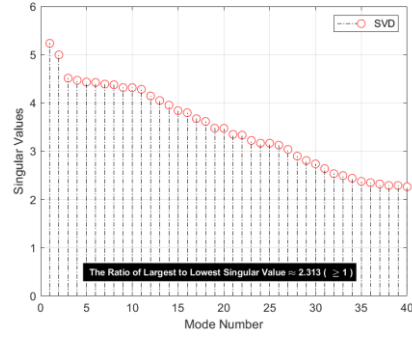
As shown from the above figure, the ratio for the *two* selections of master degrees-of-freedom (DOFs) is close to unity which reflects the independency between the basis vectors for the reduced spaces for both cases; conforming with the fact that masters selections has no effect on the ROM obtained using iterative technique nor the quality of its solution.

4.   Computational Time

From previous analysis, one-step methods (e.g. Guyan Condensation) have proven to be efficient for reduction of large-scale *static* geomechanical models. On the other hand, three-step/iterative methods have proven its efficiency in reducing the scale of large *dynamic* geomechanical models.

Based on the numerical demonstrations – presented in this paper – both one-step and three-step methods managed to achieve an intensive scale reduction (down to 10% of size of the full-order model) for their corresponding cases. The reduction in scale was reflected – in turn – on the computational speed of model runs [as shown in *Table 23*].

Table 23 displays preliminary numerical results that correspond to the iterative condensation techniques applied to the geomechanical model. As with any model reduction comparisons, this is a relative comparison for a particular computational platform. To this end, all of the simulations were performed using a laptop with the following specifications: Processor

76

Intel(R) Core(TM) i7 - 8550U CPU @ 1.80GHz 1.99 GHz; RAM: 32.0; 64-bit operating system. Initial speedups – up to 200X – were achieved using the proposed iterative techniques. It should be noted that our problem in consideration is small and any model reduction techniques applied to such systems do not perform as well as compared with problems that are more realistic. They are consistent with the problem formulation, given we are using a direct linear solver in MATLAB.

Table 23. *Comparison of Computational Time for FOM and ROM*

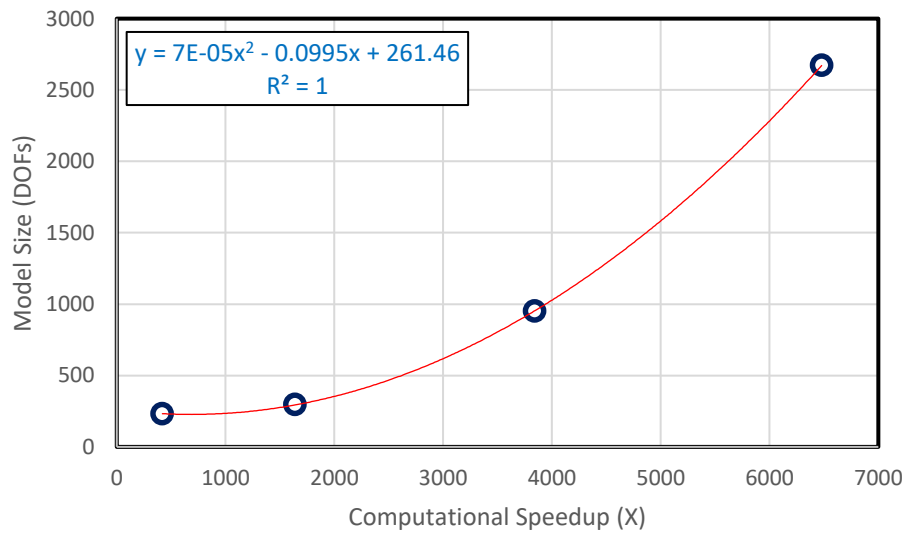| Model	FOM DOFs	FOM Runtime	ROM DOFs	ROM Runtime	Speedup
20 x 10	419	0.4156 secs	40	0.0018 secs	230
40 x 20	1639	4.5152 secs	79	0.0152 secs	297
60 x 30	3842	35.858 secs	121	0.0377 secs	951
80 x 40	6479	172.33 secs	159	0.0645 secs	2671

Figure 22: *Computational Speedups achieved using iterative condensation techniques for various model sizes*

CHAPTER IV

APPLICATION OF ROM FRAMEWORK TO COUPLED FLOW/GEOMECHANCIS

SIMULATIONS

The integration of geomechanical effects with flow systems has received a great attention in various science and engineering fields including – but not limited to – soil science [28, 29], mechanical engineering [30], civil engineering [31], environmental engineering [32,33] and bioengineering [34].

Oil & Gas industry is no different as reservoir engineering is also concerned with the study of fluid flow and the mechanical response of the reservoir. Reservoir geomechanics affect reservoir deformation, well integrity, flow response, heavy-oil production and one of the main drivers of environmental aspects of reservoir exploration [1, 2, 3]. Well and cap-rock integrity issues are often encountered in CO2 sequestration problems (CCS) and reservoir deformation can affect flow response in hydraulic fracturing processes.

Although coupled flow and geomechanics simulations can model such systems, they are computationally expensive. This is due to the nonlinear multiphysics nature of governing equations, and the complexity of the domain over which geomechanical problem must be solved. Moreover, computational demands can be excessive in applications such as optimization and uncertainty quantification, where hundreds or thousands of simulation runs might be required [3].

In this chapter, we are interested in developing a computational framework for modeling coupled flow and geomechanics in geologic systems. The focus is on sequential implicit solution methods that can solve coupled flow and geomechanics. Additionally, an extension of the previously adopted reduced-order modeling (ROM) framework to the coupled flow/geomechanics systems is implemented.

4.1.　Formulation of Coupled Equations in Flow and Geomechanics

In *coupled* flow and geomechanics system, *total stress* affects bulk volume and – accordingly – pore volume. In addition, *pore pressure* affects pore volume and – accordingly – bulk volume. In the preceding discussion we will derive both system of equations concerned with the two – previously mentioned – driving forces/effects.

4.1.1. Derivation of the First Coupling Equation

The variation in porosity is defined by both the variation in pore volume, δV_p, and the variation in bulk volume, δV_b. Variation in pore volume, δV_p, can be defined as a function of pore pressure, p_f, and volumetric stress, σ_v.

$$\delta V_p = f(p_f, \sigma_v) \tag{116}$$

Eq. (116) can be rewritten as

$$\delta V_p = \left[\frac{\partial V_p}{\partial p_f}\right]_{\sigma_v} \cdot \delta p_f + \left[\frac{\partial V_p}{\partial \sigma_v}\right]_{p_f} \cdot \delta \sigma_v \tag{117}$$

where $\left[\partial V_p / \partial p_f\right]_{\sigma_v}$ is the change in pore volume with changing pore pressure assuming constant volumetric stress. Similarly, $\left[\partial V_p / \partial \sigma_v\right]_{p_f}$ is the change in the pore volume with changing volumetric stress assuming a constant pore pressure.

Simple mathematical manipulation of Eq. (117) leads to

$$\delta V_p = \left[\frac{\partial V_p}{\partial p_f}\right]_{\sigma_v} \cdot \delta p_f - \left[\frac{\partial V_p}{\partial \sigma_v}\right]_{p_f} \cdot \delta p_f + \left[\frac{\partial V_p}{\partial \sigma_v}\right]_{p_f} \cdot \delta \sigma_v + \left[\frac{\partial V_p}{\partial \sigma_v}\right]_{p_f} \cdot \delta p_f \tag{118}$$

The definition in Eq. (118) can be rewritten in a relative sense as follows

$$\frac{\delta V_p}{V_p} = \frac{1}{V_p} \cdot \left[\frac{\partial V_p}{\partial p_f}\right]_{\sigma_v} \cdot \delta p_f - \frac{1}{V_p} \cdot \left[\frac{\partial V_p}{\partial \sigma_v}\right]_{p_f} \cdot \delta p_f + \frac{1}{V_p} \cdot \left[\frac{\partial V_p}{\partial \sigma_v}\right]_{p_f} \cdot \delta \sigma_v + \frac{1}{V_p} \cdot \left[\frac{\partial V_p}{\partial \sigma_v}\right]_{p_f} \cdot \delta p_f \tag{119}$$

$$\frac{\delta V_p}{V_p} = \left\{\frac{1}{V_p} \cdot \left[\frac{\partial V_p}{\partial p_f}\right]_{\sigma_v} - \frac{1}{V_p} \cdot \left[\frac{\partial V_p}{\partial \sigma_v}\right]_{p_f}\right\} \cdot \delta p_f + \frac{1}{V_p} \cdot \left[\frac{\partial V_p}{\partial \sigma_v}\right]_{p_f} \cdot \delta(\sigma_v + p_f) \tag{120}$$

where

$$\frac{1}{V_p} \cdot \left[\frac{\partial V_p}{\partial p_f}\right]_{\sigma_v} - \frac{1}{V_p} \cdot \left[\frac{\partial V_p}{\partial \sigma_v}\right]_{p_f} = -\frac{1}{K_s} \tag{121}$$

K_s is defined as *solid grain* modulus.

In a similar fashion, the variation in bulk volume, δV_b, can be defined as a function of pore pressure, p_f, and volumetric stress, σ_v.

$$\delta V_b = f(p_f, \sigma_v) \tag{122}$$

Then – as for Eq. (116) – Eq. (122) can be rewritten as

$$\delta V_b = \left[\frac{\partial V_b}{\partial p_f}\right]_{\sigma_v} \cdot \delta p_f + \left[\frac{\partial V_b}{\partial \sigma_v}\right]_{p_f} \cdot \delta \sigma_v \tag{123}$$

where $\left[\partial V_b / \partial p_f\right]_{\sigma_v}$ is the change in bulk volume with changing pore pressure assuming constant volumetric stress. Similarly, $[\partial V_b / \partial \sigma_v]_{p_f}$ is the change in the bulk volume with changing volumetric stress assuming a constant pore pressure.

Applying the same mathematical manipulation [as for Eq. (117)] for Eq. (123) leads to

$$\delta V_b = \left[\frac{\partial V_b}{\partial p_f}\right]_{\sigma_v} \cdot \delta p_f - \left[\frac{\partial V_b}{\partial \sigma_v}\right]_{p_f} \cdot \delta p_f + \left[\frac{\partial V_b}{\partial \sigma_v}\right]_{p_f} \cdot \delta \sigma_v + \left[\frac{\partial V_b}{\partial \sigma_v}\right]_{p_f} \cdot \delta p_f \tag{124}$$

The definition in Eq. (124) can be rewritten in a relative sense as follows

$$\frac{\delta V_b}{V_b} = \frac{1}{V_b} \cdot \left[\frac{\partial V_b}{\partial p_f}\right]_{\sigma_v} \cdot \delta p_f - \frac{1}{V_b} \cdot \left[\frac{\partial V_b}{\partial \sigma_v}\right]_{p_f} \cdot \delta p_f + \frac{1}{V_b} \cdot \left[\frac{\partial V_b}{\partial \sigma_v}\right]_{p_f} \cdot \delta \sigma_v + \frac{1}{V_b} \cdot \left[\frac{\partial V_b}{\partial \sigma_v}\right]_{p_f} \cdot \delta p_f \tag{125}$$

$$\frac{\delta V_b}{V_b} = \left\{\frac{1}{V_b} \cdot \left[\frac{\partial V_b}{\partial p_f}\right]_{\sigma_v} - \frac{1}{V_b} \cdot \left[\frac{\partial V_b}{\partial \sigma_v}\right]_{p_f}\right\} \cdot \delta p_f + \frac{1}{V_b} \cdot \left[\frac{\partial V_b}{\partial \sigma_v}\right]_{p_f} \cdot \delta(\sigma_v + p_f) \tag{126}$$

where

$$\frac{1}{V_b} \cdot \left[\frac{\partial V_b}{\partial p_f}\right]_{\sigma_v} - \frac{1}{V_b} \cdot \left[\frac{\partial V_b}{\partial \sigma_v}\right]_{p_f} = -\frac{1}{K_s} \tag{127}$$

K_s is defined as *solid grain* modulus.

Depending on the imposed conditions/constraints Eqs. (120) and (126) can be customized to account for **two** different conditions: (a) undrained and (b) drained conditions.

For the undrained conditioned, the increase (or generally, change) in both volumetric stress and pore pressure is assumed to be the same; leading to no fluid flow outside the solid rock. In other words,

$$\delta(\sigma_v + p_f) = 0 \tag{128}$$

By substitution of Eqs. (121), (127) and (128) in Eqs. (120) and (126), we get

$$\frac{\delta V_b}{V_b} = \frac{\delta V_p}{V_p} = -\frac{1}{K_s}\delta p_f = \frac{1}{K_s}\delta \sigma_v \qquad (129)$$

Unlike undrained condition, for drained condition the fluid is allowed to flow outside. This is accomplished through prohibiting any changes to pore pressure. In other words

$$\delta p_f = 0 \qquad (130)$$

Hence, pore pressure, p_f, would be same as boundary pressure. However, we are changing mean stress, σ_v, so changing bulk volume, V_b.

Substitution of Eq. (130) in Eq. (126) leads to

$$\frac{\delta V_b}{V_b} = \frac{1}{V_b} \cdot \left[\frac{\partial V_b}{\partial \sigma_v}\right]_{p_f} \cdot \delta(\sigma_v + p_f) \qquad (131)$$

where

$$\frac{1}{V_b} \cdot \left[\frac{\partial V_b}{\partial \sigma_v}\right]_{p_f} = \frac{1}{K_{dr}} \qquad (132)$$

K_{dr} is defined as *solid skeleton (drained)* modulus.

Substitution of Eqs. (127) and (132) in Eq. (126) leads to

$$\frac{\delta V_b}{V_b} = -\frac{1}{K_s} \cdot \delta p_f + \frac{1}{K_{dr}} \cdot \delta(\sigma_v + p_f) \qquad (133)$$

where $\delta V_b/V_b$ is the volumetric strain, $\delta \varepsilon_v$.

Simple manipulation of Eq. (133) leads to

$$\delta \sigma_v = K_{dr} \cdot \delta \varepsilon_v - \left(1 - \frac{K_{dr}}{K_s}\right) \cdot \delta p_f \qquad (134)$$

where

$$1 - \frac{K_{dr}}{K_s} = b \qquad (135)$$

b is the *biot coefficient*. Then,

$$\delta \sigma_v = K_{dr} \cdot \delta \varepsilon_v - b \cdot \delta p_f \qquad (136)$$

Eq. (136) is the *first equation of coupling*.

4.1.2. Derivation of the Second Coupling Equation

Before we get into the derivation/formulation of the second equation of coupling, an equally important concept/theory needs to be addressed. That is *Betti's theorem* (also known as, *Maxwell-Betti reciprocal work theorem*).

Betti's theorem states that for a linear elastic structure subject to two sets of forces $\{P\}$ and $\{Q\}$, the work done by the set $\{P\}$ through the displacements produced by the set $\{Q\}$, Δ_Q, is equal to the work done by the set $\{Q\}$ through the displacements produced by the set $\{P\}$, Δ_P.

$$P \cdot \Delta_Q = Q \cdot \Delta_P \tag{137}$$

By extending this theorem to the coupling flow/geomechanics system, we get

$$\delta\sigma_v \cdot \left(\left[\frac{\partial V_b}{\partial p_f}\right]_{\sigma_v} \delta p_f\right) = \delta p_f \cdot \left(\left[\frac{\partial V_p}{\partial \sigma_v}\right]_{p_f} \delta\sigma_v\right) \tag{138}$$

Eq. (138) can be reduced to

$$\left[\frac{\partial V_b}{\partial p_f}\right]_{\sigma_v} = \left[\frac{\partial V_p}{\partial \sigma_v}\right]_{p_f} \tag{139}$$

Considering the definition of volumetric strain and true porosity, respectively

$$\frac{1}{V_b}\left[\frac{\partial V_b}{\partial p_f}\right]_{\sigma_v} = \frac{1}{K_{dr}} - \frac{1}{K_s} \tag{140}$$

$$\phi = \frac{V_p}{V_b} \rightarrow \frac{1}{V_b} = \frac{\phi}{V_p} \tag{141}$$

Substitution of Eq. (141) into Eq. (140)

$$\frac{1}{V_p}\left[\frac{\partial V_b}{\partial p_f}\right]_{\sigma_v} = \frac{1}{\phi}\left(\frac{1}{K_{dr}} - \frac{1}{K_s}\right) \tag{142}$$

Substitution of Eq. (142) into Eq. (126)

$$\frac{\delta V_b}{V_b} = -\frac{1}{K_s}\delta p_f + \frac{1}{\phi}\left(\frac{1}{K_{dr}} - \frac{1}{K_s}\right)\delta(\sigma_v + p_f) \tag{143}$$

By taking the derivative of Eq. (141) and apply simple mathematical manipulation

$$\delta\phi = \phi\left(\frac{\delta V_p}{V_p} - \frac{\delta V_b}{V_b}\right) = \phi\left(\frac{\delta V_p}{V_p} - \delta\varepsilon_v\right) \tag{144}$$

Substitution of Eq. (144) into Eq. (143) leads to

$$\delta\phi = \phi\left[-\frac{1}{K_s}\delta p_f + \frac{1}{\phi}\left(\frac{1}{K_{dr}} - \frac{1}{K_s}\right)\delta(\sigma_v + p_f) - \delta\varepsilon_v\right] \tag{145}$$

Rearranging Eq. (133) and applying simple mathematical manipulation leads to

$$K_{dr}\left(\delta\varepsilon_v + \frac{1}{K_s}\cdot\delta p_f\right) = \delta(\sigma_v + p_f) \tag{146}$$

Substitution of Eq. (146) into Eq. (145) leads to

$$\delta\phi = \phi\left[-\frac{1}{K_s}\delta p_f + \frac{1}{\phi}\left(\frac{1}{K_{dr}} - \frac{1}{K_s}\right)K_{dr}\left(\delta\varepsilon_v + \frac{1}{K_s}\cdot\delta p_f\right) - \delta\varepsilon_v\right] \tag{147}$$

Using the definition of biot coefficient [Eq. (135)], Eq. (147) can be rewritten as

$$\delta\phi = \frac{b - \phi}{K_s}\delta p_f + (b - \phi)\delta\varepsilon_v \tag{148}$$

where $\delta\phi$ is the change in *true porosity*. Eq. (148) can be redefined in terms of *reservoir porosity*

$$\delta\Phi = \frac{b - \phi}{K_s}\delta p_f + b\,\delta\varepsilon_v \tag{149}$$

Eq. (149) is the *second coupling equation*. where $(b - \phi)/K_s = 1/M$ and $\delta\Phi = \delta m_f/\rho_f$. Then, Eq. (149) can be rewritten as

$$\frac{\delta m_f}{\delta\rho_f} = \frac{1}{M}\delta p_f + b\,\delta\varepsilon_v \tag{150}$$

4.2.   Solution Schemes for Coupled Systems

Literature is rich with various coupling methods/schemes that can be used to model the interactions between flow and geomechanics. However, this study is limited to one family of these methods, namely *Iterative methods* (traditionally known as; *sequential/staggered methods*). These iterative methods require sequential updating of flow and mechanics problems until convergence to acceptable tolerance is attained.

Iterative family of methods can be divided into **two** major groups, based on the solution scheme: **(1)** one that assumes that the mechanical problem is solved first then the fluid-flow

problem and **(2)** the other major group addresses the fluid-flow first; followed by the mechanical problem. Examples of the first major group are the drained and undrained solution schemes, while examples of the second major group are fixed-stress and fixed-strain solution schemes.

For comparison reasons, we will only consider the two solution schemes, i.e. drained and undrained, pertinent to the *first* major group. Formulation of the two schemes, detailed discussion of key distinctions, as well as, computational considerations are presented in the preceding section.

4.3.   Coupling of Static Mechanical Model w/ Static Flow Model

The linearized equations for the coupled problem are given below. The rock is assumed to be completely saturated with fluid or water. The equations are expressed in terms of the rock displacement u and pore pressure p variables as

$$K_d u - Qp = f_u \tag{151}$$

$$Q^T \dot{u} + S\dot{p} + Hp = f_p \tag{152}$$

where K_d is stiffness matrix (for drained behavior) for the rock skeleton. S and H are the compressibility/accumulation and permeability/transmissibility matrices for the pore fluid, respectively. Q is the coupling/Biot matrix.

The problems governed by Eq. (151) and Eq. (152) can be solved by the following procedure [*Figure 23*]:

Step 1. Write the equilibrium of the Eq. (151) at a time step $n + 1$ as

$$K_d u_{n+1} = (f_u)_{n+1} + Qp_n \tag{153}$$

and obtain u_{n+1} from the known values of u_n, $\dot{p}_n$ and p_n by using *Newmark's family method* with appropriate parameters (e.g. β and γ)

Step 2. writing Eq. (152) as

$$S\dot{p}_{n+1} + Hp_{n+1} = (f_p)_{n+1} - Q^T \dot{u}_{n+1} \tag{154}$$

we can solve for $\dot{p}_{n+1}$ and p_{n+1} using known p_n, $\dot{p}_n$ and $\dot{u}_{n+1}$ [evaluated in Eq. (153)] and a standard θ procedure.
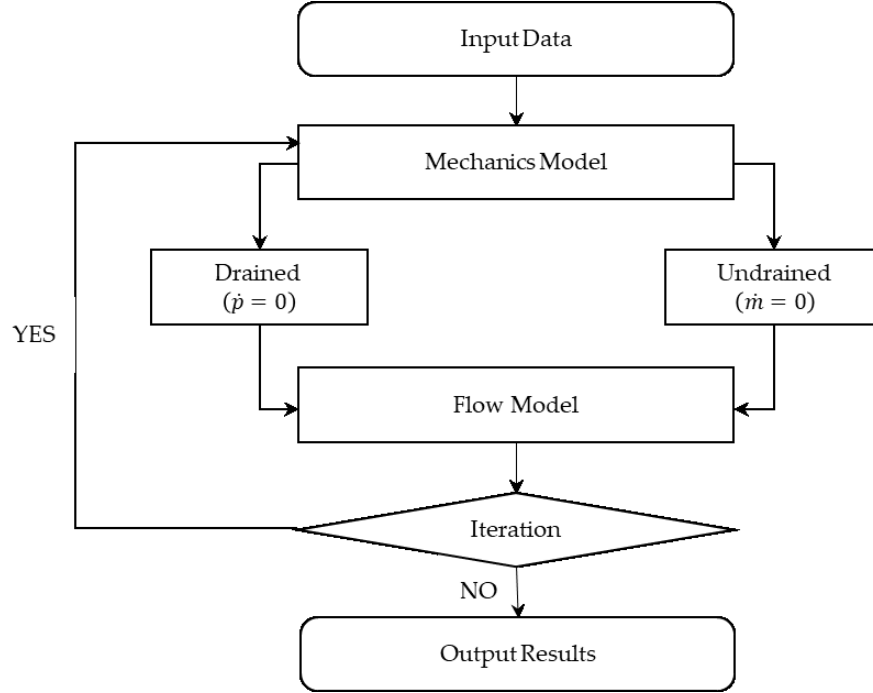
Figure 23: Iteratively coupled schemes for coupled Simulations (drained and undrained splits)

4.3.1. Undrained Solution Scheme

If the permeability approaches zero (i.e. the undrained condition is reached) then the contribution of permeability matrix H vanishes and in that case the pressure can be obtained from Eq. (152) after integrating in terms of compressibility matrix S (noting that under such condition $f_p = 0$):

$$\Delta p_{n+1} = -S^{-1}Q^T\Delta u_{n+1} \tag{155}$$

The equivalent force due to this additional pressure on the soil skeleton would be [from Eq. (151)]:

$$Q\Delta p_{n+1} = -QS^{-1}Q^T\Delta u_{n+1} \tag{156}$$

Now if Eq. (151) and (152) is modified to consider this increased pressure, a staggered scheme of the form given below appears natural. This starts with Eq. (151) at time step $n + 1$ written as

$$(K_d + QS^{-1}Q^T)u_{n+1} = (f_u)_{n+1} + Qp_n + QS^{-1}Q^T u_n \tag{157}$$

and proceeds with Eq. (152) at time step $n + 1$ written as

$$Q^T \dot{u}_{n+1} + S\dot{p}_{n+1} + Hp_{n+1} = (f_p)_{n+1} \tag{158}$$

Indeed, this staggered solution with suitably predicted values of p_{n+1}^p and u_{n+1}^p and with suitable integration formulae turns out to be unconditionally stable when stable ranges of those formulae are used for each component equation. The selection of formulae and predictors for stable solution will be discussed in the next section.

Although the process appears as simple mathematical manipulation, it has a physical significance as the new stiffness matrix is simply the *undrained* stiffness matrix, , defined as

$$K_u = K_d + QS^{-1}Q^T \tag{159}$$

The undrained split can then be written in matrix representation as follows

$$\begin{bmatrix} K_d + U & 0 \\ Q^T & S + \Delta t \cdot H \end{bmatrix} \begin{Bmatrix} u \\ p \end{Bmatrix}^{n+1} = \begin{bmatrix} U & Q \\ Q^T & S \end{bmatrix} \begin{Bmatrix} u \\ p \end{Bmatrix}^n + \begin{Bmatrix} f_u \\ f_p \end{Bmatrix} \tag{160}$$

4.3.2. Drained Solution Scheme

In this case, the mechanics problem is solved first with freezing the pressure field

$$\Delta p_{n+1} = 0 \tag{161}$$

Now if Eq. (151) and (152) is modified to consider this effect, it will take the form

$$K_d u_{n+1} = (f_u)_{n+1} + Qp_n \tag{162}$$

and proceeds with Eq. (152) at time step $n + 1$ written as

$$Q^T \dot{u}_{n+1} + S\dot{p}_{n+1} + Hp_{n+1} = (f_p)_{n+1} \tag{163}$$

Indeed, this staggered solution with suitably predicted values of p_{n+1}^p and u_{n+1}^p and with suitable integration formulae turns out to be unconditionally stable when stable ranges of those formulae are used for each component equation. The selection of formulae and predictors for stable solution will be discussed in the next section.

The drained split can then be written in matrix representation as follows

$$\begin{bmatrix} K_d & 0 \\ Q^T & S + \Delta t \cdot H \end{bmatrix} \begin{Bmatrix} u \\ p \end{Bmatrix}^{n+1} = \begin{bmatrix} 0 & Q \\ Q^T & S \end{bmatrix} \begin{Bmatrix} u \\ p \end{Bmatrix}^n + \begin{Bmatrix} f_u \\ f_p \end{Bmatrix} \tag{164}$$

4.3.3. Time Stepping Algorithm for Coupled Systems

In this section, we briefly present the basic equations used in the time integration scheme of Newmark family methods. Application of the Newmark scheme to both displacement and pressure terms is unconditionally stable for various possible.

4.3.3.1. *Formulation of Newmark set of Equations*

Considering the mechanics terms, the *Newmark family* would consist of the following equations:

$$d_{n+1} = d_n + \Delta t v_n + \Delta t^2 (0.5 - \beta) a_n + \beta \Delta t^2 a_{n+1} \tag{165}$$

$$v_{n+1} = v_n + \Delta t (1 - \gamma) a_n + \gamma \Delta t a_{n+1} \tag{166}$$

The *predictors* will take the form:

$$\tilde{d}_{n+1} = d_n + \Delta t v_n + \frac{\Delta t^2}{2} (1 - 2\beta) a_n \tag{167}$$

$$\tilde{v}_{n+1} = v_n + \Delta t (1 - \gamma) a_n \tag{168}$$

Eq. (165) and (166) may then be rewritten as

$$d_{n+1} = \tilde{d}_{n+1} + \beta \Delta t^2 a_{n+1} \tag{169}$$

$$v_{n+1} = \tilde{v}_{n+1} + \gamma \Delta t a_{n+1} \tag{170}$$

In single component equations, stability is assured if $\gamma \geq 0.5$ and $\beta \geq 0.25$

Similarly, for the predictor for the pressure term will take the form

$$\widetilde{\boldsymbol{p}}_{n+1} = \boldsymbol{p}_n + a\,\Delta t\,\dot{\boldsymbol{p}}_n + b\,\frac{\Delta t^2}{4}\,\ddot{\boldsymbol{p}}_n \tag{171}$$

allows various predictors when a and b take values ranging from 0 to 1, and on insertion of $a = b = 1$, Eq. (171) gives

$$\widetilde{\boldsymbol{p}}_{n+1} = \boldsymbol{p}_n + \Delta t\,\dot{\boldsymbol{p}}_n + \frac{\Delta t^2}{4}\,\ddot{\boldsymbol{p}}_n \tag{172}$$

Application of the aforementioned time-stepping scheme (i.e. Newmark family) for both *undrained* condition and *drained* condition are provided in **Algorithm 4** and **Algorithm 5**, respectively.

Algorithm 4: *Time-stepping scheme for displacement and pressure (*Undrained Split*)*

Initialization:
1) Geomechanics Equation:
$d(0) = d_0$
2) Flow Equation:
$p(0) = p_0$
for $n - time\ steps$:
   Predictors:
   1) Mechanics Term:
   $\widetilde{d}_{n+1} = d_n$
   2) Pressure Term:
   $\widetilde{p}_{n+1} = p_n$
   Solution:
   1) Mechanics Equation:
   $d_{n+1} = (K_d + QS^{-1}Q^T)^{-1}\big[(F_u)_{n+1} + Q\widetilde{p}_{n+1} + (QS^{-1}Q^T)\widetilde{d}_{n+1}\big]$
   2) Flow Equation:
   $p_{n+1} = (S + \Delta t\ H)^{-1}\big[(F_u)_{n+1} + S\widetilde{p}_{n+1} + Q^T\widetilde{d}_{n+1} - Q^T d_{n+1}\big]$
   Updates:
   1) Mechanics Term
   $d_n = d_{n+1}$
   2) Flow Term
   $p_n = p_{n+1}$
end

__Algorithm 5:__ Time-stepping scheme for displacement and pressure (__Drained Split__)

Initialization:
3) Geomechanics Equation:
$d(0) = d_0$
4) Flow Equation:
$p(0) = p_0$
for $n - time\ steps$:
 Predictors:
 3) Mechanics Term:
 $\widetilde{d}_{n+1} = d_n$
 4) Pressure Term:
 $\widetilde{p}_{n+1} = p_n$
 Solution:
 3) Mechanics Equation:
 $d_{n+1} = (K_d)^{-1}[(F_u)_{n+1} + Q\widetilde{p}_{n+1}]$
 4) Flow Equation:
 $p_{n+1} = (S + \Delta t\ H)^{-1}[(F_u)_{n+1} + S\widetilde{p}_{n+1} + Q^T\widetilde{d}_{n+1} - Q^T d_{n+1}]$
 Updates:
 3) Mechanics Term
 $d_n = d_{n+1}$
 4) Flow Term
 $p_n = p_{n+1}$
end

4.3.4. Numerical Demonstration

In this section, we present the performance of the proposed scheme through one structural problem. Mandel's problem is commonly used to validate simulators of coupled flow and geomechanics. For greater detail the reader can refer to Abousleiman et al. (1996). For the finite element modeling, we use the well-known 4-node quadrilateral flat shell finite elements.

A two-dimensional reservoir [**Figure 24**] is considered with boundary conditioned as specified in **Table 24**. The specifications of our model are listed in **Table 25**. In the model, a uniform mesh of the size 20×10 is used, in which 231 nodes, 200 elements and 419 degrees-of-freedom are contained.

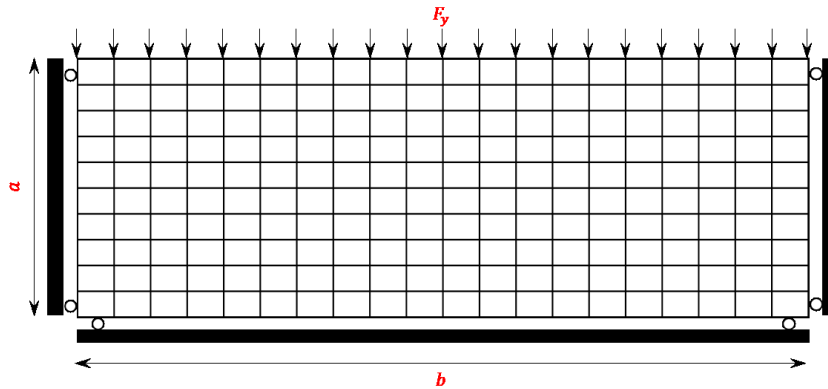**Figure 24:** *Two-dimensional reservoir*

Table 24: *Boundary Conditions for Two-dimensional Reservoir*

5. Constant vertical stress on the top ($\sigma_y = F \, / \, a$; where $F = 1.00E08 \, N$ and $a = 100 \, m$).
6. No vertical displacement in the bottom (i.e. $u_y = 0$).
7. No horizontal displacement on the right side (i.e. $u_x = 0$).
8. No horizontal displacement on the left side (i.e. $u_x = 0$).

Table 25: *Data Input for Two-dimensional Reservoir*

Young's Modulus, E *	=	2.900	GPa
Poisson Ratio, v *	=	0.000	fraction
Biot coefficient, b	=	1.000	fraction
Permeability, K	=	50.00	md
Porosity, $\emptyset_0$	=	0.300	fraction
Bulk density, ρ_b	=	2400	$Kg.m^{-3}$
Fluid density, $\rho_{f,0}$	=	1000	$Kg.m^{-3}$
Fluid viscosity, μ	=	1.000	cp
Initial pressure, p_i	=	2.125	MPa
Boundary pressure, $\bar{p}$	=	2.125	MPa
Overburden pressure	=	2.125	MPa

* *Only two elastic moduli are needed to describe fully material behavior of homogeneous, isotropic material*

Three numerical cases are considered with different master degrees-of-freedom (i.e. different reduced model size) for the two-dimensional reservoir. Summary of the three models is listed in **Table 26**.

Table 26: *Summary of three Cases for Two-Dimensional Reservoir*

Model	Number of Master DOFs	Number of Slave DOFs	Relative Size of Reduced-Order Model
A	40	379	9.55 %
B	70	347	17.1 %
C	188	231	44.8 %

The exact and estimated pressure profile at monitoring point are shown in **Figure 25**. As expected, with coupling the geomechanical model with the flow model, some control is lost over coupling procedure. *Accordingly, some error is introduced in the coupled system. Additionally, the choice of the measurement locations (i.e. the masters) is critical for the overall solution.* As shown, with the increase in the size of the reduced model, the reduced solution approximates the full solution to acceptable degree.
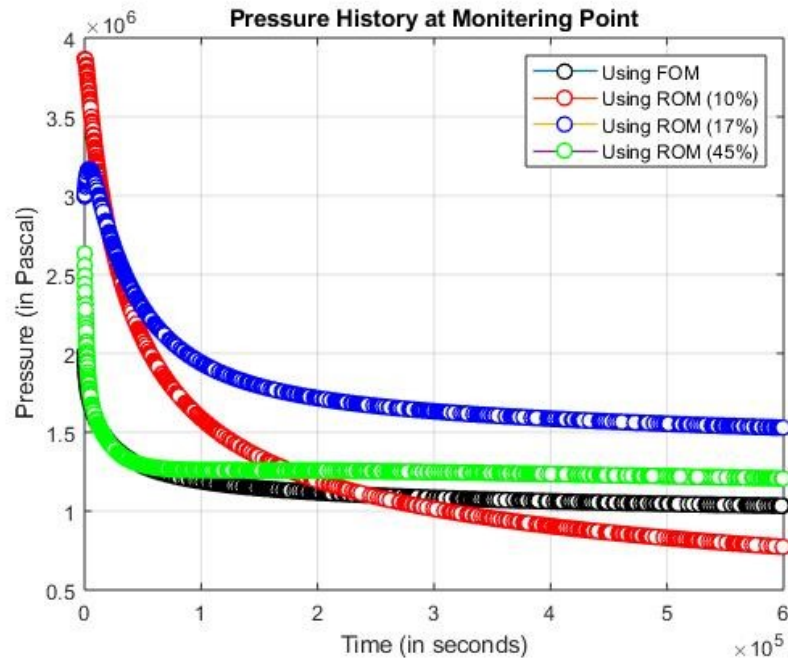
Figure 25: *Exact and estimated pressure profile (at monitoring point) for* three *reduced systems; where full system represented in **black**, first reduced system (Model A) represented in **red**, second reduced system (Model B) represented in **blue** and third reduced system (Model C) represented in **green**.*

Based on those results, a special attention should be geared towards the choice of master degrees-of-freedom; both the number and the measurement location, for coupled simulation.

CHAPTER V
CONCLUSION & FUTURE WORK

5.1. Conclusion

Throughout history, geomechanics modeling has proven its critical role in the development of oil and gas reservoirs, especially unconventional reservoirs. However, integration of geomechanical models in conventional simulations (flow only simulations) has been challenging in various aspects. One is the large scale of such models, which has been a major constraint due to the increased computational time and cost.

Historically, the finite element methods (FEM) proved to be efficient for the discretization and the analysis of complex structure mechanics. Yet, with the constant increase in the systems complexity, the discrete model size is substantially large. In turn, this motivated the development of low-order, yet, accurate models (ROM) capable of capturing the main features of the full-order model (FOM).

Much effort was devoted into the creation and development of efficient reduced-order modeling (ROM) techniques for flow only simulations. However, to date, the contributions to the mechanical models in coupled simulations have been minimal. Former ROM techniques applied to mechanics problems, such as DD and POD-DEIM, although efficient, yet they are not easy to implement and not robust.

This study proposes a relatively easy, yet efficient, ROM workflow (based on system condensation) for geomechanical models, as well as, coupled flow/geomechanics models that can guarantee:

- Easy coupling with any commercial simulation software.
- Intensive scale reduction; down to 10% of full-order model (FOM) size.
- High computational speedups; more than 20-fold, and error as low as 1%.
- Continuity of solution over the whole domain unlike domain decomposition (DD).

Based on the provided analyses:

- One-step methods (e.g. Guyan Condensation) have proven to be efficient for reduction of large-scale *static* geomechanical models. However, due to the ignorance of inertia effects, Guyan Condensation loses its accuracy for dynamic models. Besides, Guyan Condensation overall accuracy is dependent on the choice of master degrees-of-freedom (DOFs).

- Two-step methods have shown a slight improvement over one-step methods for large-scale dynamic models due to the corrections for inertia effects. However, the dependence of the quality of overall results for ROM on the selection of master degrees-of-freedom (DOFs) limited the implementation of two-step methods to large-scale dynamic models.

- Three-step (iterative) methods have proven its superiority over the aforementioned reduction, or condensation, techniques for two reasons: (1) the inclusion of inertia effects during the construction of condensation matrix for dynamic models, as well as, (2) independence of ROM accuracy from masters selection due to the iteration over reduced-order model (ROM) parameters.

Based on the presented results, an optimal choice for the reduced-order modeling (ROM) techniques was made; that is the implementation of three-step methods. Following that, optimization of the developed workflow was carried out through testing the completeness, efficiency, and convergence for all the implemented reduction techniques.

Upon testing of proposed workflow on geomechanical models, extension of the application of the ROM workflow to coupled flow/geomechanics models was carried out. Sequential methods were used for integration of geomechanical effects with conventional flow simulation models. Verification of the workflow for coupled systems using Mandel's problem has shown that:

- Some control is lost over coupling procedure. Accordingly, some error is introduced in the coupled system.

- The choice of the measurement locations (i.e. the masters) is critical for the overall solution accuracy.

- More investigation has shown that, with the increase in the size of the reduced model, the reduced solution approximates the full solution to acceptable degree.

5.2. Future Work

Based on the presented analyses, the proposed reduced-order modeling (ROM) framework shows a huge potential and comparable results as opposed to other reduction techniques. With that being considered, large-scale complex simulations – similar to those associated hydraulic fracturing – would be more feasible and less costly. This ultimately would motivate the advent of unconventional reservoirs development. However, a special consideration should be paid to the following:

- Extension of adopted reduced-Order modeling (ROM) workflow to more realistic models (e.g. coupled flow/geomechancis dynamic systems).
- Implementation of adopted workflow on far complicated systems with severe discontinuities (e.g. fractured reservoirs).
- Adjustment of developed workflow to adapt to nonlinear system.
- Integration of data analytics for control over coupling parameters.

REFERENCES

Abousleiman, Y., Cheng, A.H.D., Cui, L., Detournay, E., and Roegiers, J.C., 1996, *Mandel's problem revisited*: Geotechnique, v. 46, p. 187-195.

Allemang, R. J., and Brown, D. L.: "*A Correlation Coefficient for Modal Vector Analysis*", Proceedings of the 1st International Modal Analysis Conference (Orlando, FL), Union College, Schenectady, NY, **1982**, pp. 110-116.

Alpak, F. O. (2019, March 29). *A Multiphysics Fully-Coupled Flow and Geomechanics Simulation System with Hydraulic-Fracturing Simulation Capability*. Society of Petroleum Engineers. doi:10.2118/193825-MS

Armero F. and Simo J.C. 1992. *A new unconditionally stable fractional step method for non-linear coupled thermomechanical problems*. Int J Numer Methods Eng 35: 737–766.

Armero F. and Simo J.C. 1993. *A prior stability estimates and unconditionally stable product formula algorithms for nonlinear coupled thermoplasticity*. Int J Plasticity 9: 749–782.

Athanasios C. Antoulas. *Approximation of Large-Scale Dynamical Systems* (Advances in Design and Control). Society for Industrial and Applied Mathematics (SIAM). 2005.

Aziz, K., & Settari, A. (**2002**). Petroleum reservoir simulation. Calgary: K. Aziz & A. Settari.

Babuska, I., 1973, *Finite-Element Method with Lagrangian Multipliers*: Numerische Mathematik, v. 20, p. 179-192. Barber, J.R., 2002, Elasticity: New York, Kluwer Academic Publishers.

Bui, Van & Luu, Huong & Sun, Yanhua. (2020). Using Performance Models to Analyze the Behavior of Parallel Programs.

Belayneh, B.S.A.a.M., 2004, *Elastoplastic fracturing model for wellbore stability using non-penetrating fluids*: Journal of Petroleum Science and Engineering, v. 45, p. 179-192.

Belgacem, F.B., 1999, *The Mortar finite element method with Lagrange* multipliers: Numer. Math., v. 84, p. 173-197.

Bernardi, C., Maday, Y., and Patera, A.T., 1994a, *A new nonconforming approach to domain decomposition: the mortar element method, Nonlinear partial differential equations and their applications*: Collège de France Seminar, vol. XI (Paris, 1989–1991), Longman Sci. Tech.

Bianco, M., Bilardi, G., Pesavento, F., Pucci, G., and Schrefler, B.A., 2003, *A frontal solver tuned for fully coupled non-linear hygro-thermo-mechanical problems*: International Journal for Numerical Methods in Engineering, v. 57, p. 1801- 1818.

Biot M.A. 1941. *General theory of three-dimensional consolidation*. J Appl Phys 12: 155–164.

Bjorstad, P.E., and Widlund, O.B., 1986, *Iterative Methods for The Solution Of Elliptic Problems On Regions Partitioned Into Substructures*: Siam Journal on Numerical Analysis, v. 23, p. 1097-1120.

Booker, J.R., and Small, J.C., 1987, *A Method of Computing the Consolidation Behavior of Layered Soils Using Direct Numerical Inversion of Laplace Transforms*: International Journal for Numerical and Analytical Methods in Geomechanics, v. 11, p. 363-380.

Bourgat, J.F., Glowinsky, R., Tallec, P.L., and Vidrascu, M., 1988, *Variational Formulation and Algorithm for Trace Operator in Domain Decomposition Calculations*, Second International Symposium on Domain Decomposition Methods, SIAM, p. 3-16.

Cardoso, M.A. and Durlofsky, L.J. (2010). *Linearized reduced- order models for subsurface flow simulation*. Journal of Computational Physics, 229(3), 681–700.

Charlez, P.A., 1991, *Rock Mechanics, Volume I*: Theoretical Fundamentals: France, Editions Technip.

Chin, L.Y., Raghavan, R., and Thomas, L.K., 2000, *Fully coupled geomechanics and fluid-flow analysis of wells with stress- dependent permeability*: Spe Journal, v. 5, p. 32-45.

Coussy, O., 2004, *Poromechanics*: New York, Wiley.

Cowsar, L.C., Mandel, J., and Wheeler, M.F., 1995, *Balancing Domain Decomposition for Mixed Finite- Elements*: Mathematics of Computation, v. 64, p. 989-1015.

Dean, R.H., Gai, X., Stone, C.M., and Minkoff, S.E., 2006, *A comparison of techniques for coupling porous flow and geomechanics*: Spe Journal, v. 11, p. 132-140.

Destuynder, P., and Roux, F., 1988, *A Parallel Solver for the Linear Elasticity Equations on a Composite Beam*, in al., T.F.C.e., ed., Second International Symposium on Domain Decomposition Methods, SIAM, p. 314-320.

E. Gildin, A. C. Antoulas, D. Sorensen, R. H. Bishop: "*Model and controller reduction applied to structural control using passivity theory*". Struct. Control Health Monit.**2009**,16(3), 319.

Ferronato, M., Castelletto, N., and Gambolati, G., 2010, *A fully coupled 3-D mixed finite element model of Biot consolidation*: Journal of Computational Physics, v. 229, p. 4813-4830.

Ferronato, M., Janna, C., and Gambolati, G., 2008, *Mixed constraint preconditioning in computational contact mechanics*: Computer Methods in Applied Mechanics and Engineering, v. 197, p. 3922-3931.

Fjaer, E., Holt, R.M., Horsrud, P., Raaen, A.M., and Risnes, R., 2008, *Petroleum related rock mechanics*: Hungary, Elsevier.

Flemisch, B., Puso, M.A., and Wohlmuth, B.I., 2005*, A new dual mortar method for curved interfaces: 2D elasticity*: International Journal for Numerical Methods in Engineering, v. 63, p. 813-832.

Fritz, A., Hueber, S., and Wohlmuth, B.I., 2004, *A comparison of mortar and Nitsche techniques for linear elasticity*: Calcolo, v. 41, p. 115-137.

Funaro, D., Quarteroni, A., and Zanolli, P., 1988, *An Iterative Procedure With Interface Relaxation For Domain Decomposition Methods*: Siam Journal on Numerical Analysis, v. 25, p. 1213-1236.

Gai, X., 2004, *A Coupled Geomechanics and Reservoir Flow Model on Parallel Computers*: Austin, The University of Texas. Gassmann, F., 1951, Elastic waves through a packing of spheres: Geophysics v. 16, p. 673-685.

Gawin, D., Majoranna, C.E., Pesavento, F., and Schrefler, B.A., 1998, *A fully coupled multiphase model of hydro-thermo- mechanical behaviour of concrete at high temperature*, Fourth World Congress on Computational Mechanics, p. 1-19.

Geertsma, J., 1957, *The effect of fluid pressure decline on volumetric changes of porous rocks*: Trans. AIME, v. 210, p. 331- 340.

Girault, V., Pencheva, G.V., Wheeler, M.F., and Wildey, T.M., 2009, *Domain decomposition for linear elasticity with DG jumps and mortars*: Computer Methods in Applied Mechanics and Engineering, v. 198, p. 1751-1765.

Glowinski, R., and Wheeler, M.F., 1988, *Domain decomposition and mixed finite element methods for elliptic problems*, in R. Glowinski, G.H.G., G.A. Meurant, J. Periaux, ed., First International Symposium on Domain Decomposition Methods for Partial Differential Equations, SIAM.

Gutierrez, M., Lewis, R.W., and Masters, I., 2001, *Petroleum reservoir simulation coupling fluid flow and geomechanics*: Spe Reservoir Evaluation & Engineering, v. 4, p. 164-172.

H. Florez and E. Gildin. "*Global/local model order reduction in coupled flow and linear thermal-poroelasticity*". Comput Geosci (2019). https://doi.org/10.1007/s10596-019-09834

H. Florez and E. Gildin: "*Model-order Reduction Applied to Coupled Flow and Geomechanics*", in Proceedings of the ECMOR XVI – 16th European Conference on the Mathematics of Oil Recovery, Barcelona, Spain, EAGE, **2018**.

H. Florez, "*Applications of model-order reduction to thermo-poroelasticity*," in 51st US Rock Mechanics/Geomechanics Symposium, American Rock Mechanics Association, 2017.

Hansbo, P., Lovadina, C., Perugia, I., and Sangalli, G., 2005*, A Lagrange multiplier method for the finite element solution of elliptic interface problems using non-matching meshes*: Numerische Mathematik, v. 100, p. 91-115.

Hauret, P., and Le Tallec, P., 2007, *A discontinuous stabilized mortar method for general 3D elastic problems*: Computer Methods in Applied Mechanics and Engineering, v. 196, p. 4881-4900.

Hauret, P., and Ortiz, M., 2006, *BV estimates for mortar methods in linear elasticity*: Computer Methods in Applied Mechanics and Engineering, v. 195, p. 4783-4793.

Hyun C. Yoon, Xuyang Guo, Jihoon Kim, John Killough, *Flexible and practical parallel implementation for coupled elastoplastic geomechanics and non-isothermal flow*. International Journal of Rock Mechanics and Mining Sciences, Volume 120, 2019, Pages 96-107.

J. E. T. Penny, M. I. Friswell, S. D. Garvey: "*Automatic Choice of Measurement Locations for Dynamic Testing*". AIAA Journal, Vol. 32, No. 2, February **1994.**

J. H. Ong: "*Improved Automatic Masters for Eigenvalue Economization*". January **1987**

J. He and L. J. Durlofsky, "*Reduced-order modeling for compositional simulation by use of trajectory piecewise linearization,*" SPE Journal, vol. 19, no. 05, pp. 858–872, 2014.

Jansen, J.D., Durlofsky, L.J. *Use of reduced-order models in well control optimization*. Optim Eng 18, 105–132 (2017). https://doi.org/10.1007/s11081-016-9313-6

Jihoon Kim, George J. Moridis, *Numerical analysis of fracture propagation during hydraulic fracturing operations in shale gas systems*. International Journal of Rock Mechanics and Mining Sciences, Volume 76, 2015, Pages 127-137.

Jin, Z. L., Garipov, T., Volkov, O., & Durlofsky, L. J. (2019, November 1). *Reduced-Order Modeling of Coupled Flow and Quasistatic Geomechanics*. Society of Petroleum Engineers. doi:10.2118/193863-PA

Jun Xiong, Nathan Deisman, Rick Chalaturnyk, Xiolan Huang. "*Reservoir-geomechanical analysis for caprock integrity evaluation during oilsand development*". September 2012. Disaster Advances 5(4):1713-1717

Kaasschieter, E.F., and Frijns, A.J.H., 2003, *Squeezing a sponge: a three-dimensional solution in poroelasticity*: Computational Geosciences, v. 7, p. 49-59.

Kim, C., Lazarov, R.D., Pasciak, J.E., and Vassilevski, P.S., 2001, *Multiplier spaces for the mortar finite element method in three dimensions*: Siam Journal on Numerical Analysis, v. 39, p. 519-538.

Kim, J., Tchelepi, H.A., and Juanes, R., 2009, *Stability; Accuracy and Efficiency of Sequential Methods for Coupled Flow and Geomechanics*, 2009 SPE Reservoir Simulation Symposium, Volume SPE 119084: The Woodlands, SPE.

Kim, K., Yi, D., and Lee, S., 2005, *Mortar method for nonconforming finite elements*: Applied Mathematics and Computation, v. 167, p. 650-669.

L. Sirovich, "*Turbulence and the dynamics of coherent structures, i-iii*". Quarterly of applied mathematics, vol. 45, no. 3, pp. 561–590, 1987.

Lamichhane, B.P., Stevenson, R.P., and Wohlmuth, B.I., 2005, *Higher order mortar finite element methods in 3D with dual lagrange multiplier bases*: Numerische Mathematik, v. 102, p. 93-121.

Lewis, R.W., and Schrefler, B.A., 1998, *The Finite Element Method in the Static and Dynamic Deformation and Consolidation of Porous Media*: New York, John Wiley and Sons.

Liu, R., 2004, *Discontinuous Galerkin Finite Element Solution for Poromechanics*: Austin, The University of Texas.

Longuemare, P., Mainguy, M., Lemonnier, P., Onaisi, A., Gerard, C., and Koutsabeloulis, N., 2002, *Geomechanics in reservoir simulation: Overview of coupling methods and field case study*: Oil & Gas Science and Technology-Revue De L Institut Francais Du Petrole, v. 57, p. 471-483.

M. Ghommem, E. Gildin, and M. Ghasemi: "*Complexity Reduction of Multiphase flows in heterogeneous porous media*", SPE Journal, **2015**.

M. I. Friswell, S. D. Garvey and J. E. T. Penny: "*Model Reduction Using Dynamic and Iterated IRS Techniques*". October 11th, **1994**

Maday, Y., and Magoules, F., 2006, *Absorbing interface conditions for domain decomposition methods*: A general presentation: Computer Methods in Applied Mechanics and Engineering, v. 195, p. 3880-3900.

Maday, Y., Mavriplis, C., and Patera, A.T., 1988, *Nonconforming Mortar Element Methods: Application to Spectral Discretization*, in al., T.F.C.e., ed., Second International Symposium on Domain Decomposition Methods, SIAM, p. 392-418.

Mandel, J., 1953, *Consolidation des sols (etude mathhatique)*: Géotechnique, v. 3, p. 287-299.

Mandel, J., and Brezina, M., 1996, *Balancing domain decomposition for problems with large jumps in coefficients*: Mathematics of Computation, v. 65, p. 1387-1401.

Miga M.I., Paulsen K.D., and Kennedy F.E. 1998. *Von Neumann stability analysis of Biot's general two dimensional theory of consolidation*. Int J Numer Methods Eng 43: 955–974.

Minkoff, S.E., Stone, C.M., Bryant, S., Peszynska, M., and Wheeler, M.F., 2003, *Coupled fluid flow and geomechanical deformation modeling*: Journal of Petroleum Science and Engineering, v. 38, p. 37-56.

Morris J. 2009a. *Injection and Reservoir Hazard Management: The Role of Injection-Induced Mechanical Deformation and Geochemical Alteration at In Salah CO2 Storage Project*. Lawrence Livermore National Laboratory.

Morris J.P. 2009b. *Simulations of injection-induced mechanical deformation: A study of the In Salah CO2 storage project*. SEG 2009 Summer Research Work CO2 Seq Geophy, Banff Canada, 23-27 Aug.

Muller, A.L., Jr, E.d.A.V., Vaz, L.E., and Goncalves, C.J., 2009, *Borehole stability analysis considering spatial variability and poroelastoplasticity*: International Journal of Rock Mechanics and Mining Sciences, v. 46, p. 90-96.

Pao, W.K.S., Lewis, R.W., and Masters, I., 2001, *A fully coupled hydro-thermo-poro-mechanical model for black oil reservoir simulation*: International Journal for Numerical and Analytical Methods in Geomechanics, v. 25, p. 1229-1256.

Park K.C. 1983. *Stabilization of partitioned solution procedure for pore fluid-soil interaction analysis*. Int J Numer Methods Eng 19(11): 1669–1673.

Peter Benner, Serkan Gugercin, and Karen Willcox. *A Survey of Projection-Based Model Reduction Methods for Parametric Dynamical Systems.* SIAM Review 2015 57:4, 483-531

Phillips, P.J., 2005, *Finite Element Methods in Linear Poroelasticity*: Theoretical and Computational Results: Austin, The University of Texas

Phillips, P.J., and Wheeler, M.F., 2007a, *A coupling of mixed and continuous Galerkin finite element methods for poroelasticity I*: the continuous in time case: Computational Geosciences, v. 11, p. 131-144.

Puso, M.A., **2004**, *A 3D mortar method for solid mechanics*: International Journal for Numerical Methods in Engineering, v.59, p. 315-336.

Qu, Z.-Q.: "*Model Order Reduction Techniques: With Applications in Finite Element Analysis*", Springer, London, **2004**.

Quarteroni, A., and Valli, A., **1999**, *Domain Decomposition Methods for Partial Differential Equations*: Oxford Oxford University Press.

Reddy, J.. (**2006**). An Introduction to Finite Element Method. 10.1115/1.3265687.

R. J. Guyan: "*Reduction of Stiffness and Mass Matrices*". AIAA Journal Vol. 3, No. 2, **1965**, p., 380.

Rice, J.R., and Cleary, M.P., 1976, *Some Basic Stress Diffusion Solutions for Fluid-Saturated Elastic Porous-Media with Compressible Constituents*: Reviews of Geophysics, v. 14, p. 227- 241.

Sandhu, R.S., and Wilson, E.L., 1969, *Finite element analysis of seepage in elastic media*: J. Eng. Mech. Div., ASCE, v. 95, p. 641-652.

Santarelli, F.J., Dahen, D., Baroudi, H., and Sliman, K.B., 1992, *Mechanisms of Borehole Instability in Heavily Fractured Rock Media*: Int. J. Rock Mech. Min. Sci. and Geomech. Abstr., v. 29, p. 457-467.

Settari, A., and Walters, D.A., 2001, *Advances in coupled geomechanical and reservoir modeling with applications to reservoir compaction*: Spe Journal, v. 6, p. 334-342.

Shao, J.F., 1997, *A numerical solution for a thermo-hydro-mechanical coupling problem with heat convection*: International Journal of Rock Mechanics and Mining Sciences, v. 34, p. 163-166.

Souza-Neto, E.A.d., Peric, D., and Owen, D.R.J., 2008, *Computational Methods for Plasticity: Theory and Applications*: United Kingdom, John Wiley and Sons Ltd.

Stavroulakis, G.M., and Papadrakakis, M., 2009, *Advances on the domain decomposition solution of large scale porous media problems*: Computer Methods in Applied Mechanics and Engineering, v. 198, p. 1935-1945.

T. Kidambi, A. Hanegaonkar, A. Dutt, G.S. Kumar, "*A fully coupled flow and geomechanics model for a tight gas reservoir: Implications for compaction, subsidence and faulting*", Journal of Natural Gas Science and Engineering, Volume 38, 2017, Pages 257-271.

Terzaghi, K., 1923, Die Berechnung der Durchlassigkeitsziffer des Tones aus dem Verlauf der hydrodynamischen Spannungserscheinungen: Sitzung Berichte. Akadamie der Wissenschaften, Wien Mathematisch- Naturwissenschaftliche Klasse, Abteilung IIa, v. 132, p. 105-124, 1943, Theoretical Soil Mechanics: New York, Wiley.

Toselli, A., and Widlund, O.B., 2004, *Domain Decomposition Methods: Algorithms and Theory*, publisher Springer.

Turska, E., and Schrefler, B.A., 1993, *On Convergence Conditions of Partitioned Solution Procedures for Consolidation Problems*. Computer Methods in Applied Mechanics and Engineering, v. 106, p. 51-63.

Turska, E., Wisniewski, K., and Schrefler, B.A., 1994, *Error Propagation of Staggered Solution Procedures for Transient Problems*: Computer Methods in Applied Mechanics and Engineering, v. 114, p. 177-188.

V. N. Shah and M. Raymund: "*Analytical Selection of Masters for the Reduced Eigenvalue Problem*". International Journal for Numerical Methods in Engineering, Vol. 18, 89-98 (**1982**)

Wheeler, M.F., 1978, *Elliptic Collocation-Finite Element Method with Interior Penalties*: Siam Journal on Numerical Analysis, v. 15, p. 152-161.

Wohlmuth, B.I., 2000, *A mortar finite element method using dual spaces for the Lagrange multiplier: Siam Journal on Numerical Analysis*, v. 38, p. 989-1012.

X. Tan, E. Gildin, H. Florez, S. Terhan, Y. Yang, N. Hoda, et al., "*Trajectory-Based DEIM (TDEIM) Model Reduction Applied to Reservoir Simulation*". Computational Geosciences, Vol. 23, No. 1, pp. 35-53, **2019**.

Yin, S.D., Dusseault, M.B., and Rothenburg, L., 2009, *Thermal reservoir modeling in petroleum geomechanics: International Journal for Numerical and Analytical Methods in Geomechanics*, v. 33, p. 449-485.

Yoon, HC, Kim, J. *Spatial stability for the monolithic and sequential methods with various space discretizations in poroelasticity*. Int J Numer Methods Eng. 2018; 114: 694– 718. https://doi.org/10.1002/nme.5762

Zienkiewicz, O.C., and Shiomi, T., 1984, *Dynamic behavior of saturated porous media: the generalized Biot formulation and its numerical solution*: Int. J. Numer. Anal. Methods Geomech., v. 8, p. 71-96.

Zienkiewicz, O.C., Humpheson, C., and Lewis, R.W., 1977, *A unified approach to soil mechanics problems including plasticity and viscoplasticity*, in Gudehus, G., ed., Finite Elements in Geomechanics, Wiley, New York, p. 151–-177.

Zu-Qing Qu and Zhi-Fang Fu: "*An Iterative Method for Dynamic Condensation of Structural Matrices*". May 13th , **1998**.